Atomic many-body theory and variation of constants of nature

by

Michael Marchenko

A thesis submitted in satisfaction of
the requirements for the degree of
Doctor of Philosophy
in the Faculty of Science.

20 September 2015

THE UNIVERSITY OF
NEW SOUTH WALES

SYDNEY · AUSTRALIA

Statement of Originality

I hereby declare that this submission is my own work and to the best of my knowledge it contains no materials previously published or written by another person, or substantial proportions of material which have been accepted for the award of any other degree or diploma at UNSW or any other educational institution, except where due acknowledgement is made in the thesis. Any contribution made to the research by others, with whom I have worked at UNSW or elsewhere, is explicitly acknowledged in the thesis. I also declare that the intellectual content of this thesis is the product of my own work, except to the extent that assistance from others in the project's design and conception or in style, presentation and linguistic expression is acknowledged.

(Signed)

Abstract

Fundamental physical constants are the only absolutes which exist at the moment. If they are not really constants then this is a serious philosophical problem. All measurements are binding to the fundamental physical constants. The cutting edge of the modern physics is high energy physics which can allow to go beyond Standard Model, to discover New Physics, and to understand better how the Universe came into existence (evolved). This may result in better sources of energy than the ones which are used now. Theories unifying gravity with other interactions (such as string theories and M- theory) allow or require variation of the fundamental physical constants. If one can determine precise enough limits for variation of fundamental physical constants it may help to choose the most adequate theory of unifying gravity with other interactions. This would be indirect theoretical verification of high energy physics. This verification is not feasible by experimental methods.

We use Big Bang Nucleosynthesis calculations and light element abundance data to constrain the relative variation of the deuteron binding energy since the universe was a few minutes old, $\delta Q = Q(\mathrm{BBN}) - Q(\mathrm{present})$. Two approaches are used, first treating the baryon to photon ratio, η, as a free parameter, but with the additional freedom of varying δQ, and second using the WMAP value of η and solving only for δQ. Including varying Q yields a better fit to the observational data than imposing the present day value, rectifying the discrepancy between the ^{4}H e abundance and the deuterium and ^{7}Li abundances, **and** yields good agreement with the independently determined $\eta_{\mathbf{WMAP}}$. The minimal deviation consistent with the data is significant at about the 4-σ level; $\delta Q/Q = -0.019 \pm 0.005$. If the primordial ^{4} He abundance lies towards the low end of values in the literature, this deviation is even larger and more statistically significant. Taking the light element abundance data at face-value, our result may be interpreted as variation of the dimensionless ratio $X = m_s / \Lambda_{\mathbf{QCD}}$ of the strange quark mass and strong scale: $\delta X/X = (1.1 \pm 0.3) \times 10^{-3}$. These results provide a strong motivation for a more thorough exploration of the potential systematic errors in the light element abundance data.

Key words: physical constants, high energy physics, Big Bang nucleosynthesis (nuclear synthesis), atomic clocks, Grand Unification, Standard Model, quasar spectra, signal processing, sensitivity, precision.

Contents

Introduction

Recently there was an intensive discussion of the possible space-time variation of the fine structure constant

$\alpha = e^2/hc$ at the cosmological scale.

The first evidence for such variation has been reported in [1, 2, 3, 4, 5, 6] from the analysis of the astrophysical data. These results are to be compared with the number of experimental up-per bounds on this variation obtained from other astrophysical observations (see, e.g. [7, 8, 9]) and from the precision laboratory measurements [10, 11, 12]. Recently a number of new laboratory tests have been proposed (see, e.g. [13]). The analysis of the microwave back-ground radiation can also give some restrictions on time variation of α as suggested in [14, 15, 16]. Implementations of the space-time variation of the fine structure constant to the theory of the fundamental interactions are discussed e.g. in Refs. [17, 18, 19, 20, 21, 22, 23] (see also discussion and references in [3]).

The most straightforward way to look for the variation of is to measure the ratio of some fine structure interval to an optical transition frequency, such as $\omega(np_{1/2} \rightarrow np_{3/2})$ and $\omega(n's_{1/2} \rightarrow np_{3/2})$ [37]. This ratio can be roughly estimated as $0.2\ \alpha^2 Z^2$, where Z is the nuclear charge [24]. Therefore, any difference in this ratio for a laboratory experiment and a measurement for some distant astrophysical object can be easily converted into the space-time variation of α. However, as it was pointed out in [25], one can gain about an order of magnitude in the sensitivity to the α-variation by comparing optical transitions for different atoms. In this case the frequency of each transition can be expanded in a series in α^2 :

α_0 stands for the laboratory value of the fine structure constant. Note, that Eq. (1a) corresponds to the expansion at $\alpha = 0$, while Eq. (1b) — to the expansion at $\alpha = \alpha_0$. In both cases parameters $\omega_i^{(2)}$ and q_i appear due to relativistic corrections.

For a fine structure transition the first coefficient on the right hand side of (1a) turns to zero, while for the optical transitions it does not. Thus, for the case of a fine structure and an optical transition one can write:

Quite often the coefficients $\omega_i^{(2)}$ for optical transitions are about an order of magnitude larger than corresponding coefficients for the fine structure transitions $\omega_{fs}^{(2)}$ (this is because the relativistic correction to a ground state electron energy is substantially larger than the spin-orbit splitting in an excited state [25, 26]). Therefore, the ratio (3) is, in general, more sensitive to the variation of α than the ratio (2). It is also important that the signs of coefficients $\omega_i^{(2)}$ in (3) can vary. For example, for s-p transitions the relativistic corrections are positive while for d-p transitions they are negative. This allows to suppress possible systematic errors which "do not know" about the signs and magnitude of the relativistic corrections [25]. On the other hand, for many cases of interest, the underlying atomic theory is much more complicated for Eq. (3). In particular, the most difficult case corresponds to transitions to highly excited states of a multi-electron atom, where the spectrum is very dense. And this happens to be a typical situation for astrophysical spectra, in particular, for large cosmological red shifts. Corresponding atomic calculations have to account very accurately for the electronic correlations, which may affect such spectra quite dramatically.

TABLE I: Final results for parameters q from Eq. (1) for Si II, Cr II, Fe II, Ni II, and Zn II. Estimated errors are in brackets.

Ion	Transition			ω_0 (cm^{-1})	q (cm^{-1})	
Si II	$^2P^o_{1/2}$	$\rightarrow$	$^2D_{3/2}$	55309.3365	520	(30)
		$\rightarrow$	$^2S_{1/2}$	65500.4492	50	(30)
Cr II	$^6S_{5/2}$	$\rightarrow$	$^6P^o_{3/2}$	48398.868	−1360	(150)
		$\rightarrow$	$^6P^o_{5/2}$	48491.053	−1280	(150)
		$\rightarrow$	$^6P^o_{7/2}$	48632.055	−1110	(150)
Fe II	$^6D_{9/2}$	$\rightarrow$	$^6D^o_{9/2}$	38458.9871	1330	(150)
		$\rightarrow$	$^6D^o_{7/2}$	38660.0494	1490	(150)
		$\rightarrow$	$^6F^o_{11/2}$	41968.0642	1460	(150)
		$\rightarrow$	$^6F^o_{9/2}$	42114.8329	1590	(150)
		$\rightarrow$	$^6P^o_{7/2}$	42658.2404	1210	(150)
		$\rightarrow$	$^4F^o_{7/2}$	62065.528	1100	(300)
		$\rightarrow$	$^6P^o_{7/2}$	62171.625	−1300	(300)
Ni II	$^2D_{5/2}$	$\rightarrow$	$^2F^o_{7/2}$	57080.373	−700	(250)
		$\rightarrow$	$^2D^o_{5/2}$	57420.013	−1400	(250)
		$\rightarrow$	$^2F^o_{5/2}$	58493.071	−20	(250)
Zn II $^2S_{1/2}$		$\rightarrow$	$^2P^o_{1/2}$	48481.077	1584	(25)
		$\rightarrow$	$^2P^o_{3/2}$	49355.002	2490	(25)

The first calculations of the coefficients q from Eq. (1) for the transitions suitable for astronomical and laboratory measurements were done in Refs. [25, 26, 27, 28]. Here we present a new and more accurate calculations of the coefficients q for the transitions, which are currently used in the analysis of the astrophysical data. A full list of these transitions was given in [3]. We have not re-calculated here the lightest and the most-simple atoms Mg and Al, for which the previous calculation [25] should be sufficiently accurate and focused on more complicated ions Si II, Cr II, Fe II, Ni II, and Zn II. Our final results for them are given in Table I. Note, that here we use the single parameter q instead of two parameters q_1 and q_2 used in the earlier works and $q \equiv \partial\omega/\partial x|_{x=0} = q_1 + 2q_2$. Details of the calculations and discussion of the accuracy will be given in Sec. III. Before that we briefly address few theoretical points in Sec. II.

Theories unifying gravity with other interactions suggest that fundamental constants could vary in space-time (see, e.g. [1]). Recent evidence of variation of the fine structure constant α in quasar absorption spectra [2] elevated interest to the search of variation of α in laboratory experiments. Comparing frequencies of different atomic transitions over long period of time is a good way to do such search due to extremely high accuracy of measurements achieved for certain types of transitions. The best limit on local present-time variation of the fine structure constant published so far was obtained by comparing Hg^+ microwave atomic clock vs hydrogen maser [3]. Recently this limit was further improved by more than an order of magnitude in comparing cesium and rubidium atomic clocks [4]. There are also many proposals for the search of variation of α in atomic optical transitions, some of which were analyzed in our previous works (see [5] and references therein). In the present paper we analyze three new proposals involving strontium/calcium, dual beam [6], dysprosium atom [5,7] and ytterbium positive ions $Y\,b^+$ [8] and $Y\,b^{2+}$ [9]. We perform relativistic many-body calculations to link variation of α with the variation of the frequencies of atomic transitions. Then we use this connection to find out what accuracy of measurements is needed to improve current best limit on time variation of the fine structure constant.

In the proposal suggested by S. Bergeson strontium-calcium dual beam is to be used to compare the frequencies of the $^1S_0 -^3 P_1$ clock transitions in these atoms over a long period of time. Ca and Sr have similar electron structure. However, due to higher nuclear charge, relativistic effects are larger for strontium. If α is changing, corresponding change in frequency of the clock transition for Sr would go considerably faster than for Ca. Precise measurements might be able to indicate this or, at least, put strong constrain on possible variation of α. Calculations of the

relativistic effects for Ca were done in our previous work [5]. In present paper we do similar calculations for Sr.

Experiments with ytterbium positive ion have advantages of greater relativistic effects due to larger nuclear charge and the convenience of working with two different transitions of the same element. There are two transitions in Yb^+ involving metastable states for which comparison of frequencies is considered. One is quadrupole transition $4f\,^{14}6s\,^2S_{1/2} - 4f\,^{14}5d\,^2D_{5/2}$ and another is octupole transition $4f\,^{14}6s\,^2S_{1/2} - 4f\,^{13}6s^2\,^2F_{7/2}$. The quadrupole transition is basically a s−d transition while the octupole one is a f −s transition. According to simple analytical formula presented in Ref. [5] relativistic energy shifts for s electrons, and electrons with high total momentum j (like d and f electrons) are large but have opposite sign. This means that we should expect that two metastable states of Yb^+ move in opposite directions if α is changing. This brings extra enhancement to the sensitivity of the measurements for Yb^+ to the variation of α. Our accurate calculations presented below support these considerations.

The proposal for dysprosium is quite different from what was considered so far. Instead of comparing two very stable atomic clock frequencies the authors of this proposal [5] suggest to measure very small frequency of the transition between two almost degenerate states of opposite parity in dysprosium. The states are $4f\,^{10}5d6s\,^3[10]_{10}$ E = 19797.96cm^{-1} and $4f\,^9 5d^2 6s\,^9K_{10}$ E = 19797.96cm^{-1}. These states were used before for the search of parity non-conservation in Dy [11]. Small energy splitting and different electron structure of these two states lead to very strong enhancement of the sensitivity of the frequency of transition

between the states to variation of α. The enhancement (about eight orders of magnitude) seems to be strong enough to overcome the disadvantage of dealing with states which are not very narrow.

In the present paper we calculate the values of relativistic energy shifts for Sr, Yb^+ and Dy and discuss what accuracy of measurements is needed to improve current best constrain on local time variation of the fine structure constant.

Chapter1 Many-Body Theory

Standard many-body perturbation theory

The quantum-mechanical treatment of many-electron systems, based on the Schr□odinger equation and the Coulomb interaction between the electrons,was developed shortly after the advent of quantum mechanics, particularlyby John Slater in the late 1920's and early 1930's [214]. Self-consistent-field(SCF) schemes were early developed by Slater, Hartree, Fock and others.1

Perturbative schemes for quantum-mechanical system, based on the Rayleigh-Schr□odinger and Brillouin-Wigner schemes, were developed in the 1930's and 1940's, leading to the important linked-diagram expansion, introduced by Brueckner [37] and Goldstone [73] in the 1950's, primarily for nuclear applications. That scheme was in the 1960's and 1970's also applied to electronic systems [100] and extended to degenerate and quasi-degenerate energy levels [31, 112]. The next step in this development was the introduction of " all-order methods" of coupled-cluster type, where certain effects are taken to all orders of the perturbation expansion. This represents the last and probably major step of the development of a non-relativistic many-body perturbation theory (MBPT).2

The first step towards a relativistic treatment of many-electron systems was taken in the early 1930's by Gregory Breit [32], extending works made somewhat earlier by J. A. Gaunt [68]. Physically, the Gaunt interaction represents the magnetic interaction between the electrons, which is a purely relativistic effect. Breit augmented this treatment by including the leading retardation effect, due to the fact that the Coulomb interaction is not instantaneous, which is an effect of the same order.

A proper relativistic theory should be Lorentz covariant, like the Dirac single-electron theory.3 The Dirac equation for the individual electrons together with the instantaneous Coulomb and Breit interactions between the electrons represent for a many-electron system all effects up to order2 H(Hartree atomic units) or 4mec2.4 This procedure, however, is NOT Lorentz covariant, and the Breit interaction can only be treated to first-order in perturbation theory, unless projection operators are introduced to prevent the intermediate states from falling into the "Dirac sea" of negative-energy states, as discussed early by Brown and Ravenhall [36] and later by Joe Sucher [222]. The latter approach has been successfully employed for a long time in relativistic many-body calculations and is known as the no-virtual-pair approximation (NVPA). A fully covariant relativistic many-body theory requires a field-theoretical approach, i.e., the use of quantum-electrodynamics (QED). In principle, there is no sharp distinction between relativity

and QED, but conventionally we shall refer to effects beyond the no-virtual-pair approximation as QED effects. This includes effects of retardation, virtual pairs and radiative effects (selfenergy, vacuum polarization, vertex correction). The systematic treatment of these effects requires a covariant approach, where the QED effects are included in the wave function. It is the main purpose of the present book to formulate the foundations of such a procedure.

Quantum-electrodynamics

Already in the 1930's deviations were observed between the results of precision spectroscopy and the Dirac theory for simple atomic systems, primarily the hydrogen atom. Originally, this deviation was expected to be due to vacuum polarization, i.e., spontaneous creation of electron-positron pairs in the vacuum, but this effect turned out to be too small and even of the wrong sign. An alternative explanation was the electron self-energy, i.e., the emission and absorption of a virtual photon on the same electron another effect that is not included in the Dirac theory. Early attempts to calculate this effect, however, were unsuccessful, due to singularities (infinities) in the mathematical expressions.

The first experimental observation of a clear-cut deviation from the Dirac theory was the detection in 1947 by Lamb and Retherford of the so-called Lamb shift [111], namely the shift between the 2 s and 2 p 1 = 2 levels in atomic hydrogen, levels that are exactly degenerate in the Dirac theory [53, 54]. In the same year Hans Bethe was able to explain the shift by a non-relativistic calculation, eliminating the singularity of the self energy by means of a renormalization process[16]. At about the same time Kusch and Foley observed that the magnetic g-factor of the free electron deviates slightly but significantly from the Dirac value -2 [105, 106]. These observations led to the development of the modern form of the quantum-electrodynamics theory by Feynman, Schwinger, Dyson, Tomanaga and others by which the deviations from the Dirac theory could be explained with good accuracy [210, 228, 64, 63, 58].5 The original theory of QED was applied to free electrons. During the last four decades several methods have been developed for numerical calculation of QED effects in bound electronic states. The scattering-matrix or S-matrix formulation, originally developed for dealing with the scattering of free particles, was made applicable also to bound states by Joe Sucher [220], and the numerical procedure was refined in the 1970's particularly by Peter Mohr [146]. During the last two decades the method has been extensively used in studies of highly charged ions in order

to test the QED theory under extreme conditions, works that have been pioneered by Mohr and So (for a review, see ref. [152]).

The Green's function is one of the most important tools in mathematical physics with applications in essentially all branches of physics.6 During the1990's the method was adopted to bound-state QED problems by Shabaev et al. [211]. This procedure is referred to as the Two-times Green's function and has recently been extensively applied to highly-charged ions by the St Petersburg group. During the first decade of this century another procedure for numerical QED calculations was developed by the Gothenburg atomic theory group, termed the Covariant-evolution-operator (CEO) method [124], which has been applied to the fine structure and other energy-level separations of heliumlike ions. [1.111]

Chapter 2

THEORY

In order to find parameters $q = \partial\omega/\partial x|_{x=0}$ in Eq. (1) we perform atomic calculations for three values of x: $x_- = -1/8$, $x_0 = 0$, and $x_+ = 1/8$. That allows us to determine q: $q = 4\,(\omega(x_+) - \omega(x_-))$ and also estimate the second derivative $\partial^2\omega/\partial x^2|_{x=0}$. The large value of the latter signals that interaction between levels is strong (level pseudo-crossing), and there is a risk of large errors. For these cases further analysis was done as described below.

a. Relativistic calculations of multi-electron ions.

In order to accurately account for the dominant relativistic effects we use the Dirac-Hartree-Fock approximation as a starting point for all calculations of atomic spectra. Though most of the calculations were done for the Coulomb potential, we have also estimated Breit corrections by including the magnetic part of the Breit inter-action in the self-consistent field [1.29].

The ions we are dealing with in this paper have from one to nine electrons in the open shells. For one valence electron in Zn II the Dirac-Fock V^{N-1} approximation already gives rather good results. On the next step the core-valence correlations can be accounted for by means of the many-body perturbation theory (MBPT). Already the second order MBPT correction allows to reproduce the spectrum with the accuracy, better than 1%, which is more than sufficient for our current purposes.

Other ions of interest to us have at least three valence electrons. Here the dominant correlation correction to transition frequencies corresponds to the valence-valence correlations. This type of correlations can be accounted for with configuration interaction (CI) method. If necessary, the core-valence correlations can be included within combined CI+MBPT technique [1.30]. The latter usually provides an accuracy of the order of 1% or better for the lower part of the spectra of atoms and ions with two or three valence electrons [1.30, 31, 32]. However, the accuracy of ab initio methods decreases with the number of valence electrons and with excitation energy.

Indeed, for a large number of valence electrons and/or sufficiently high excitation energy the spectrum becomes dense and the levels with the same exact quantum numbers strongly interact with each other. The part of the spectrum of Fe II above 55000 cm^{-1} and, to a somewhat lesser extent, the spectrum of Ni II represent this situation. There-fore, for these ions we developed a semi-empirical fitting procedure, which is described below.

In order to have additional control of the accuracy of our CI we performed calculations for most of the ions with two different computer packages. One package was used earlier in Refs. [30, 32, 33] and another one was used in Refs. [3, 25, 26, 27, 28, 31]. The former pack-age allows to construct flexible basis sets and optimize configuration space, while the latter allows for a larger CI space as it works with the block of the Hamiltonian matrix, which corresponds to a particular total angular momentum of atom J . When there were no significant difference between two calculations, we only give results obtained with the first package. Nevertheless, our final results presented in Table I are based on both calculations.

b. Semi-empirical treatment of the strong interaction of levels: pseudo-crossing.

In the nonrelativistic limit $\alpha \to 0$, all multi-electron states are accurately described by the LS-coupling scheme: $E_{\alpha\to 0} = E_{p,n,L,S,J}$, where p = ±1 is the parity and n numerates levels with the same p, L,S, and J. For sufficiently small values of α the LS-coupling holds and the energy has the form:

$$E_{p,n,L,S,J} = E^{(0)}_{p,n,L,S} + \left(\frac{\alpha}{\alpha_0}\right)^2 \Big(C_{p,n,L,S} + \frac{1}{2}A_{p,n,L,S}\left[J(J+1) - L(L+1) - S(S+1)\right]\Big), \quad (4)$$

The first term in the parentheses gives the slope for the centre of the multiplet and the second term gives the fine structure. With growing α the multiplets start to overlap and when the levels with the same p and J come close, the pseudo-crossing takes place.

Near the pseudo-crossing the slope of the energy curves changes dramatically. If such crossing

takes place at $x \approx 0$, where x is defined by Eq. (1), i.e. near the physical value of α, it can cause significant uncertainty in the values of parameters q.

Let us first analyze the behavior of the slopes q(x) in the vicinity of the pseudo-crossing in the two-level approximation. Consider two levels E_1 and E_2 which cross at $x = x_c$:

$$E_1 = q_1(x - x_c), \qquad (5a)$$
$$E_2 = q_2(x - x_c). \qquad (5b)$$

If the interaction matrix element between these two levels is V , the exact adiabatic levels will be

$$E_{a,b} = \frac{1}{2}\Big((q_1 + q_2)(x - x_c) \pm \sqrt{(q_1 - q_2)^2(x - x_c)^2 + 4V^2}\Big). \qquad (6)$$

It is easy now to calculate the energy derivative in respect to x in terms of the mixing angle φ between unperturbed states 1 and 2:

$$\frac{\partial E_{a,b}}{\partial x} = \cos^2\phi\, q_{1,2} + \sin^2\phi\, q_{2,1}. \qquad (7)$$

Note, that at the crossing the angle φ varies from 0 on one side through π/4 in the centre to π/2 on the other side, which leads to the change of the slope

$q_a(x) = \partial E_a/\partial x$ from q_1 through $(q_1 + q_2)/2$ to q_2. The narrow crossings with small V are particularly dangerous, as the slopes change very rapidly within the interval $x \approx V/|q_1 - q_2|$. Then, even small errors in the position of the crossing point x_c , or the value of V can cause

large errors in $q_{a,b}$. In this model we assume that non-diagonal term V = const. For the real atom V $\propto \alpha^2$. However, if the crossing region $x \ll 1$, we can neglect the dependence of V on α.

b. Semi-empirical treatment of the strong interaction of levels: multi-level case.

Eq. (7) can be easily gener-alized to a multi-level case as it simply gives the slope of a physical level a as a weighted average of the mixed levels. Thus, if the level a can be expressed as a linear combination of some unperturbed LS-states $\psi_{Ln,Sn}$:

$$|a\rangle = \sum_n C_n |\psi_{L_n,S_n}\rangle, \tag{8}$$

the resultant slope q_a is given by:

$$q_a = \sum_n C_n^2 \, q_n. \tag{9}$$

Here again we neglect weak dependence of interaction V on x in comparison to strong dependence of C_n^2 on x near crossing points.

Eq. (9) allows to improve ab initio coefficients q if we can find the expansion coefficients C_n in

Eq. (8). That can be done, for example, by fitting g-factors. The magnetic moment operator $\mu = g_0(L + 2S)$ is diagonal in L and S and, therefore, does not mix different LS-states. Thus, in the LS-basis the resultant g-factor for the state *a* has exactly the same form as q_a:

$$g_a = \sum_n C_n^2 \, g_n. \tag{10}$$

If the experimental g-factors are known, one can use Eq. (10) to find weights C_n^2 and, then find the corrected values of the slopes q_a.

Sometimes, the experimental data on g-factors are in-complete. Than, one can still use a simplified version of Eqs. (9) and (10):

$$\begin{aligned} g_a &= C^2 g_a^0 + (1 - C^2)\,\bar{g}, \Rightarrow C^2 = \frac{g_a - \bar{g}}{g_a^0 - \bar{g}}, \\ q_a &= C^2 q_a^0 + (1 - C^2)\,\bar{q}. \end{aligned} \tag{11a,b}$$

C^2 here is the weight of the dominant LS-level in the experimental one, and the bar means the averaging over the admixing levels. Of course, there is some arbitrariness in calculation of averages $\bar{g}$ and $\bar{q}$. However, the advantage of Eqs. (11) is that only one experimental g-factor is required.

III. DETAILS OF THE CALCULATION AND RESULTS

As we mentioned above, we performed calculations of energy levels for three values of the parameter x: $x_- = -1/8$, $x_0 = 0$, and $x_+ = 1/8$. All three calculations were done at exactly same level of approximation, to minimize the error caused by the incompleteness of the basis sets and configuration sets. From these calculations we found two approximations for q: $q_- = 8(\omega(x_0) - \omega(x_-))$ and $q_+ = 8(\omega(x_+) - \omega(x_0))$. If there were problems with level identification we performed

additional calculation for x = 0.01, where the LS-coupling should be very accurate and identification is straitforward. The noticeable difference between q_- and q_+ signaled the possibility of the level crossing. In these cases we applied the semiempirical procedure described in Sec. II to find the corrected values for q; otherwise, we simply took the average: $q = (q_+ + q_-)/2$.

A. Zn II

Zn II has the ground state configuration $[1s^2 \ldots 3d^{10}]4s$

and we are interested in the $4s \rightarrow 4p_j$ transitions. As the theory here is much simpler than for other ions, we

TABLE II: Transition frequencies and parameters q for Zn II (in cm^{-1}). Calculations were done in four different ap-proximations: Dirac-Hartree-Fock-Coulomb (DHFC), Dirac-Hartree-Fock-Coulomb-Breit (DHFCB), Brueckner-Coulomb (BC), and Brueckner-Coulomb-Breit (BCB).

Transition	Exper.	DHFC	DHFCB	BC	BCB
		transition frequencies			
$^{4s}1/2 \rightarrow 4p_{1/2}$	48481.077	44610.1	44608.1	48391.2	48389.4
$\rightarrow {}^{4p}3/2$	49355.002	45346.9	45330.0	49263.8	49244.6
		parameters $q = (q_+ + q_-)/2$			
$^{4s}1/2 \rightarrow 4p_{1/2}$		1362	1359	1594	1590
$\rightarrow {}^{4p}3/2$		2129	2109	2500	2479

used Zn II to study the importance of the core-valence correlation correction and Breit correction to the slopes q. The former correction was calculated in Brueckner approximation:

$$\left(H_{\mathrm{DHF}} + \Sigma(E)\right)\Psi = E\Psi, \tag{12}$$

with the self-energy operator Σ(E) calculated in the second order of MBPT (the perturbation here is the difference between the exact and Dirac-Hartree-Fock Hamiltonians, $V = H - H_{DHF}$). The H_{DHF} was calculated with the magnetic part of the Breit operator included self-consistently. The retardation part of the Breit operator is known to be significantly smaller [29] and we completely neglected it here.

B. Si II

Si II has three valence electrons and the ground state configuration $[1s^2 \ldots 2p^6]3s^2 3p$. Excited configurations of interest are $3s3p^2$ and $3s^2 4s$. We made the CI calculation in the Coulomb approximation on the basis set, which included 1s − 8s, 2p − 8p, 3d − 8d, and 4f, 5f orbitals, which we denote as the basis set [8spd5f]. Note, that we use virtual orbitals, which are localized within the atom [34], rather than Dirac-Fock ones. This pro-vides fast convergence. CI included all single-double (SD) and partly triple excitations from three valence configurations listed above. The results of these calculations are given in Table III.

TABLE III: Transition frequencies ω from the ground state $^2P_1{}^o{}_{/2}$, fine structure splitting $_{FS}$, and parameters $q_\pm$ for Si II (in cm^{-1}).

	Experiment [35]		Theory			
	ω	FS	ω	FS	q−	q+
$^2P_3{}^o{}_{/2}$	287	287	293	293	295	291
$^4P_{1/2}$	44080		41643		453	451
$^4P_{3/2}$	44191	111	41754	111	565	564
$^4P_{5/2}$	44364	174	41935	181	746	744
$^2D_{3/2}$	55304		54655		509	507
$^2D_{5/2}$	55320	16	54675	20	530	530
$^2S_{1/2}$	65495		65148		40	39

Like in Zn, the left and write derivatives q_- and q_+ are close to each other, and all levels with equal exact quantum numbers are well separated. The astrophysical data exist for the levels $^2S_{1/2}$ and $^2D_{5/2}$. The former corresponds to the 3p → 4s, while the latter corresponds to the 3s → 3p transition and has much larger positive q.

(H_{DHF} = EΨ, (12)

That is in agreement with the fact that relativistic corrections to the energy usually decrease with the principle quantum number n and with the orbital quantum number l. Therefore, for the ns → np transition one should expect large and positive q, while for np → (n + 1)s, there should be large cancellation of relativistic corrections to upper and to lower levels, resulting in smaller q (see discussion in [25, 26]). The dominant correction to our results should be from the core-valence correlations. In the recent calculations of Mg, which has the same core as Si II, the core-valence corrections to transition frequencies were found to be about 4% [33, 36]. We conservatively estimate corresponding correction to q to be 6% of the larger q, i.e. 30 cm^{-1}

C. Cr II

Cr II has the ground state configuration $[1s^2 \ldots 3p^6]3d^5$ with five valence electrons. The astrophysical data cor-respond to the 3d → 4p transition, for which one may expect negative value of q. CI calculations here are much more complicated, than for Si II. There is strong relaxation of the 3d shell in the discussed transition, which requires more basic d-orbitals. Therefore, we used the [6sp9d6f] basis set. In CI we included only single and double (SD) excitations. Some of the triple, quadruple, and octuple excitations were accounted for by means of the second order perturbation theory. It was found that corresponding corrections to transition frequencies were of the order of few percent, and were even smaller for parameters q. In general, these corrections did not improve the agreement with the experiment, so we present only CI results in Table IV.

As we mentioned above, there is strong relaxation of the 3d-shell in the 3d → 4p transition. We were not able to saturate CI space and completely account for this relaxation. Because of that, we estimate the error for q here to be close to 10%.

TABLE IV: Transition frequencies ω from the ground state $^6S_{5/2}$, fine structure splitting $_{FS}$, and parameters q for Cr II (in cm^{-1}). CI single-double approximation was used for the Coulomb-Breit interaction.

	Experiment		Theory		
	ω	FS	ω	FS	q+
$^6D_{5/2}$	12148		13123		−2314
$^6D_{7/2}$	12304	156	13289	165	−2153
$^6F_1{}^o{}_{/2}$	46824		47163		−1798
$^6F_3{}^o{}_{/2}$	46906	82	47244	81	−1715
$^6F_5{}^o{}_{/2}$	47041	135	47378	134	−1579
$^6F_7{}^o{}_{/2}$	47228	187	47565	187	−1387
$^6F_9{}^o{}_{/2}$	47465	237	47803	238	−1148
$^6F_{11}{}^o{}_{/2}$	47752	287	48091	288	−862
$^6P_1{}^o{}_{/2}$	48399		48684		−1364
$^6P_2{}^o{}_{/2}$	48491	92	48790	106	−1278
$^6P_3{}^o{}_{/2}$	48632	141	48947	157	−1108

We have seen before for Zn II and Si II, that in the absence of level-crossing the difference between q_+ and q_- is smaller than other theoretical uncertainties. In Cr II there are no close levels which may interact with each other, so in the calculation presented in Table IV we determined only the right derivative q_+ . In calculations with different basis sets we checked that the difference between q_+ and q_- is much smaller than the given above theoretical error (see Table I).

D. Fe II

Fe II ion has 7 valence electrons in configuration $3d^6 4s$ and represents the most complicated case. The astrophysical data includes 5 lines in the band 38000 cm^{-1}– 43000 $cm^{-1}$and two lines with the frequency close to 62000 cm^{-1}. The first band consists of three close, but separated multiplets with a regular fine structure split-tings. The 62000 cm^{-1} band is completely different as the multiplets here strongly overlap and fine structure inter-vals are irregular [35]. Characteristic distance between the levels with identical exact quantum numbers is few hundred cm^{-1} , which is comparable to the fine structure splittings. This means that the levels strongly interact and even their identification may be a problem.

In fact, in Moore Tables [1.35] one of the multiplets of interest, namely y $^6P^o$, is erroneously assign to the con-figuration $3d^6(^7S)4p$. It is an obvious misprint, as there is no term ^7S for configuration $3d^6$. This term appears, however, in the configuration $3d^5$ and the correct assign-ment of this multiplet should be $3d^5(^7S)4s4p$. This as-signment is in agreement with our calculations and with the experimental g-factor of the level with J = 7/2. We checked that all close levels of the configuration $3d^6 4p$ have significantly smaller g-factors.

This reassignment has dramatic consequences in terms of the corresponding parameter q as configurations $3d^6 4p$ (4s − 4p transition from the ground state) and $3d^5 4s4p$ (3d − 4p transition) move in the opposite directions from the ground state configuration $3d^6 4s$ when x is changed. It also causes a number of pseudo-crossings to occur right in the vicinity of x = 0 (see Fig. 1).

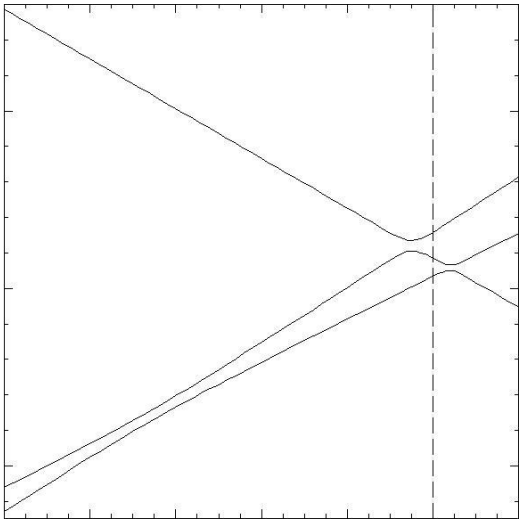

0 0.2 0.4 0.6 0.8 1 1.2

FIG. 1: Examples of typical interaction of levels in the upper band of Fe II. Levels are shown in arbitrary units as function of $(\alpha/\alpha_0)^2 = x + 1$. Levels of configuration $3d^6$ 4p have similar slopes and strongly interact with each other. That causes wide pseudo-crossings, similar to one shown on the left side of the plot. The level $^6P_7{}^o{}_{/2}$ of the configuration $3d^5$ 4s4p moves in the opposite direction. A series of sharp pseudo-crossings takes place near the physical value of α, marked by a vertical dotted line.

CI calculations for Fe II were done on the basis set [6spdf] in the SD approximation (see Table V). Triple excitations were included within second order perturbation theory and corresponding corrections were found to be relatively small. One can see from Table V that for the lower band both frequencies and g-factors are reproduced rather accurately.

The first anomaly takes place at 44000 cm^{-1}, where the levels $^4D_7{}^o{}_{/2}$ and $^4F_7{}^o{}_{/2}$ appear in the reverse order. Theoretical g-factors are also much further from LS values (1.429 and 1.238). That means that theoretical levels are at pseudo-crossing, while experimental levels already passed it. Indeed, calculations for x = 1/8 show that the right order of levels is restored, though the g-factors are still too far from LS values.

The second anomaly corresponds to the band above 60000 cm^{-1}. Here the order of calculated levels differs from that of the experimental ones. Note, that for this band only levels of negative parity with J = 7/2 are given in Table V. Thus, all of them can interact with each other. Let us estimate, how this interaction can affect the slopes q.

TABLE V: Transition frequencies ω from the ground state $^6D_{9/2}$, g-factors, and parameters $q_\pm$ for Fe II (in cm^{-1}).

	Experiment		Theory				
	ω	g	ω	gg(LS)		q_-	q_+
$^6D_9{}^o{}_{/2}$	38459	1.542	38352		1.556	1359	1363
$^6D_7{}^o{}_{/2}$	38660	1.584	38554	1.586	1.587	1522	1510
$^6F_{11}{}^o{}_{/2}$	41968		41864		1.455	1496	1508
$^6F_9{}^o{}_{/2}$	42115	1.43	42012		1.434	1615	1631
$^6F_7{}^o{}_{/2}$	42237	1.399	42141	1.396	1.397	1738	1737
$^6P_7{}^o{}_{/2}$	42658	1.702	42715	1.709	1.714	1241	1261
$^4D_7{}^o{}_{/2}$	44447	1.40	44600	1.345	1.429	1791	1837
$^4F_7{}^o{}_{/2}$	44754	1.29	44386	1.327	1.238	1608	1601
$^8P_7{}^o{}_{/2}$	54490		54914	1.936	1.937	−2084	−2086
$^4G_7{}^o{}_{/2}$	60957	0.969	63624	0.978	0.984	1640	1640
$^4H_7{}^o{}_{/2}$	61157	0.720	63498	0.703	0.667	1296	1247
$^4D_7{}^o{}_{/2}$	61726	1.411	66145	1.398	1.429	1194	1240
$^4F_7{}^o{}_{/2}$	62066	1.198	65528	1.252	1.238	1071	1052
$^6P_7{}^o{}_{/2}$	62172	1.68	65750	1.713	1.714	−1524	−1514
$^2G_7{}^o{}_{/2}$	62323		64798	0.882	0.889	1622	1605

Five levels from this band belong to configuration $3d^64p$ and have close slopes with the average $q^- = 1360\ cm^{-1}$. Only the level $^4F_7{}^o{}_{/2}$ has the slope, which is 300 cm^{-1} smaller, than the average. The remaining level $^6P_7{}^o{}_{/2}$ belongs to configuration $3d^54s4p$ and has the slope of the opposite sign $q_1 = -1519\ cm^{-1}$. Its absolute value is 500 cm^{-1} smaller, than for the level $^8P_7{}^o{}_{/2}$ of the same

configuration $3d^5 4s4p$. That suggests that the levels $^4F_7{}^o{}_{/2}$ and $^6P_7{}^o{}_{/2}$ strongly interact with each other. This is also in agreement with the fact, that these levels are the closest neighbors both experimentally and theoretically and that they cross somewhere between x_- and x. There is also strong interaction be-tween the levels $^2G^o{}_{7/2}$, $^4F_7{}^o{}_{/2}$, and $^4D_7{}^o{}_{/2}$. That can be seen if one calculates the scalar products (overlaps) be-tween corresponding wave functions for different values of x, such as: $hi(x_-)|k(x_+)i$. For weekly interacting levels $hi(x_-)|k(x_0)i \approx hi(x_-)|k(x_+)i \approx \delta_{i,k}$, so large non-diagonal matrix elements signal, that corresponding levels interact.

Interaction of levels $^2G^o{}_{7/2}$, $^4F_7{}^o{}_{/2}$, and $^4D_7{}^o{}_{/2}$ does not affect the slopes q as strongly, as the interaction of $^4F_7{}^o{}_{/2}$ and $^6P_7{}^o{}_{/2}$, so we can account for the former in a less accurate way, but it is important to include the latter as accurately as possible.

The level $^6P_7{}^o{}_{/2}$ interacts with some linear combination of levels $^2G^o{}_{7/2}$, $^4F_7{}^o{}_{/2}$, and $^4D_7{}^o{}_{/2}$. The slopes and g-factors of the latter are relatively close to each other, so we can simply take the average for all three:

$$g^- = 1.185; \quad q^- = 1297. \quad (13)$$

Now we can use experimental g-factor of the state $^6P_7{}^o{}_{/2}$

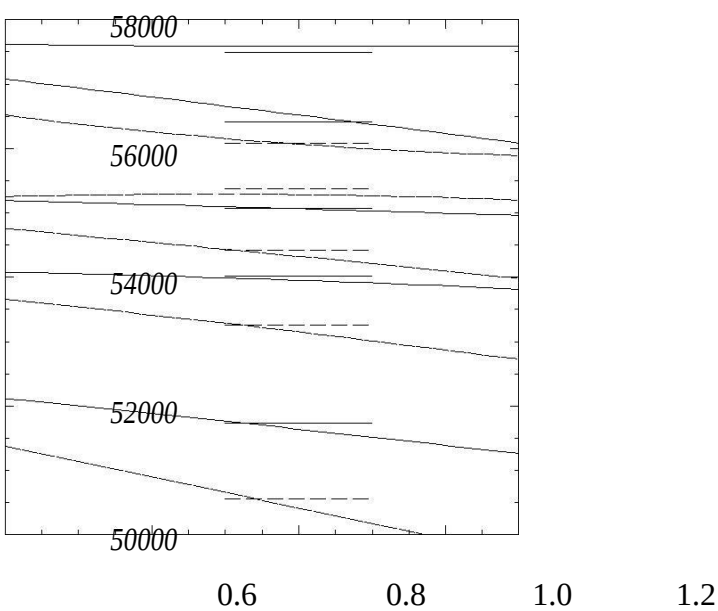

FIG. 2: Dependence of the odd levels of Ni II on $(\alpha/\alpha_0)^2 = x + 1$. Solid lines correspond to J = 5/2 and dashed lines to J = 7/2. The experimental positions of the lines are shown as short

horizontal lines and are all shifted by 1000 cm^{-1} . The order of levels from bottom up: $^4D_7{}^o{}_{/2,5/2}$, $^4G^o{}_{7/2,5/2}$, $^4F_7{}^o{}_{/2,5/2}$, $^2G^o{}_{7/2}$, $^2F_5{}^o{}_{/2}$, $^2D_5{}^o{}_{/2}$, and $^2F_5{}^o{}_{/2}$. and Eq. (11) to determine the mixing:

$$C^2 = \frac{1.68 - \bar{g}}{1.713 - \bar{g}} = 0.937, \tag{14}$$

$$q(^6P^o_{7/2}) = -1342. \tag{15}$$

Eq. (15) corresponds to the correction δq = +177.

Eq. (15) corresponds to the correction _q = +177. Therefore, for the closest level $_4F_{o\ 7/2}$ this model gives an estimate:

$$q(^4F^o_{7/2}) = \bar{q} - \delta q = 1120. \tag{16}$$

Eqs. (15) and (16) show that correction for the mixing is not very large. That corresponds to the fact that experimental g-factor of the level $^6P_7{}^o{}_{/2}$ is significantly larger than any g-factors of the levels of the configuration $3d^64p$. Thus, the interaction for this level is relatively small. On the contrary, the levels of the configuration $3d^64p$ strongly interact with each other, but corresponding changes of the slopes are also relatively small (since the q values for these strongly interacting levels are approximately the same).

We estimate the accuracy of our calculations for the lower band of Fe II to be about 150 cm^{-1}, and approximately 300 cm^{-1} for the values (15) and (16).

E. Ni II

Ni II has the ground state configuration $3d^9$. The spectrum is somewhat simpler, than for Fe II. There are als0 pseudo-crossings here, but they either lie far from x = 0, or are rather wide. That makes their treatment slightly easier. Nevertheless, our results significantly differ from previous calculations [28].

TABLE VI: Transition frequencies ω from the ground state, g-factors, and parameters $q_{\pm}$ for Ni II (in cm^{-1}).

	Experiment		Theory				
	ω	g	ω	gg(LS)		q_-	q_+
$^2D_{3/2}$	1507		1579		0.800	1559	1552
$^4D_7{}^o{}_{/2}$	51558	1.420	50415	1.423	1.429	−2405	−2425
$^4D_5{}^o{}_{/2}$	52739	1.356	51640	1.360	1.371	−1217	−1245
$^4G_7{}^o{}_{/2}$	54263	1.02	53150	1.016	0.984	−1334	−1387
$^4G_5{}^o{}_{/2}$	55019	0.616	53953	0.617	0.571	−370	−418
$^4F_7{}^o{}_{/2}$	55418	1.184	54323	1.183	1.238	−1104	−1124
$^4F_5{}^o{}_{/2}$	56075	0.985	55063	0.986	1.029	−332	−334
$^2G_7{}^o{}_{/2}$	56372	0.940	55284	0.933	0.889	−60	−188
$^2F_7{}^o{}_{/2}$	57080	1.154	56067	1.128	1.143	−911	−713

$^2D_5{}^o{}_{/2}$	57420	1.116	56520	1.108	1.200	−1419	−1438
$^2F_5{}^o{}_{/2}$	58493	0.946	57589	0.959	0.857	−35	−5

CI calculations were done for the Coulomb potential and included SD and partly triple excitations on the basis set [5spdf]. We calculated 5 lower odd levels with
J = 5/2 and 5 with J = 7/2 for x_-, x_0, and x_+ , and used parabolic extrapolation for the interval $-0.4 \le x \le +0.3$ (see Fig. 2). It is seen that the theory accurately repro-duce relative positions of all levels. An overall agreement between the theory and the experiment becomes close to perfect if all experimental levels are shifted by 1000 cm^{-1} down, as it is done in Fig. 2. Note, that this shift constitutes only 2% of the average transition frequency.

Calculated g-factors are generally in agreement with the experiment [1.35] and noticeably different from the pure LS-values (see Table VI). However, for the level $^2F_7{}^o{}_{/2}$ theoretical g-factor is smaller than the LS value, while experimental one is larger. There are no nearby levels who may mix to this one and move g-factor closer to experiment. On the other hand, the difference with experiment is only 2% and may be within experimental accuracy.

Fig. 2 shows that the levels $^2G^o{}_{7/2}$ and $^2F_7{}^o{}_{/2}$ cross at $x \approx 0.3$ and they already strongly interact at x = 0. Theoretical splitting for these levels is 10% larger than experimental one. Thus, they are in fact even closer to the crossing point than is predicted by the theory. The experimental splitting is equal to the theoretical one for larger value of α corresponding to $x \approx 0.15$. At x = 0.15 the slopes of these levels are −265 and −590, and for x = 0 they are −124 and −812 correspondingly. Note, that the sum of the slopes at x = 0.15 differs by 80 cm^{-1} from the sum at x = 0. According to Eq. (7) for a two-level system the sum is constant. This means that these two levels repel from the lower lying level $^4F_7{}^o{}_{/2}$. Taking this analysis into account we suggest an average between x = 0 and x = 0.15 as our final value: $q(^2F_7{}^o{}_{/2}) = -700(250)$.

$$\omega_i = \omega_i^{(0)} + \omega_i^{(2)}\alpha^2 + \ldots \quad (1.1a)$$

$$= \omega_{i,lab} + q_i x + \ldots, x \equiv (\alpha/\alpha_0)^2 - 1, \quad (1.1b)$$

$$\frac{\omega_{fs}}{\omega_k} = \frac{\omega_{fs}^{(2)}}{\omega_{op}^{(0)}}\alpha^2 + O(\alpha^4), \quad (1.2)$$

$$\frac{\omega_i}{\omega_k} = \frac{\omega_i^{(0)}}{\omega_k^{(0)}} + \left(\frac{\omega_i^{(2)} - \omega_k^{(2)}}{\omega_k^{(0)}} \right) \alpha^2 + O(\alpha^2). \qquad (1.3)$$

$$E_{p,n,L,S,J} = E_{p,n,L,S}^{(0)} + \left(\frac{\alpha}{\alpha_0} \right)^2 (C_{p,n,L,S} + \frac{1}{2} A_{p,n,L,J} [J(J+1) - L(L+1) - S(S+1)]), \qquad (1.4)$$

$$E_1 = q_1 (x - x_c), \quad (1.5a)$$

$$E_2 = q_2 (x - x_c). \quad (1.5b)$$

$$E_{a,b} = \frac{1}{2} ((q_1 + q_2)(x - x_c) \pm \sqrt{(q_1 - q_2)^2 (x - x_c)^2 + 4V^2}). \qquad (1.6)$$

$$\frac{\partial E_{a,b}}{\partial x} = \cos^2 \phi q_{1,2} + \sin^2 \phi q_{2,1}. \qquad (1.7)$$

$$| a >= \sum_n C_n | \psi_{L_n, S_n} >, \qquad (1.8)$$

$$q_a = \sum_n C_n^2 q_n. \qquad (1.9)$$

$$g_a = \sum_n C_n^2 g_n. \qquad (1.10)$$

$$g_a = C^2 g_a^0 + (1 - C^2) \bar{g}, \Rightarrow C^2 = \frac{g_a - \bar{g}}{g_a^0 - \bar{g}}, \qquad (1.11a)$$

$$q_a = C^2 q_a^0 + (1 - C^2) \bar{q}. \quad (1.11b)$$

$$(H_{DHF} + \Sigma(E)) \Psi = E \Psi, \qquad (1.12)$$

$$\bar{g} = 1{,}185; \bar{q} = 1297. \qquad (1.13)$$

$$C^2 = \frac{1{,}68 - \bar{g}}{1{,}713 - \bar{g}} = 0{,}937, \quad (1.14)$$

$$q(^6 P_{7/2}^o) = -1342. \qquad (1.15)$$

$$q(^4 F_{7/2}^o) = \bar{q} - \delta q = 1120. \qquad (1.16)$$

Chapter 3

I. CALCULATIONS OF ENERGIES

We use relativistic Hartree-Fock (RHF) and configuration interaction (CI) methods to do the calculations.

RHF Hamiltonian is used to generate a set of single-electron orbitals. We use a form of singe-electron wave function which explicitly depends on the fine structure constant α. Then the RHF equation for $\psi(r)_n$ has the following form (in atomic units)

The value of relativistic effects is studied by varying the value of α in (2). In particular, non-

relativistic limit corresponds to $\alpha = 0$.

In the CI calculations we use approach similar to what was first developed in Ref. [2.12]. Electrons occupying open shells are considered as valence electrons and all other are core electrons. Correlations between valence electrons are treated within the CI method while correlations between valence and core electrons are included by means of the many-body perturbation theory.

It describes correlations between a particular valence electron and core electrons (see Ref. [2.12] for details). Note that in contrast with Ref. [2.12] we don't include in present work the Σ_2 operator, which is a two-electron operator describing different type of correlations between valence and core electrons. Terms with Σ_2 can be considered as screening of Coulomb interaction between valence electrons by core electrons. These terms are less important than those with Σ, but much more time consuming in calculations. We either neglect them or simulate their effect by introducing screening factors.

We are now going to discuss the specifics of the calculations for each atom/ion. Apart from the states of interest we also calculate energies of the other states of the same con-figurations to ensure that the accuracy is systematically good. We also calculate magnetic g-factors to ensure correct identification of states. This is particularly important for dysprosium.

A. Strontium

Strontium in its ground state is a closed-shell atom. It has two 5s-electrons on its outermost shell and we need to consider energy intervals between $^1S_0$ ground state and states of the 5s5p configuration where the $^3P_1$ metastable state is of most interest. The RHF calculations for Sr were done in V^N approximation, for a closed-shell atom in its ground state. For the CI calculations we considered Sr as an atom with two valence electrons and followed the similar calculations for Ba [2.13]. Basis states for the CI+MBPT method were calculated using the B-spline technique [2.14] with 40 B-splines in a cavity of radius $R = 40a_B$.

The same basis functions were used to calculate $\hat{\Sigma}_1$ and for the CI calculations. Thirteen lowest states above core in each of the $s_{1/2}$, $p_{1/2}$, $p_{3/2}$, $d_{3/2}$ and $d_{5/2}$ waves were used to construct two-electron wave function for both $5s^2$ and 5s5p configurations. Large number of basis functions is needed mostly for adequate description of the 5s5p configuration. This is because the V^N approximation doesn't provide us with a good 5p single-electron state. Also, the 5s single-electron state in the 5s5p configuration is different from the 5s state in the $5s^2$ configuration for which Hartree-Fock calculations were done. However, with thirteen states in each wave the saturation of the basis was clearly achieved and adding more states to the basis didn't change the energy. Two-electron basis states for the CI calculations were obtained by distributing valence electrons over 65 basis states (13 × 5) in all possible ways with a restriction of fixed parity and total momentum.

The results are presented in Table I. As one can see the accuracy for the state of the interest $^3P_1$ is better than 1% while accuracy for other states is also good.

B. Ytterbium

The ground state of ytterbium positive ion is $4f^{14}6s\ ^2S_{1/2}$ and we need to consider transitions into the $4f^{14}5d\ ^2D_{5/2}$ and $4f^{13}6s^2\ ^2F_{7/2}$ states. Therefore it is convenient to do the RHF calculations in the V^{N-1} approximation, for the Yb^{2+} ion with the $4f^{14}$ closed-shell configuration. The 6s, 5d and other basis states for the CI method are calculated then in the field of frozen closed-shell core of Yb^{2+}. Then, in the CI calculations, we need to consider all 4f electrons as valence ones since one of the transitions of the interest involves excitation from the 4f subshell. So, the total number of valence electrons in present CI calculations is fifteen. This is very different from our previous calculations for Yb^+ [5] in which the $4f^{13}6s^2\ ^2F_{7/2}$ state was not considered and we were able to treat ytterbium ion as a system with one external electron above closed shells.

Our final set of single-electron states for the CI calculations consisted of $4f_{5/2}$, $4f_{7/2}$, $6s_{1/2}$, $5d_{3/2}$, $5d_{5/2}$ and few more s and f states above 4f and 6s. Note that in contrast with Sr we don't need many basis functions here because all our single-electron wave functions correspond to the Yb^+. This makes initial approximation to be very good and leads to fast convergence of the CI calculations with respect to the basis set used.

We also don't include $\hat{\Sigma}_1$ in calculations for Yb^+. In a case of many valence electrons (fifteen for Yb^+) correlations are dominated by correlations between them which are taken into account accurately via the CI technique. Correlations between valence electrons and core electrons mostly manifest themselves via screening of the Coulomb interaction between valence electrons. We take this effect into account semi-empirically, by introducing screening factors f_k. Namely, we multiply every Coulomb integral of the multi-polarity k by a numerical factor f_k which is chosen to fit the energies. It turns out that good fit for Yb^+ is achieved with $f_2 = 0.8$ and $f_k = 1$ for all other k.

Many-electron basis states for the CI calculations were obtained by allowing all possible single and double excitations from the base configuration with the restriction of fixed parity and total momentum.

Results for energies of Yb^+ are presented in Table I. The theoretical accuracy for energies as

compared to the experiment is 2- 3% for the states of interest and is not worse than 5% for other states.

C. Dysprosium

Dysprosium atom is the most difficult for calculations because of its complicated electron structure. Ground state configuration of Dy is 4f ^{10}6s^2 which means that there is no realistic RHF approximation which corresponds to a closed-shell system. We do the RHF calculations for Dy in the V ^{N} approximation with an open-shell version of the RHF method. Contribution of the 4f electrons into the RHF potential is calculated as for a closed shell and then multiplied by a numerical factor to take into account its fractional occupancy. This factor is 10/14 when interaction of the 4f electrons with other core electrons is considered and 9/13 when interaction of a 4f electron with other 4f electrons is considered. When convergence is achieved we have the 4f and 6s basis states for the CI calculations. To calculate other states of valence electrons we remove one 6s electron, freeze all RHF orbitals, including 4f and 6s and calculate the $6p_{1/2}$, $6p_{3/2}$, $5d_{3/2}$, $5d_{5/2}$ and few more d-states above 5d in the field of frozen RHF core.

In the CI calculations states below 4f are considered as core states and all other as valence states. Total number of valence electrons is therefore twelve. As for the case of Yb we neglect $\hat{\Sigma}_1$ and use screening factors as fitting parameters to improve agreement with experiment. It turns out that best fit for the 4f ^{10}6s6p configuration is achieved with $f_1 = 0.7$ and $f_k = 1$ for all other k. No fitting was used for other configurations.

To calculate states of the 4f ^{10}6s^2, 4f ^{10}6s6p and 4f ^{10}6s5d configurations we use the $4f_{5/2}$, $4f_{7/2}$, $6s_{1/2}$, $6p_{1/2}$, $6p_{3/2}$, $5d_{3/2}$ and $5d_{5/2}$ single-electron basis functions and all possible configurations which can be obtained from these basis functions by exciting of one or two electrons from the base configuration. Same approach doesn't work for the 4f ^{9}5d^{2}6s configuration because of huge number of many-electron basis states generated this way and as a consequence, the CI matrix is of so large size that it could not be handled by our computers. On the other hand test calculations with pairs of configurations showed that mixing of our state of interest with other configurations is small and can be neglected. We do need however to include mixing with the 4f ^{9}5d6d6s, 4f ^{9}5d7d6s and 4f ^{9}6d^{2}6s configurations. This is because our basis 5d state corresponds rather to the 4f ^{10}5d6s configuration and extra d-states are needed to correct it.

The result are presented in Table I. Note that they are considerably better than in our previous calculations [2.15]. This is because of better basis and more complete CI treatment.

III. FREQUENCY SHIFT: RESULTS AND DISCUSSIONS

In the vicinity of the physical value of the fine structure constant ($\alpha = \alpha_0$) frequency (ω) of an atomic transition can be presented in a form

$$\omega = \omega_0 + qx, \qquad (5)$$

where $x = (\alpha^2/\alpha_0^2) - 1$, ω_0 is the experimental value of the frequency and q is a coefficient which determines the frequency dependence on the variation of α.

The results for coefficients q are presented in Table II. Note that we have included in the Table the results of our old calculations for Yb^+ . These calculations were done in a very different way, assuming that Yb^+ is an atom with one external electron above closed shells. Comparison of the results obtained by different methods gives estimate of the accuracy of calculations.

Search for the time variation of the fine structure constant can be conducted by comparing two frequencies of atomic transitions over long period of time.

Current best laboratory limit on the time variation of α is $\alpha/\dot{\alpha} < 10^{-15}yr^{-1}$ [4].

In the first experiment considered in this paper a dual calcium-strontium beam is to be used to compare the frequencies of the $^1S_0 -^3 P_1$ transitions in both atoms. Substituting $\omega_1 = 15210cm^{-1}$, $q_1 = 230cm^{-1}$ for Ca [5], $\omega_2 = 14504cm^{-1}$, $q_2 = 667cm^{-1}$ for Sr (Tables I,II) and $\alpha/\dot{\alpha} = 10^{-15}yr^{-1}$ we get are to be compared.

$$\Delta(t)(Yb^+) = 6.1 \times 10^{-15}yr^{-1}.$$

Note that the width of $^3P_1$ state in Sr may be a problem in this case. In the case of Yb frequencies of the $^2S_{1/2} -^2 D_{5/2}$ and $^2S_{1/2} -^2 F_{7/2}$ Substituting the numbers we get (9)

Note two orders of magnitude improvement in the magnitude in comparison with the Sr-Ca dual beam experiment.

We have also calculated q-coefficient for $4f^{14}\,{}^1S_0$ - $4f^{13}5d\,{}^3P_0$ (ω = 45276 cm^{-1}) transition from YbIII ground state. This was motivated by the proposed measurements [9] of α-variation using comparison of ${}^1S_0$ - ${}^3P_0$ transition frequencies in In^+, Tl^+ and odd isotope of Yb^{++}. The different signs and magnitudes of relativistic corrections in In^+ (q= 4414 cm^{-1}), Tl^+ (q=19745 cm^{-1}) and Yb^{++} (q= -27800 cm^{-1}) provide an excellent control of systematic errors since systematic errors are not correlated with signs and magnitudes of the frequency shifts qx, where $x = (\alpha^2/\alpha_0^2) - 1$. The same idea (combination of anchors, positive shifters and negative shifters) has been used to control systematic errors in Ref. [2.2].

In our view, a very interesting possibility is that for dysprosium. Instead of comparing frequencies of different transitions one should measure the energy difference between two very close states of opposite parity. The corresponding q-coefficient is q = 6008 + 23708 = 29716cm^{-1} (see Table II). The frequency of this transition ranges from few MHz to few GHz depending on isotopes and hfs components used. If we take, e.g. ω = 3.1MHz [2.10] we get

$$\Delta(t)(Dy) = 5.7 \times 10^8 \left(\frac{\alpha^{\cdot}}{\alpha_0}\right). \qquad (11)$$

This is an eight orders of magnitude enhancement in the relative value of the effect compared to atomic clock transitions! Substituting $\alpha/\alpha^{\cdot} = 10^{-15} yr^{-1}$ we get

$$\Delta(t)(Dy) = 5.7 \times 10^{-7} yr^{-1}. \qquad (12)$$

This means that to improve current best limit on local time variation of α the frequency of this transition in Dy should be measured to the accuracy of about 10^{-7} over about a year time interval. This seems to be feasible [2.7].

$$\psi(r)_{njlm} = \frac{1}{r}\begin{pmatrix} f_n(r)\Omega(n)_{jlm} \\ i\alpha g_n(r)\tilde{\Omega}(n)_{jlm} \end{pmatrix}. \quad (2.1)$$

$$f_n^{'}(r) + \frac{\kappa_n}{r} f_n(r) - [2 + \alpha^2(\varepsilon_n - \hat{V}_{HF})]g_n(r) = 0,$$

$$g_n^{'}(r) - \frac{\kappa_n}{r} g_n(r) + (\varepsilon_n - \hat{V}_{HF}) f_n(r) = 0, \quad (2.2)$$

$$\hat{H}^{CI} = \sum_{j=1}^{N} \hat{h}_i + \sum_{i<j} \frac{e^2}{r_{ij}}. \quad (2.3)$$

$$\hat{h}_i = c\alpha p + (\beta - 1)mc^2 - \frac{Ze^2}{r_i} + \hat{V}_{core} + \hat{\Sigma}_1. \quad (2.4)$$

$$\omega = \omega_0 + qx, \quad (2.5)$$

$$x = (\alpha^2 / \alpha_0^2) - 1,$$

$$q = 4(\omega_+ - \omega_-), \quad (2.6)$$

$$\Delta(t) = \left(\frac{\dot{\omega}_1}{\omega_1} - \frac{\dot{\omega}_2}{\omega_2}\right). \quad (2.7)$$

$$\Delta(t) = \left(\frac{2q_1}{\omega_1} - \frac{2q_2}{\omega_2}\right)\left(\frac{\dot{\alpha}}{\alpha_0}\right). \quad (2.8)$$

Chapter 4

The possibility that the fundamental constants vary is suggested by theories unifying gravity with other interactions (see, e.g. [3.1, 2, 3] and review [3.4]). The analysis of quasar absorption spectra by means of the many-multiplet method reveals anomalies which can be interpreted in terms of varying fine structure constant α [3.5, 6, 7]. The first indication that α might have been smaller at early epoch came from the analysis of magnesium and iron lines [3.5, 6]. Later inclusion of other lines belonging to many different atoms and ions (Si, Cr, Ni, Zn, etc.) as well as many samples of data from differ-ent gas clouds not only confirmed the initial claim, but made it even stronger [3.7]. However, there are some recent works in which a similar analysis indicates no variation of α in quasar absorption spectra [3.8, 9]. These works use the same many-multiplet method and the results of our calculations of the relativistic effects in atoms, but analyze different samples of data from a different telescope. It is important to include as much data as possible into the analysis to resolve the differences, and to verify or discard the claim of a varying fine structure constant.

It is natural to analyze fine structure intervals in the search of variation of α. Indeed, initial searches of variation of α in quasar absorption spectra were based on alkali-doublet lines (alkali-doublet method) [3.10, 11, 12] and on the fine structure of O III [3.13]. However, all of the present evidence for varying fine structure constant has come from the analysis of the E1-transition frequencies (many-multiplet method) rather than fine structure intervals. These frequencies are about an order of magnitude more sensitive to the variation of α [3.6]. However, the corresponding analysis is much more complicated. One needs to perform accurate ab initio calculations of the atomic structure to reveal the dependence of transition frequencies on the fine structure constant. We have done such calculations for many atoms and ions in our previous works [3.14, 15]. In the present work we do similar calculations for some other atoms and ions for which data on quasar absorption spectra are available [3.16], and for which corresponding calculations have not previously been done.

We use the relativistic Hartree-Fock (RHF) method as a starting point of our calculations. Correlations are included by means of configuration-interaction (CI) method for many valence electron atoms, or by the many-body perturbation theory (MBPT) and Brueckner-orbital method for single valence electron atoms. The dependence of the frequencies on α is revealed by varying in computer codes.

The results are presented in the form

$$\omega = \omega_0 + qx, \qquad (1)$$

where $x = (\alpha^2/\alpha^2_0) - 1$, α_0 is the laboratory value of the fine structure constant, ω and ω_0 are the frequencies of the transition in quasar absorption spectra and in the laboratory, respectively, and q is the relativistic energy shift that comes from the calculations. Comparing the laboratory frequencies, ω_0, with those measured in the quasar absorption spectra, ω, allows one to obtain the value of α billions of years ago.

The method of calculations is described in detail in our early works [3.14, 15]. Here we only discuss the details specific for current calculations.

Some atoms and ions considered in the present work represent open-shell (many valence electron) systems. Therefore, the Hartree-Fock procedure needs to be further specified. The natural choice is to remove all open-shell electrons and start the Hartree-Fock calculations for the closed-shell core. However, this usually leads to poor convergence of the subsequent CI method. Better convergence can be achieved using the so called V^{N-1} approximation in which only one valence electron is removed. Since we calculate not only the ground state but also ex-cited states of different configurations, it is convenient to remove the electron which changes its state in the transition. Single-electron basis states for valence electrons are calculated in the V^{N-1} potential of the frozen-core.

The V^{N-1} potential corresponds to an open-shell sys-tem. We include the contribution of the open shells into the Hartree-Fock potential as if they were totally filled and then multiply them by a weighting coefficient. Note that this procedure must not destroy the cancellation of the self-action (we would like to remind the reader that there is exact cancellation between direct and exchange

self-action in the Hartree-Fock equations for the closed-shell systems).

For the CI calculations we use B-splined single-electron basis set similar to those developed by Johnson et al [3.17, 18, 19]. The main difference is that we use the open-shell RHF Hamiltonian described above to calculate the B-splined states.

There are two major sources of inaccuracy in the stan-dard CI calculations. One is incompleteness of the basis set and another is core-valence correlations. We use a fitting procedure to model both effects. We add an extra term into a single-electron part of the Hamiltonian for the valence electrons:

$$U(r) = -\frac{\alpha_c}{2(r^4 + a^4)}. \qquad (3.2)$$

Here α_c is the polarizability of the atomic core and a is a cut-off parameter that is introduced to remove the singularity at r = 0. We use $a = a_b$ (Bohr radius) and treat α_c as a fitting parameter. The values of α_c for each partial wave (s, p, d) are chosen to fit the experimental energy levels of the many-electron atom.

The term (3.2) describes polarization of the atomic core by valence electrons. It can be considered as a semi-empirical approximation to the correlation interaction of a particular valence electron with the core. It also allows us to improve the convergence of the CI calculations by modifying the single-electron basis states. Our calculations for rare-earth ions [3.20, 21] have demonstrated that using this term allows one to obtain good accuracy of calculations with the minimum number of single-electron basis states (one in each partial wave in the cited works).

Below we present the details and results of calculations for the atoms and ions considered. All transition frequencies are presented with respect to the ground state. Therefore we use the term “energy levels” instead. If a transition between excited states is needed, the corresponding relativistic energy shift q is the difference be-tween the level shifts ($q_{2\to1} = q_2 - q_1$).

a. Manganese (Z = 25): The ground state of Mn^+ is $3d^5 4s\ ^7S_3$ and we need to consider transitions into the $3d^4 4s4p$ configuration. Earlier we also considered transitions to the states of the $3d^5 4p$ configuration [3.14]. Since in the present work we use different basis set, we have repeated calculations for this configuration in order to check their accuracy.

The RHF calculations are done in the V^{N-1} approximation with the $3d^5$ configuration of external electrons. The 4s, 4p and higher states are calculated in the same V^{N-1} potential. We use $\alpha_c = 2.05a^3_B$ for the p-wave as a fitting parameter (see formula (3.2)). The results are presented in Table I. Fitting changes both energies and q-coefficients by less than 10%, and agreement with previous calculations is also within 10%. Therefore, we use 10% as a conservative estimate of the accuracy of q.

Note that the relativistic shift is positive for the s − p singe-electron transitions and negative for the d −p transitions. Having transitions with different signs of q- coefficients in the same atom (ion) helps to fight systematic errors in the search for variation of α (see Ref. [3.14] for details).

b. Titanium (Z = 22): We perform calculations for both Ti^+ and Ti^{2+} starting from the same RHF approximation, and using the same single-electron basis set. The ground state of Ti^+ is $3d^2 4s\ ^4F_{3/2}$ and we need to consider transitions into states of the $3d^2 4p$ configuration. The ground state of Ti^{2+} is $3d^2\ ^3F_2$ and we need to con-sider transitions into the states of the 3d4p configuration. Therefore it is convenient to do the RHF calculations for the Ti^{2+} ion with the $3d^2$ open-shell configuration. The 4s, 4p and other basis states for the CI method are calculated in the frozen-core field of Ti^{2+}.

The fitting parameters chosen are $\alpha_c = 0.38a^3_B$ for s-electrons and $\alpha_c = 0.065a^3_B$ for d-electrons. The results are presented in Table II. As in the case of Mn^+, there are negative and positive relativistic shifts. The effects of fitting and change of basis set does not exceed 10%. The values of the q-coefficients for titanium are consistent with calculations for other atoms and with semi-empirical estimations using the formulas presented in [3.14]. In particular, the values of the negative q-coefficients for the d − p transitions are very close to the values for similar transitions in Cr II [3.14]. The positive coefficients for Ti^+ are very close to those for Mn^+ after rescaling by Z^2 according to the semi-empirical formula [3.14].

TABLE 1: Energies and relativistic energy shifts (q) for Mn^+ (cm^{-1})

State	Energy			q	
	theory		experiment		
	no fitting	fitted	[22]	this work	[15]
$3d^5\ 4p\ \ ^7P_2$	36091	38424	38366	869	918
$3d^5\ 4p\ \ ^7P_3$	36252	38585	38543	1030	1110
$3d^5\ 4p\ \ ^7P_4$	36483	38814	38807	1276	1366
$3d^4\ 4s4p\ \ ^7P_2$	97323	83363	83255	-3033	
$3d^4\ 4s4p\ \ ^7P_3$	97554	83559	83376	-2825	
$3d^4\ 4s4p\ \ ^7P_4$	97858	83818	83529	-2556	

TABLE 11: *Energies and relativistic energy shifts (q) for* Ti^{+} *and* Ti^{2+} (cm^{-1})

State		Energy			q
		theory		*experiment*	
		no fitting	*fitted*	[22]	
		Ti^{+}			
$3d^2\ 4p$	$^4G_{5/2}$	27870	29759	29544	396
$3d^2\ 4p$	$^4F_{3/2}$	28845	30691	30837	541
$3d^2\ 4p$	$^4F_{5/2}$	28965	30813	30959	673
$3d^2\ 4p$	$^4D_{1/2}$	30582	32416	32532	677
$3d^2\ 4p$	$^4D_{3/2}$	30670	32510	32603	791
$3d4s4p$	$^4D_{1/2}$	50651	52185	52330	-1564
		Ti^{2+}			

3d4p	$^3D_1$	80558	77000	-1644

TABLE III: Energies and relativistic energy shifts (q) for Na (cm^{-1})

State		Energy		q
		theory	experiment [22]	
3p	$^2P_{1/2}$	16858	16956	45
3p	$^2P_{3/2}$	16876	16973	63
4p	$^2P_{1/2}$	30124	30267	53
4p	$^2P_{3/2}$	30130	30273	59

TABLE IV: Energies and relativistic energy shifts (q) for the carbon atom and its ions (cm^{-1})

State		Energy theory	Energy experiment [3.22]	q
		C		
$2s2p^3$	$^3D_3$	66722	64087	151
$2s2p^3$	$^3D_1$	66712	64090	141
$2s2p^3$	$^3D_2$	66716	64091	145
$2s2p^3$	$^3P_1$	75978	75254	111
$2s2p^3$	$^3S_1$	100170	105799	130
		C^+		
$2s^22p$	$^2P_{1/2}$	74	63	63
$2s2p^2$	$^2D_{5/2}$	76506	74930	179
$2s2p^2$	$^2D_{3/2}$	76503	74933	176
$2s2p^2$	$^2S_{1/2}$	97993	96494	161
		$_C2+$		
2s2p	$^1P_1$	104423	102352	162
		$_C3+$		
2p	$^2P_{1/2}$	65200	64484	104
2p	$^2P_{3/2}$	65328	64592	232

c. Sodium (Z = 11): In contrast to the ions considered above, sodium is an atom with one external

electron above closed shells. Its ground state is $1s^2 2s\ ^2 2p^6 3s\ ^2S_{1/2}$. Very accurate calculations are possible for such systems by including certain types of correlation diagrams to all orders (see, e.g. [3.23, 24]). However, since both relativistic and correlation effects for sodium are small we use a simplified approach. We calculate the correlation potential $\hat{\Sigma}$ (the average value of this operator is the correlation correction to the energy of the external electron) in the second order only. Then we use it to modify the RHF equations for the valence electron and to calculate the so called Brueckner-orbitals. Note that due to iterations of $\hat{\Sigma}$ certain types of correlation diagrams are still included in all orders in this procedure. The final accuracy of the energy is better than 1%, and for the fine structure accuracy is 2-6% (see Table III). We believe that the accuracy for the relativistic shifts q is on the same level.

d. Carbon (Z = 6): Relativistic effects for carbon and its ions are small and calculations can be done with-out fitting parameters. The ground state of neutral car-bon is $1s^2 2s^2 2p^2\ ^3P_0$. Our RHF calculations for this atom include all electrons, however, since we need to con-sider configurations with excitations from both 2s and 2p states, we treat both as valence states in CI.

TABLE V: Energies and relativistic energy shifts (q) for oxy-gen ions (cm^{-1})

State		Energy theory	Energy experiment [3.22]	q
		O^+		
$2s2p^4$	$^4P_{5/2}$	122620	119873	346
$2s2p^4$	$^4P_{3/2}$	122763	120000	489

$2s2p^4$	$^4P_{1/2}$	122848 $_{O}2+$	120083	574
$2s2p^3$	$^3D_1$	121299	120058	723
$2s2p^3$	$^3P_1$	143483 $_{O}3+$	142382	726
$2s2p^2$	$^2D_{3/2}$	129206 $_{O}5+$	126950	840
$1s^2 2p$	$^2P_{1/2}$	97313	96375	340
$1s^2 2p$	$^2P_{3/2}$	97913	96908	872

For neutral carbon we have performed the calculations for the ground state configuration as well as for excited configurations $2s^22p3s$, $2s2p^3$, $2s^22p4s$,$2s^22p3d$, $2s^22p4d$, $2s^22p5d$ and $2s^22p6d$. However, we present in Table IV only results for the $2s2p^3$ configuration. The relativistic energy shift for all other configurations is small ($q < 50$ cm^{-1}). This is smaller than uncertainty of the q-coefficients for heavier atoms and ions. Since the analysis of quasar spectra is based on comparison of the relativistic effects in light and heavy atoms (ions), small relativistic energy shifts in light atoms can be neglected. The q-coefficients for the $2s2p^3$ configuration are larger because this configuration corresponds to the $2s - 2p$ transition from the ground state. These are the lowest valence single-electron states with the largest relativistic effects. Other excited configurations correspond to the $2p - ns$ or $2p - nd$ ($n \geq 3$) transitions. However, relativistic energy shifts for higher states are smaller [3.14].

The calculations for C^{2+} and C^{3+} are done in the potential of the closed-shell (helium) core. As can be seen from Table IV, accuracy for the energies is within 10%. We estimate the accuracy of q-coefficients at around 10-20%.

e. Oxygen (Z = 8): Relativistic effects for oxygen ions are comparatively large, and become larger with in-creasing electric charge. This is in agreement with semi-empirical formulae presented in [3.14]. For neutral oxygen, however, q-coefficients are approximately 20 cm^{-1} or less; these results are not presented here.

$$\omega = \omega_0 + qx, \quad (3.1)$$

$$x = (\alpha^2 / \alpha_0^2) - 1,$$

$$U(r) = -\frac{\alpha_c}{2(r^4 + a^4)}. \quad (3.2)$$

Chapter 5

TABLE I: High-priority lines observed in QSO spectra. The first column is the ion; the second and third columns are the rest wavelength and the transition frequency, respectively; the fourth column is the oscillator strength; the relativistic shift (q value) is shown in the fifth column, where known. Those transitions for which high-accuracy laboratory data are needed are marked with either ‘A’ (very important) or ‘B’ (mildly important). Lines for which there is no measured isotopic structure are marked ‘I’. Additionally, there are some lines for which both the transition frequency and isotope shift are known; these are marked with an ‘M’. They are included here for reference only (of course, verification would still be useful). References for precisely measured lines are given in the last column. The second set of references are for isotope shift measurements, where available. The wavelengths and oscillator strengths are taken from the compilation by Morton [4.12, 13].

Atom/ Ion	Wavelength λ (Å)	Frequency ω_0 (cm^{-1})	Oscillator Strength	q value (cm^{-1})			Refs.
C I	945.188	105799.1	0.272600	130	(60)	M	[20]
	1139.793	87735.30	0.013960	0	(100)	B	
	1155.809	86519.47	0.017250	”		B	
	1157.186	86416.55	0.549500	”		B	
	1157.910	86362.52	0.021780	”		B	
	1188.833	84116.09	0.016760	”		B	
	1193.031	83820.13	0.044470	”		B	
	1193.996	83752.41	0.009407	”		B	
	1260.736	79318.78	0.039370	30	(10)	A	
	1276.483	78340.28	0.004502	17	(10)	A	
	1277.245	78293.49	0.096650	−13	(10)	A	
	1280.135	78116.74	0.024320	−21	(10)	A	
	1328.833	75253.97	0.058040	117	(10)	A	
	1560.309	64089.85	0.080410	137	(10)	A	
	1656.928	60352.63	0.140500	−24	(10)	A	
C II	1037.018	96430.32	0.123000	168	(10)	A	
	1335.662	74869.20	0.012770	178	(10)	A	
	1335.707	74866.68	0.114900	181	(10)	A	
C III	977.020	102352.0	0.762000	165	(10)	B	
C IV	1548.204	64590.99	0.190800	232	(20)	A	[4.21]
	1550.781	64483.65	0.095220	104 (20)		A	[4.21]
O I	1025.762	97488.54	0.020300	0 (20)		B	
	1026.476	97420.72	0.002460	”		B	
	1039.230	96225.05	0.009197	”		B	
	1302.168	76794.98	0.048870	”		A	

TABLE I: (continued)

Atom/ Ion	Wavelength λ (Å)	Frequency ω_0 (cm^{-1})	Oscillator Strength	q value (cm^{-1})			Refs.
Na I	3303.320	30272.58	0.013400	59	(4)	B	
	3303.930	30266.99	0.006700	53	(4)	B	
	5891.583	16973.37	0.655000	63	(4)	M	[22][23, 24]
	5897.558	16956.17	0.327000	45	(4)	M	[4.22][25]
Mg I	2026.477	49346.73	0.112000	87		I	[4.26]
	2852.963	35051.27	0.181000	86	(10)	M	[26, 27][28, 29]
Mg II	1239.925	80650.04	0.000267			B	
	2796.354	35760.85	0.612300	211	(10)	M	[26, 27][30]
	2803.532	35669.30	0.305400	120	(10)	I	[4.26, 27]
Al II	1670.789	59851.97	1.880000	270	(30)	M	[4.21]
Al III	1854.718	53916.54	0.539000	464	(30)	M	[4.21]
	1862.791	53682.88	0.268000	464	(30)	M	[4.21]
Si II	1190.416	84004.26	0.250200			B	
	1193.290	83801.95	0.499100			B	
	1260.422	79338.50	1.007000			A	
	1304.370	76665.35	0.094000			A	
	1526.707	65500.45	0.117094	50	(30)	I	[4.21]
	1808.013	55309.34	0.002010	520	(30)	I	[4.21]
Si IV	1393.760	71748.64	0.528000	862		A	[4.21]
	1402.773	71287.54	0.262000	346		A	[4.21]
S II	1250.583	79962.61	0.005350			A	
	1253.808	79756.83	0.010700			A	
	1259.518	79395.39	0.015900			A	
Ca II	3934.775	25414.41	0.688000	452		A	[4.13]
	3969.590	25191.52	0.341000	224		A	[4.13]

Ti II	1910.600	52339.58	0.202000	−1564	(150)	A	
	1910.938	52330.32	0.098000	−1783	(300)	A	
	3067.245	32602.55	0.041500	791	(50)	I	[4.26]
	3073.877	32532.21	0.104000	677	(50)	I	[4.26]
	3230.131	30958.50	0.057300	673	(50)	I	[4.26]
	3242.929	30836.32	0.183000	541	(50)	I	[4.26]
	3384.740	29544.37	0.282000	396	(50)	I	[4.26]
Cr II	2056.256	48632.06	0.105000	−1110	(150)	I	[4.26, 31]
	2062.236	48491.05	0.078000	−1280	(150)	I	[4.26, 31]
	2066.164	48398.87	0.051500	−1360	(150)	I	[4.26, 31]
Mn II	1197.184	83529.35	0.156600	−2556	(450)	B	
	1199.391	83375.65	0.105900	−2825	(450)	B	
	1201.118	83255.77	0.088090	−3033	(450)	B	
	2576.877	38806.66	0.288000	1420	(150)	I	[4.26]
	2594.499	38543.08	0.223000	1148	(150)	I	[4.26]
	2606.462	38366.18	0.158000	986	(150)	I	[4.26]

TABLE I: (continued)

Atom/ Ion	Wavelength λ (Å)	Frequency ω_0 (cm^{-1})	Oscillator Strength	q value (cm^{-1})		Refs.
Fe II	1063.176	94057.80	0.060000		B	
	1063.971	93987.52	0.003718		B	
	1096.877	91167.92	0.032400		B	
	1121.975	89128.55	0.020200		B	
	1125.448	88853.51	0.016000		B	
	1143.226	87471.77	0.017700		B	
	1144.939	87340.98	0.106000		B	
	1260.533	79331.52	0.025000		A	
	1608.450	62171.63	0.058000	−1300 (300)	A	[4.32]
	1611.200	62065.53	0.001360	1100 (300)	A	[4.32]
	2249.877	44446.88	0.001821		A	
	2260.780	44232.51	0.002440		I	[4.26]
	2344.212	42658.24	0.114000	1210 (150)	I	[4.26, 33]
	2367.589	42237.06	0.000212	1904	A	
	2374.460	42114.83	0.031300	1590 (150)	I	[4.26, 33]
	2382.764	41968.06	0.320000	1460 (150)	I	[4.26, 33]
	2586.649	38660.05	0.069180	1490 (150)	I	[4.26, 33]
	2600.172	38458.99	0.238780	1330 (150)	I	[4.26, 33]
Ni II	1317.217	75917.64	0.146000		A	
	1370.132	72985.67	0.076900		A	
	1393.324	71770.82	0.022220		A	
	1454.842	68735.99	0.032300		A	
	1467.259	68154.29	0.009900		A	
	1467.756	68131.22	0.006300		A	
	1502.148	66571.34	0.006000		A	

	1703.412	58705.71	0.012240			A	[4.31]
	1709.604	58493.07	0.032400	−20	(250)	A	[4.31]
	1741.553	57420.01	0.042700	−1400	(250)	A	[4.31]
	1751.915	57080.37	0.027700	−700	(250)	A	[4.31]
Zn II	2026.137	49355.00	0.489000	2479	(25)	M	[4.26, 31][34]
	2062.660	48481.08	0.256000	1584	(25)	I	[4.26, 31]

Chapter 6

Field shift

5.1 Method

To calculate the field shift (also called the volume shift), we add a finite perturbation due to the field shift to the nuclear potential, and then calculate the energy spectrum directly. The field shift potential is

$$U(r) = U(R + \;\; R; r) \quad U(R; r) \tag{5.1}$$

where R is the nuclear radius and U (R; r) is the nuclear potential. In our codes we use a Fermi distribution for the nuclear charge density (see Fig. 5.1).

To obtain the change in energy of a state due to the field shift, we add the potential

U (r) to the nuclear potential in our Hartree-Fock calculations. By introducing a scaling factor we can increase the size of the effect and take the limit as **!** 0. To calculate the field-shift constant, we take the gradient of a level energy E vs. graph and extract F as

$$F = \frac{E}{\mathbf{h}r^2\mathbf{i}} = \frac{5}{3}\frac{1}{2R\;R}\lim_{!0}\frac{dE}{d} \;: \tag{5.2}$$

where $\mathbf{h}r^2\mathbf{i}$ is the mean-square radius. The nuclear charge distribution can be approximated by a uniformly charged sphere of radius R, thus $\mathbf{h}r^2\mathbf{i} = \frac{3}{5}R^2$. Note that the field-shift constant, F , is defined here as having opposite sign to the definition in some previous papers, e.g. Refs. [72] and [68].

Figure 5.1: Schematic graph of the nuclear charge density distribution, , and the corresponding potential, U for two different values of the nuclear charge radius R (arbitrary units).

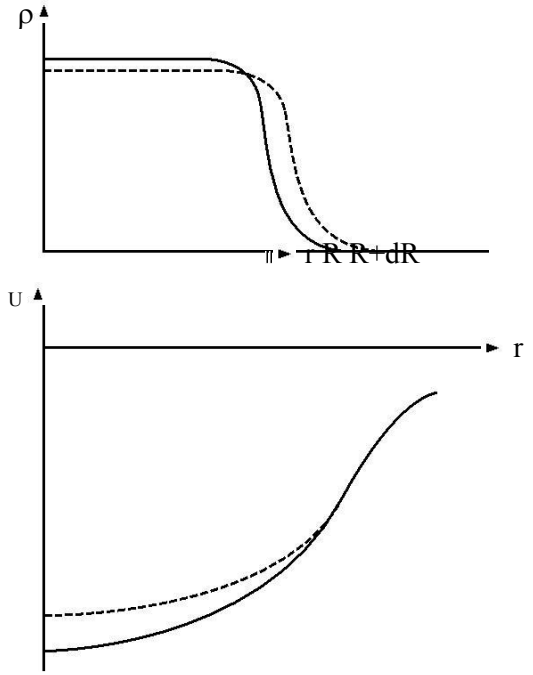

Higher-order correlation effects in the field shift are not too large, and are localised at the nucleus. For single-valence-electron atoms and ions we can include them easily by creating approximate Brueckner orbitals (solutions of the modified Hamiltonian, $h = h^{DF} + {}^{(1)}$) using the second-order operator, defined in Equation (3.12). The field shift is proportional in first order to the square of the wavefunction at the nucleus. Hence we can include higher-order effects quite simply by multiplying the matrix element by the square of the ratio of the Brueckner wavefunction to the Dirac-Fock wavefunction at the nucleus,

$$\frac{F_{DF+}}{} = \frac{{}^{DF+}(0)}{}^{2} \qquad (5.3)$$

5.2 King Plots

Using King plots[a], we can extract the ratios of field-shift constants for different transitions, provided we have experimental data for a number of different isotopes. Taking Eq. (2.7) for two transitions and , we can write

$$_{A;A^0} = F \; \mathbf{h}r^2\mathbf{i}^{A;A_0} + k \quad \frac{1}{A} \quad \frac{1}{A^0}; \tag{5.4}$$

where k is the total mass shift constant (including normal and specific mass shifts) for transition . A similar equation can be written for transition . We wish to eliminate the $\mathbf{h}r^2\mathbf{i}$ and obtain useful information about the constants F and k. The two axes of our King plot are defined by

$$y(A) = \frac{_{A;A^0}}{\frac{1}{A} \quad \frac{1}{A^0}} = F \; \frac{\mathbf{h}r^2\mathbf{i}^{A;A_0}}{\frac{1}{A} \quad \frac{1}{A^0}} + k \tag{5.5}$$

$$x(A) = \frac{_{A;A^0}}{\frac{1}{A} \quad \frac{1}{A^0}} = F \; \frac{\mathbf{h}r^2\mathbf{i}^{A;A^0}}{\frac{1}{A} \quad \frac{1}{A^0}} + k \; :$$

x and y are often called \modi ed isotope shifts" (MIS). Plotting the points (x(A); y(A)) for several pairs of isotopes (A; A^0) yields a straight line

$$y = \frac{F}{F} x + k \quad \frac{F}{F} k: \tag{5.6}$$

This equation is useful for extracting the ratios of eld-shift constants (from the gradient), but has proven less useful for extracting mass shift constants due to the generally small value of the intercept. The value of A^0 is often xed for all experiments in a partic-ular element (it usually corresponds to the leading isotope, e.g. for barium A^0 = 138), however this is not a necessary condition, and can be relaxed without changing the method.

As an illustrative example, we present in Fig. 5.2 a King plot of the 6497A and 5854A lines in Ba II. The isotope shifts were taken from Villemoes **et al.**, 1993 [5.102].

[a] introduced by King, 1963 [5.57] to explain anomalies in isotope shifts of samarium; see also

Hansen
et al., 1965 [5.101]

Figure 5.2: King plot of the Ba II 6497 and 5854 lines. The axes are the modified isotope shifts (Eq. (5.5)) in units of GHz amu.

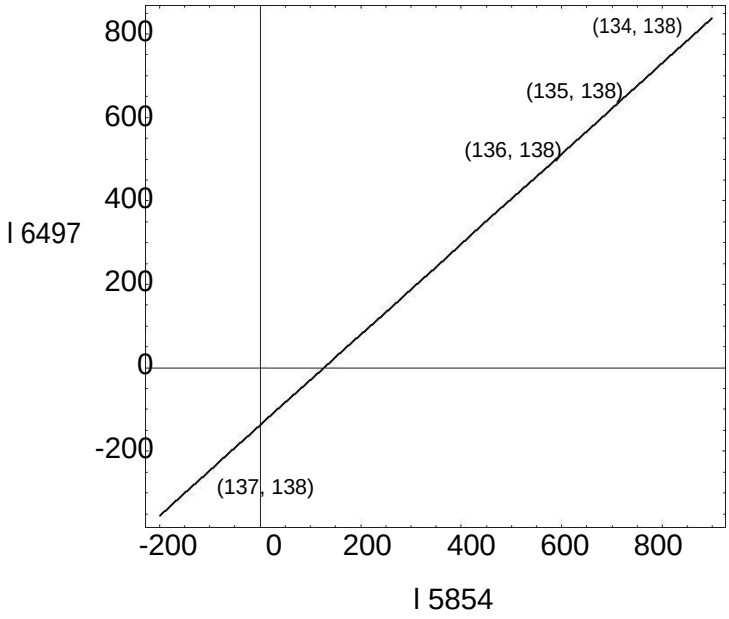

5.3 Results

We tested our method for the calculation of field shift in Ba II because in barium the field shift dominates over the mass shift, and there is a lot of experimental data to compare with. We present the results of our calculations of specic-mass-shift and field-shift constants in Ba II in Table 5.2. The method for calculating SMS is discussed in Section 6.1.

Our results for field-shift constants in Ba II were found to be consistent within a few percent of the previous theoretical work by Martensson-Pendrill (Table 5.1). In the same paper, Ref. [5.68], they say that they have underestimated the $6p_{1=2}$ field-shift constant by around 7%, based on the difference between experimental and theoretical calculations of the hyper ne constant A. Also, their 6s constant is said to be overestimated, leading to a corrected value of $F_{6\mathbf{p}_{3=2}\ 6\mathbf{s}}$ = 4:20(13) GHz/fm^2. These corrected values are in better agreement with the **ab initio** values obtained in this work ($F_{6\mathbf{p}_{3=2}\ 6\mathbf{s}}$ = 4:076 GHz/fm^2).

Table 5.1: Level field-shift constants, F , in Ba II. Due to a difference in the definition of F , the values calculated in Ref. [5.68] have been presented here with opposite sign.

State	Energy[a] (cm^{-1})	F (MHz/fm^2) Ref. [68]	This work
6s	80686:87	4096	3851
$6p_{1=2}$	60425:31	111:1	150:1
$6p_{3=2}$	58734:45	242:6	225:4
$5d_{3=2}$	75813:02		1223
$5d_{5=2}$	75012:05		1148

[a] Experimental results tabulated by Moore [98]

Table 5.2: Calculated specific-mass-shift (k_{SMS}) and field-shift constants (F) in Ba II transitions.

Transition	(A)	k_{SMS} (GHz amu)	F (MHz/fm^2)
$6p_{1=2}$ 6s	4934	105	-4001
$6p_{3=2}$ 6s	4554	257	-4077
$5d_{5=2}$ 6s	17622	-550	-4999
$6p_{1=2}$ $5d_{3=2}$	6497	653	1073
$6p_{3=2}$ $5d_{3=2}$	5854	805	997
$6p_{3=2}$ $5d_{5=2}$	6142	807	922

In Table 5.3 we compare our calculated values of field-shift constant ratios with King plot data obtained by combining several different experiments and transitions. We have used a simple weighted least squares t to obtain an experimental value for the ratio $F_{455}=F_{614}$. A two point formula was used for ratios involving the 1762 nm transition as experimental data exists only for the $^{134;138}$ and $^{136;138}$ isotope shifts [5.103]. Other ratios were extracted by the groups that performed the experiments, with much higher accuracy. Our values were found to be consistent with experimental values to within 5%.

We have shown in this section that we can calculate field shift in heavy atoms, where it dominates over mass shift. In the rest of this thesis we can now simply remove its (relatively minor) contribution from the experimental data in light atoms, so that we can compare the SMS part directly.

Table 5.3: Ratios of eld-shift constants in Ba II transitions. In the second column we list the measured values, obtained using King plots. In some cases we obtain the ratio ourselves by combining the results of two separate studies.

Transitions (/)	F =F This work	F =F Experiment
$6p_{1/2}$ { 6s / $6p_{3/2}$ { 6s	0:982	0:975(3)[a]
$6p_{3/2}$ { 6s / $6p_{3/2}$ { $5d_{5/2}$	4:42	4:50(6)[bc]
$6p_{3/2}$ { 6s / $5d_{5/2}$ { 6s	0:816	0:82(4)[bd]
$5d_{5/2}$ { 6s / $6p_{3/2}$ { $5d_{5/2}$	5:42	5:5(3)[cd]
$6p_{1/2}$ { $5d_{3/2}$ / $6p_{3/2}$ { $5d_{3/2}$	1:076	1:087(4)[c]
$6p_{3/2}$ { $5d_{5/2}$ / $6p_{3/2}$ { $5d_{3/2}$	0:925	0:961(3)[c]
$6p_{3/2}$ { $5d_{3/2}$ / $6p_{3/2}$ { 6s	0:245	0:2312(6)[c]

[a] Wendt **et al.** [104]
[b] Wendt **et al.** [105]
[c] Villemoes **et al.** [102]
[d] Zhao **et al.** [103]

Chapter 7

Specific mass shift

The specific mass shift has proven very di cult to calculate in the past (see Section 2.3). In this Chapter we describe a method of calculation which may make such calculations possible even in very di cult cases. The SMS operator is (see Eq. (2.5))

$$\Pi_{SMS} = \frac{1}{\ } \times \quad \mathbf{p_i}\ \mathbf{p_j} \tag{6.1}$$

Using many-body perturbation theory in the residual Coulomb operator and specic mass shift (SMS) operator to calculate isotope shift shows poor convergence (see Section 2.3.1). Therefore, we are looking for an \all order" method of calculation. The finite- field scaling method is used, which reduces the task to an energy calculation, and includes the SMS in all parts of the calculation.

To calculate k_{SMS} we include a scaled specific-mass-shift operator directly into our energy calculation from the very beginning. We add the two-body SMS operator to the Coulomb potential $\bar{Q} = 1= \mathbf{r}_1 \quad \mathbf{r}_2 + \mathbf{p}_1\ \mathbf{p}_2$. The operator Q replaces the Coulomb operator everywhere that it appears in an energy calculation. We recover the specific-mass-shift constant as

$$\kappa_{SMS} = \frac{d!}{\ } =0: \tag{6.2}$$

The operator $\bar{Q}$ has the same symmetry and structure as the Coulomb operator (see Appendix A).

6.1 Single-valence-electron atoms and ions

In this section, we develop a method for calculating the isotope shift of atoms and ions that can be treated as a single electron above a closed-shell core. These include the alkali metals and singly-ionised alkaline-earths, as well as other ions such as Zn II that are fairly well approximated by a single electron above a closed-subshell core.

We test our technique by calculating the isotope shift for several light atoms. The eld shift dominates in heavy atoms, and having tested it in Ba II (Chapter 5), we can now simply remove its contribution from the experimental data in light atoms so that we can compare the SMS part directly. After obtaining good agreement with experiment in a number of species, we apply the technique to calculate isotope shift for astronomically relevant transitions in Mg II, Zn II, Ge II, Si II and Si IV.

6.1.1 Calculation of k_{SMS}

As a zero approximation we use the Dirac-Fock (relativistic Hartree-Fock) method. At the Hartree-Fock stage we include the isotope shift in the exchange potential and iterate to obtain self-consistent \dressed" wavefunctions. In the MBPT terms explained in Ref. [6.72], the SMS matrix element at this stage is roughly equivalent to the rst-order and second-order contributions of the one-particle operator, plus higher-order corrections from the random-phase approximation (this corresponds to $P^{(1)} + S^{(2)}$ in the notation of Ref. [6.72]). It is interesting to note that k_{SMS} at this stage does not give meaningful results, and can even be of the wrong sign (it is labelled as \DF" in Table 6.1). We need to include correlation corrections in order to obtain any reasonable accuracy.

We include correlation effects to second order of MBPT; this approach gives good accuracy for energies. The perturbation is the difference between the exact and zero-order Dirac-Fock (DF) Hamiltonians, $\mathbf{V} = \mathbf{H}\ \mathbf{H}_0$ (see Eq. (3.18)). The many-body corrections start in second order; all first-order diagrams have been included in the self-consistent Hartree-Fock procedure. There are just four second-order diagrams, illustrated in Fig. 3.1. However, now we replace the Coulomb operator in these diagrams

Table 6.1: Level specic-mass-shift constants, k_{SMS}, in Na I and Mg II. The Dirac-Fock (DF) value, which does not include MBPT effects, is shown separately (this is approximately equivalent to the values labelled \$P^{(1)} + S^{(2)}$" in Ref. [6.72]). This table shows that MBPT effects are very important for accurate calculation of specific mass shift in single-valence-electron atoms and ions.

Ion	State	k_{SMS} (GHz amu)			
		Ref. [72]		This work	
		$P^{(1)} + S^{(2)}$	Final	DF	Final
Na I	3s	-54	54	-52	69
	3p 1=2	-67	-43	-68	-40
	3p 3=2	-67	-43	-67	-39
Mg II	3s		38	-171	83
	3p 1=2		-324	-408	-296
	3p 3=2		-323	-402	-290

with our two body operator $\tilde{Q}$, and use dressed Hartree-Fock wavefunctions as described above. This gives our final value of k_{SMS} as listed in Table 6.1.

In Table 6.1 we compare our results to those obtained by Safronova and Johnson (Ref. [6.72]) who calculated the isotope shift to third order in standard MBPT. Our values are significantly different, in particular the Mg II 3s level shift is more than twice that given in Refs. [70] and [72] (Refs. [70] and [72] are broadly in agreement with each other). However we find that this difference is not so large in the 3p { 3s transition due to cancellation of higher-order terms between the two levels. We compare our final results and those of Ref. [6.72] with experiment in Table 6.2. Agreement is at the level of 1%, which is much smaller than our error estimates (see section 6.1.2).

Our method includes many-body diagrams that are different from those of Ref. [6.72], including some chains of diagrams in all orders. It is also arguably simpler to implement since it does not require term-by-term calculation of a large number of matrix elements.

6.1.2 Estimation of error

For single-valence-electron atoms and ions, an estimate of the size of neglected higher-order diagrams can be obtained by calculating a new value of k_{SMS} that includes

Table 6.2: Comparison of calculated values of the specific mass shift (SMS) of transitions in Na I and Mg II with experiment.

Isotopes	Transition	SMS (MHz)		
		Ref. [72]	This work	Expt.[a]
^{23} ^{22}Na I	$3p_{1=2}$ { 3s	192	214 (48)	215 (1) 214 (2)
	$3p_{3=2}$ { 3s	192	212 (48)	214
^{26} ^{24}Mg II	$3p_{3=2}$ { 3s	1157	1196 (18)	1207 (100)

[a] these values are extracted from isotope shift experiments in Table 6.3

some higher-order chains of diagrams. We add the operator $^{(1)}{}_2$ (see Eq. (3.12)) to the exchange potential in the Dirac-Fock Hamiltonian (3.2) for the valence electron, h = h^{DF} + . Thus, we calculate the single electron Brueckner orbital. We also include a scaling factor f with the operator (**!** f) in order to t the experimental energy. The rescaling of simulates some higher order correlation corrections that were omitted in our calculation. Including in our Hartree-Fock calculation allows us to obtain another value for k_{SMS}, and the difference between this new value and the old second-order value gives us an estimate of the error.

6.1.3 Comparison with experiment

We compare our results with experimental data for alkali-metal atoms and ionised alkaline-earth metals in Table 6.3. In these systems it is more valuable to compare only the specific mass shift with those extracted from experiment than to compare the entire isotope shift. This is because the mass shift dominates strongly in these atoms and ions, and also because the SMS is generally considered more di cult to calculate. We have removed the field shift and the normal mass shift from the experimental values of the isotope shift in order to obtain an experimental value for the specific mass shift. The field shift values used in Table 6.3 were calculated using the method presented in Chapter 5. While our calculation of F has been shown to be good, the field shift also depends on having knowledge of $\mathbf{h}r^2\mathbf{i}$ for the relevant isotopes.

For Na I we use the value quoted in Ref. [6.72] of $\mathbf{h}r^2\mathbf{i}^{23;22}$ = 0:205(3) fm^2. This value is only from an empirical t, and shouldn't be trusted too far. The field shift is very

Table 6.3: Comparison of calculated values of the specific mass shift (SMS) with experiment for several transitions in single-valence-electron species. The experimental values of the SMS in the final column are extracted by subtracting the normal mass shift (NMS) and field shift (FS) from the experimental isotope shift (IS).

Isotopes	Transition	Energy (cm^{-1})	IS (expt.) (MHz)	NMS (MHz)	FS (MHz)	SMS (MHz) This work	SMS (MHz) Expt.
^{23} ^{22}Na I	$3p_{1=2}$ { 3s	16956.18	758:5 (7)[a]	551	8	214 (48)	215 (1)
			756:9 (1:9)[b]				214 (2)
	$3p_{3=2}$ { 3s	16973.38	757:72 (24)[c]	552	8	212 (48)	214
^{26} ^{24}Mg II	$3p_{3=2}$ { 3s	35760.97	3050 (100)[d]	1185	42	1196 (18)	1207 (100)
^{41} ^{39}K I	$4p_{1=2}$ { 4s	12985.17	235:25 (75)[e]	267	13 (5)	32 (21)	19 (6)
	$4d_{1=2}$ { 4s	27398.11	585 (9)[f]	564	13 (5)	20 (30)	34 (13)
^{43} ^{40}Ca II	$4p_{1=2}$ { 4s	25191.54	706 (42)[g]	723	36 (3)	22 (1)	19 (45)
			672 (9)[h]				15 (11)
			685 (36)[i]				2 (39)
	$4p_{3=2}$ { 4s	25414.43	713 (31)[g]	729	36 (3)	5 (1)	20 (34)
			677 (19)[h]				16 (22)
			685 (36)[i]				8 (39)
	$3d_{3=2}$ { 4s	13650.21	4180 (48)[g]	392	47 (4)	3502 (217)	3835 (52)
	$3d_{5=2}$ { 4s	13710.90	4129 (10)[g]	393	47 (4)	3487 (215)	3783 (14)
	$4p_{1=2}$ { $3d_{3=2}$	11541.33	3464:3 (3:0)[j]	331	12 (1)	3479 (218)	3807 (4)
			3483 (40)[g]				3826 (41)
	$4p_{3=2}$ { $3d_{3=2}$	11764.22	3462:4 (2:6)[j]	337	12 (1)	3507 (217)	3811 (4)
			3446 (20)[g]				3795 (21)
	$4p_{3=2}$ { $3d_{3=2}$	11703.53	3465:4 (3:7)[j]	336	12 (1)	3492 (216)	3813 (5)
			3427 (33)[g]				3774 (34)

[a] Pescht **et al.** [106]
[b] Huber **et al.** [107]
[c] Gangrsky **et al.** [108]
[d] Drullinger **et al.** [109]
[e] Touchard **et al.** [110]
[f] H•orb•ack **et al.** [64]
[g] Kurth **et al.** [111]
[h] extracted from Martensson-Pendrill **et al.** [67]
[i] Maleki and Goble [112]
[j] N•ortersh•auser **et al.** [113]

small in this atom, so the errors do not matter too much. For Mg II we have used the value $\mathbf{h}r^2\mathbf{i}^{26;24}$ = 0:33 fm^2 from another empirical t, the equation R_{nuc} = 1:1$A^{1=3}$ fm. This is a poor approximation, but in this case the field shift is small even in relation to the error in the experimental isotope shift. In Table 6.3 we have not included an error contribution for the field shift in either of these atoms, since we really do not know how accurate these approximations are.

The values of $\mathbf{h}r^2\mathbf{i}$ are known for K I and Ca II from muonic x-ray experiments, allowing us to calculate the field shift much more accurately. This is fortunate because the SMS is relatively small for the p { s transitions in these atoms, and hence the field shift plays a much larger role. We use the values $\mathbf{h}r^2\mathbf{i}^{41;39}$ = 0:117(40) fm^2 for K I from Ref. [114], and $\mathbf{h}r^2\mathbf{i}^{43;40}$ = 0:1254(32) fm^2 for Ca II from Ref. [6.115]. In Ca II the change in mean-square nuclear radius is given to high precision, so we have included an additional error of 5% in the field shift that comes from the constant F . This is a pessimistic estimate of error based on the accuracy we achieved calculating F for transitions in Ba II.

Table 6.3 shows that our method can reliably calculate the isotope shift in alkali-metal atoms and singly-ionised alkaline-earth metals, including those transitions with a large specific mass shift.

6.1.4 Results

We have shown that our method works in atoms for which we have available experimental data (Section 6.1.3). In Table 6.4 we tabulate values for the mass and field-shift constants for some astronomically useful transitions. We have not given errors for F , however we can say that they are less than 5% based on comparison of calculation with experiment in Ba II (Section 5.3).

In Table 6.5 we present the results of isotope shift calculations between common isotopes of astronomically important ions (meaning important for astronomy, rather than really ridiculously important). We have used the isotope shift constants presented in Table 6.4 with Equation (2.7) in order to calculate the isotope shift between particular

Table 6.4: Mass (k_{NMS} and k_{SMS}) and eld-shift constants (F) for some useful transitions in ions that can be treated as having a single valence electron.

Ion	Transition	F (MHz/fm^2)	K NMS (GHz amu)	K SMS (GHz amu)
Mg II	$3p_{1=2}$ { 3s	-127	-587	373 (12)
	$3p_{3=2}$ { 3s	-127	-588	373 (6)
Si II	4s { $3p_{1=2}$	171	-1077	1257 (29)
	4s { $3p_{3=2}$	171	-1072	1243 (28)
Si IV	$3p_{1=2}$ { 3s	-484	-1172	1535 (11)
	$3p_{3=2}$ { 3s	-485	-1180	1505 (7)
Zn II	$4p_{1=2}$ { 4s	-1596	-797	1310 (69)
	$4p_{3=2}$ { 4s	-1596	-812	1266 (69)
Ge II	5s { $4p_{1=2}$	1088	-1026	1046 (69)
	5s { $4p_{3=2}$	1083	-997	960 (62)

isotopes. Results of measurements for Zn II were brought to our attention [116] after we had performed our calculations. These results matched our prediction extremely well.

In Ge II and Si II, the specific mass shift cancels the normal mass shift entirely, making the field shift, and hence $\mathbf{h}r^2\mathbf{i}$, important. We have just used the empirical formula $R_{nuc} = 1{:}1A^{1=3}$ fm^2 to obtain values of $\mathbf{h}r^2\mathbf{i}$ in these ions. This is extremely rough, and although it seems to work in Zn II to within a 20% accuracy based on the experimental data given, we really don't know if this holds for Si and Ge at all. In the Si IV transitions presented, it is less important to have good values for the field shift because there is no cancellation between the NMS and SMS.

6.2 Mg I

Magnesium is one of the simplest and well-studied two-electron atoms. Because of that it is often used as a test ground for different methods of atomic calculations. In this section we show that we can calculate the isotope shift of some magnesium transitions for which experimental values are available.

Table 6.5: Total isotope shifts for some astronomically relevant transitions in single-valence-electron ions. We have presented two errors: the rst comes from our uncertainty in calculation of the specific-mass-shift constant, k_{SMS}; and the second comes from the field shift, which is mainly due to lack of knowledge of $\mathbf{h}r^2\mathbf{i}$. A negative sign means that the total shift is opposite to the normal mass shift. The experimental value for the $4p_{3=2}$ { 4s transition in Zn II is 676(6) MHz [6.116], in agreement with our prediction.

Isotopes	Transition	Energy[a] (cm^{-1})	Isotope Shift (MHz)
$^{30}\ ^{28}$Si II	4s { $3p_{1=2}$	65495.1	375 (70)(11)
	4s { $3p_{3=2}$	65208.1	351 (67)(11)
$^{30}\ ^{28}$Si IV	$3p_{1=2}$ { 3s	71289.6	6294 (26)(31)
	$3p_{3=2}$ { 3s	71749.9	6241 (18)(31)
$^{66}\ ^{64}$Zn II	$4p_{1=2}$ { 4s	48480.6	653 (32)(78)
	$4p_{3=2}$ { 4s	49354.4	632 (33)(79)
$^{74}\ ^{70}$Ge II	5s { $4p_{1=2}$	62402.4	491 (53)(101)
	5s { $4p_{3=2}$	60635.3	533 (48)(101)

[a] Moore [98]

6.2.1 Configuration interaction

It is interesting to examine the contribution of various parts of the CI Hamiltonian to the SMS. We can separate the contribution of the specific mass shift from the Hamiltonian operator of Eq. (3.7):

$$H = H_0 + H_{SMS} = H_0 + \sum_{i<j} \mathbf{p}_i \cdot \mathbf{p}_j \; : \tag{6.3}$$

The SMS operator for the valence electrons in the frozen core approximation can be divided into the core, one-valence-electron and two-valence-electron parts:

$$H_{SMS} = H_{SMS}^{(0)} + H_{SMS}^{(1)} + H_{SMS}^{(2)} \tag{6.4}$$

The rst term in Eq. (6.4) corresponds to the change of the core potential. It accounts for the change of the core orbitals when the Dirac-Fock equations are solved for the operator H . The term $H_{SMS}^{(1)}$ accounts for the exchange interaction of the valence electrons with the core:

$$\sum_{j=1}^{N_{core}} \langle \mathbf{h}_i; j j \mathbf{p}_1 \cdot \mathbf{p}_2 j j; k \mathbf{i} \rangle \; : \tag{6.5}$$

The last term, $H_{SMS}^{(2)}$, corresponds to the specific mass shift between the two valence electrons, $\mathbf{p}_1\ \mathbf{p}_2$.

In order to study the role of the valence correlations we made three different calculations:

1. The basic one-configurational calculation for the ground state $3s^2\ {}^1S_0$ and for the $3s3p\ {}^{1;3}P_J$ states. All core orbitals and orbitals 3s and 3p are formed in the $V^{N\ 2}$ approximation (i.e. by solving Dirac-Fock equations for the core).

2. Full two-electron CI for a medium sized **r** basis set [8sp5d], which includes the orbitals $1\ 8s_{1=2}$, $2\ 8p_j$ and $3\ 5d_j$. The 3s, 3p and 3d orbitals are solutions of the $V^{N\ 2}$ Dirac-Fock potential. The remaining virtual orbitals are constructed by multiplying the previous orbital of the same partial wave by the simple radial function and orthogonalizing with the other orbitals.

3. Full two-electron CI for the B-spline basis set [12spd9f].

Below we refer to these calculations as small, medium, and large. The large calculation is already very close to the saturation of the valence CI. Here the difference between the theoretical spectrum and experiment is mostly caused by the neglect of the core-valence correlations.

Table 6.6 presents the resulting SMS level shift constants, k_{SMS} of Eq. (2.7), in different approximations. The contributions of individual terms in Eq. (6.4) are given, as well as their sum. It is interesting to note that all of the terms are large in comparison to the total SMS. There is a large cancellation between contributions within levels, and also between different levels. This shows that high accuracy is required in each term, so that the residual SMS in transitions is still correct after cancellation.

Comparison of the different approximations shows a strong dependence on the size of the basis sets. We see that it is very important to saturate the basis as completely as possible. In some cases the SMS changes drastically even between the medium and the large basis sets. In particular, the difference between large and medium SMS calculation for the level $3s3d\ {}^3D_1$ is 39%. This is mostly due to the f -wave contribution, which

Table 6.6: Level specific-mass-shift constants, k_{SMS}, in Mg I. Individual contributions from Eq. (6.4) are presented [(0), (1), (2)], as well as the total. For some levels we give medium CI (M) and one-configurational results (S) in addition to the large CI (L) ones.

	k_{SMS} (GHz amu)				
Level	(0)	(1)	(2)	Total	CI
$3s^2\ ^1S_0$	559	883	131	193	L
"	561	881	135	186	M
"	857	1125	0	268	S
$3s4s\ ^3S_1$	422	615	44	149	L
"	431	624	52	142	M
$3s4s\ ^1S_0$	415	615	21	179	L
"	424	630	30	177	M
$3s3d\ ^1D_2$	343	616	267	541	L
$3s3d\ ^3D_1$	375	561	41	144	L
"	381	571	10	200	M
$3s3d\ ^3D_2$	375	561	41	144	L
$3s3d\ ^3D_3$	375	561	41	144	L
$3s3p\ ^3P^o_0$	428	853	144	570	L
$3s3p\ ^3P^o_1$	428	852	145	569	L
$3s3p\ ^3P^o_2$	428	850	145	567	L
"	431	850	142	561	M
"	759	1161	266	668	S
$3s3p\ ^1P^o_1$	408	698	329	38	L
"	411	700	341	52	M
"	946	1163	265	49	S
$3s4p\ ^3P^o_0$	402	630	13	215	L
$3s4p\ ^3P^o_1$	402	629	13	215	L
$3s4p\ ^3P^o_2$	402	629	13	214	L

is absent in the medium basis set. Note that the SMS operator can only mix orbitals with l = 1. That is why the f -wave contribution is more important for the levels of the configuration 3s3d. On the other hand, for the same reason, the contribution of higher partial waves to the considered levels is suppressed.

Analysis of Table 6.6 shows that valence correlations tend to decrease the contributions of the first two terms of the SMS operator. The third (two-particle) term of

the SMS operator is generally not screened. On the contrary, for some levels the two-particle contribution grows with the size of the basis set. Note that the nal value

Table 6.7: Speci c-mass-shift constants, k_{SMS}, of transitions from the ground state ($3s^2\ ^1S_0$) in Mg I.

Upper Level	Energy[a] (cm^{-1})	k_{SMS} (GHz amu) CI	CI + $^{(1)}$	CI + $^{(1;2)}$
$3s3p\ ^3P^o_0$	21850	378	487	492
$3s3p\ ^3P^o_1$	21870	377	486	491
$3s3p\ ^3P^o_2$	21911	375	485	489
$3s3p\ ^1P^o_1$	35051	231	120	134
$3s4s\ ^3S_1$	41197	43	59	49
$3s4s\ ^1S_0$	43503	13	94	85
$3s3d\ ^1D_2$	46403	345	500	477
$3s4p\ ^3P^o_0$	47841	17	136	126
$3s4p\ ^3P^o_1$	47844	16	136	126
$3s4p\ ^3P^o_2$	47851	16	136	126
$3s3d\ ^3D_3$	47957	52	87	77
$3s3d\ ^3D_2$	47957	52	87	77
$3s3d\ ^3D_1$	47957	52	87	77
$3s4p\ ^1P^o_1$	49347	5	120	108
$3s4d\ ^1D_2$	53135	100	246	239
$3s4d\ ^3D_1$	54192	32	99	88
$3p^2\ ^3P_0$	57813	225	469	464

[a] Experimental values tabulated by Moore [98]

of the two-particle contribution to the ground state SMS is of the same order as the other contributions (as it is for most other states), while in the one-con gurational approximation it is zero.

6.2.2 Role of

The B-spline basis used in this section is the same that was used to calculate energies and relativistic shift for Mg I in Section 4.1. For a comparison of energies, see Table 4.1. Agreement with experiment is within 0.4% for all considered levels. Table 6.7 presents the resulting SMS level shift constants, k_{SMS} of Eq. (2.7). In each table we present results of the pure CI calculation (which agree with our previous calculation, Sec-tion 6.2.1), as well as calculations including $^{(1)}$ only, and both $^{(1)}$ and $^{(2)}$.

The core-valence e ects are very important for the SMS calculation. In particular the single-valence-electron diagrams (included in $^{(1)}$) can improve accuracy drastically

in cases where the pure CI method is not very good. Although $^{(2)}$ is important for calculation of energy, it appears to make little difference to k_{SMS}. This is easily understood since the most important two-body diagram (the direct diagram, Fig. 3.3.1, corresponding to the screening of the electron-electron interaction by the core electrons) makes no contribution to the SMS. The exchange diagrams in $^{(2)}$ do have an effect, but this is much smaller than the one-body contribution.

6.2.3 Comparison with experiment

In Table 6.8 we compare experimental and calculated frequency shifts between isotopes ^{26}Mg and ^{24}Mg ($^{26;24}$). We compare the SMS part only, which is extracted from experiment by subtracting the NMS. We have ignored the eld shift for simplicity; it is approximately 20-30 MHz or 2% of the NMS, which is less than the experimental uncertainty in most cases, and is of the order of the error in our SMS calculations.

Also presented in Table 6.8, for a theoretical comparison, are the results of Veseth (Ref. [71], 1987) and Johnsson **et al.** (Ref. [79], 1999). Veseth used non-relativistic many-body perturbation theory within the algebraic approximation to calculate the isotope shift to third order for some transitions. Jonsson **et al.** used a non-relativistic multiconfigurational Hartree-Fock approach, which allowed for both core and valence excitations in the CI. These calculations are discussed in more detail in Section 2.3.

An under-studied transition that is seen in quasar absorption spectra is the 2026 A line of Mg I ($3s^2\ ^1S_0$ **!** $3s4p\ ^1P_1^{\mathbf{o}}$). From Table 6.7, we calculate the isotope shift of this line as $^{26;24}$ = 2950(50) MHz (the error here is based on the absence of eld shift as well as the incompleteness of saturation of the basis set used to calculate k_{SMS}).

6.3 Carbon

The isotope shift of carbon is particularly important for testing models of chemical evolution; this is explained in Section 1.2.2. We also have one more reason to study carbon: it is a well studied atom, and we can compare the results of our method with those of other theoretical analyses, as well as a few experiments. In particular, much progress

Table 6.8: Comparison of calculated values of the specific mass shift of several transitions in Mg I with experiment. All isotope shifts are between ^{26}Mg and ^{24}Mg. The experimental values of the SMS are obtained by subtracting the normal mass shift (NMS) from the experimental isotope shift (IS). We have neglected the field shift; it is of the order of 20-30 MHz. Also presented are the results of Refs. [71] and [79] for theoretical comparison.

Transition	(A)	IS (expt.) (MHz)	NMS (MHz)	SMS (MHz) CI	CI + (1)	CI + (1;2)	Expt.	Ref. [71]	Ref. [79]
$3s^2\ ^1S_0$! $3s3p\ ^3P_1^o$	4572	2683 (0)[a]	1153	1208	1559	1573	1530	1378	1666
$3s^2\ ^1S_0$! $3s3p\ ^1P_1^o$	2853	1412 (21)[b]	1848	-740	-383	-428	-436		-409
		1390 (31)[c]					-458		
$3s3p\ ^3P_0^o$! $3s4s\ ^3S_1$	5169	396 (6)[d]	1020	-1347	-1371	-1419	-1416		
$3s3p\ ^3P_1^o$! $3s4s\ ^3S_1$	5174	390 (5)[d]	1019	-1345	-1369	-1416	-1409		
$3s3p\ ^3P_2^o$! $3s4s\ ^3S_1$	5185	390 (7)[d]	1017	-1339	-1363	-1411	-1407		
$3s3p\ ^3P_1^o$! $3p^2\ ^3P_0$	2782	1810 (80)[a]	1895	-486	-56	-86	-85		
$3s3p\ ^3P_0^o$! $3s3d\ ^3D_1$	3830	60 (15)[b]	1376	-1377	-1283	-1329	-1316	-1269	
$3s3p\ ^3P_1^o$! $3s3d\ ^3D_{1;2}$	3833	61 (3)[b]	1375	-1374	-1280	-1326	-1314		
$3s3p\ ^3P_2^o$! $3s3d\ ^3D_{1;2;3}$	3839	58 (4)[b]	1373	-1368	-1274	-1321	-1315		
$3s3p\ ^3P_1^o$! $3s4d\ ^3D_1$	3094	420 (20)[e]	1704	-1309	-1241	-1291	-1284		
$3s3p\ ^1P_1^o$! $3s4d\ ^1D_2$	5530	2107 (15)[d]	953	1059	1173	1195	1154		

[a] Sterr **et al.** [117]
[b] Hallstadius [118]
[c] Le Boiteux **et al.** [119]
[d] Hallstadius and Hansen [120]
[e] Novero **et al.** [121]

has been made to calculate isotope shifts using the multiconfigurational Hartree-Fock (MCHF) and configuration interaction (CI) approach [77{80]; see Section 2.3.2.

In this section we show that our CI + MBPT method has accuracy comparable to that of the MCHF calculations, and are accurate enough to be used to measure isotope abundances. We present results for each species of carbon separately, in order of increasing number of valence electrons. The basis sets used in this section are the same as those described in Section 4.2. The MBPT basis is fully saturated in the sense that the energies and isotope shifts do not change with the addition of more basis functions. The saturation achieved for the CI basis is described below.

6.3.1 C IV

C IV has one electron above a closed $1s^2$ core. It can therefore be treated as a single valence electron atom using MBPT, or as a three electron atom using CI. We have used both methods; the results are presented for comparison in Table 6.9. In each case, the calculations were done using the $\mathbf{B}_1$ basis set. The isotope shift results have also been compared with previous theoretical approaches, namely the MCHF { CI calculations presented in Ref. [77], and the combined the Hylleraas [85] and full-core plus correlation (FCPC) calculations [86] also presented in Ref. [77].

As noted previously, the MBPT basis was completely saturated, however we have only included second-order diagrams in our calculation. By contrast, the CI calculations are complete (although they do not include the Breit interaction and QED effects), but the basis is not completely saturated. We have used an effective 22spd8f basis for the CI calculation, including only single and double excitations from the leading configurations (SD-CI). We included triple excitations for a smaller basis, 14spd8f : this made a difference of less than 2 cm^{1} in the transition energy, and less than 1 GHz amu for k_{SMS}. Other f -wave and higher partial waves were also found to be unimportant.

All methods give the same value for the transition energies and SMS constants to within 0.5%.

Table 6.9: Energies and speci c-mass-shift constants, k_{SMS} of transitions from the ground state ($2s\ ^2S_{1=2}$) in C IV. The transition energies presented do not include the addition of mass shift e ects. Note that all results presented by other groups are non-relativistic and hence do not distinguish ne-structure.

Level	Expt.[a]	DF + $^{(1)}$	Full CI	Other works
			Energy (cm^{-1})	
$2p\ ^2P^o_{1=2}$	64484	64551	64594	64564[b]
$2p\ ^2P^o_{3=2}$	64592	64681	64725	64399[c]
				64449[d]
			k_{SMS} (GHz amu)	
$2p\ ^2P^o_{1=2}$		-4511	-4521	-4526[b]
$2p\ ^2P^o_{3=2}$		-4504	-4514	-4527[c]
				-4528[d]

[a] Moore [98]
[b] MCHF-CI: Carlsson **et al.** [77]
[c] MCHF: Godefroid **et al.** [80]
[d] Hylleraas + FCPC: Results of King [85], and Wang **et al.** [86], combined and presented in Ref. [77]

6.3.2 C III

The ground state for C III is $1s^2 2s^2\ ^1S_0$. We have done our calculations both as a four-electron CI problem (full CI) and by combining two-valence-electron CI with MBPT, considering $1s^2$ as the frozen core (CI + $^{(1;2)}$). All results are presented in Table 6.10. Also included are CI results (the pure two-electron CI method) and CI + $^{(1)}$ results (that do not include $^{(2)}$). This allows us to examine the roles of the different parts of the core-correlation. The CI and CI + $^{(1)}$ results are calculated with the $\mathbf{B}_2$ basis set; the complete CI + $^{(1;2)}$ results have been calculated using both the $\mathbf{B}_1$ and $\mathbf{B}_2$ sets. Additionally we have presented the MCHF results of Ref. [79].

For the full four-electron CI method we used a very large basis 16spdf , in the SD-CI approximation. This was not enough to saturate the basis entirely, and we could go no further because the Hamiltonian matrix became too large. The error in k_{SMS} from the full CI calculation could be as large as 100 GHz amu. Nonetheless, they are in agreement with the calculations of Ref. [79], as well as the results of our own CI + MBPT.

Table 6.10: Energies and specific-mass-shift constants, k_{SMS}, of transitions from the ground state ($2s^2\ ^1S_0$) in C III. Note that the MCHF results are non-relativistic and hence do not distinguish ne-structure.

Level	Expt.[a]	CI	CI + $^{(1)}$	CI + $^{(1;2)}$ $\mathbf{B}_2$	CI + $^{(1;2)}$ $\mathbf{B}_1$	Full CI	MCHF[b]
				Energy (cm^{-1})			
$2s2p\ ^3P_0^o$	52367	52750	52322	52349	52383	52506	52280
$2s2p\ ^3P_1^o$	52391	52784	52357	52383	52418	52534	
$2s2p\ ^3P_2^o$	52447	52852	52427	52453	52488	52592	
$2s2p\ ^1P_1^o$	102352	103719	103365	102725	102775	103109	102598
				k_{SMS} (GHz amu)			
$2s2p\ ^3P_0^o$		-3439	-3478	-3473	-3470	-3483	-3475
$2s2p\ ^3P_1^o$		-3438	-3476	-3472	-3468	-3480	
$2s2p\ ^3P_2^o$		-3434	-3473	-3468	-3465	-3474	
$2s2p\ ^1P_1^o$		-2688	-2759	-2790	-2784	-2882	-2817

[a] Moore [98]
[b] J•onsson **et al.** [79]

In Ref. [79] the MCHF results were given an error of 1%; our CI + MBPT results are within this range, and so we believe that we have obtained a similar accuracy. It is also worth noting again that we have excluded the extra box diagrams with \wrong" parity from the results presented. The inclusion of these diagrams in $^{(2)}$ makes a difference of around 0.1% to the k_{SMS} constants.

6.3.3 C II

We have treated C II as a three-valence-electron ion; its ground state is $2s^22p\ ^2P_{1=2}^o$. We have used the $\mathbf{B}_2$ basis 20spdf , which corresponds to the $V^{N\ 1}$ potential, and we have restricted ourselves in the CI problem to single and double excitations from the leading configurations $2s^22p$ and $2s2p^2$.

In Table 6.11 we present all results for C II. Again we have presented the breakdown of the various parts of the CI + MBPT method. We have also performed our calculations using the $\mathbf{B}_1$ basis: this changed the results by less than 1% for all results except

for the $^2S_{1=2}$ transition, in which the difference was around 3%. For this transition, neither basis set was enough to completely saturate k_{SMS}. Furthermore, the difference

Table 6.11: Specific-mass-shift constants, k_{SMS}, of transitions from the ground state ($2s^2 2p\ ^2P_{1=2}^{o}$) in C II. Note that the MCHF-CI results are non-relativistic and hence do not distinguish ne-structure.

Level	Energy[a] (cm^{-1})	k_{SMS} (GHz amu) CI	CI + (1)	CI + (1;2)	MCHF-CI[b]
$2s2p^2\ ^4P_{1=2}$	43003	-2913	-2956	-2960	
$2s2p^2\ ^4P_{3=2}$	43025	-2912	-2954	-2958	
$2s2p^2\ ^4P_{5=2}$	43054	-2910	-2952	-2956	
$2s2p^2\ ^2D_{5=2}$	74930	-2604	-2666	-2672	-2672
$2s2p^2\ ^2D_{3=2}$	74933	-2604	-2666	-2671	
$2s2p^2\ ^2S_{1=2}$	96494	-1204	-1301	-1321	-1411
$2s2p^2\ ^2P_{1=2}$	110624	-1323	-1410	-1471	-1531
$2s2p^2\ ^2P_{3=2}$	110666	-1320	-1407	-1468	

[a] Experimental results tabulated by Moore [98]
[b] J•onsson **et al.** [78]

between the results of CI + MBPT and MCHF-CI is fairly large for this transition (around 7%). Adding the next most important configuration, $2s^2 3s$, to the leading set changes the energy of the $^2S_{1=2}$ transition by 30 cm^{-1} (0.03%) and k_{SMS} by 14 GHz amu (around 1%). The e ect on all other transitions was much smaller.

6.3.4 C I

Transition energies in neutral carbon were presented in Table 4.7. The ground state of C I is $2s^2 2p^2\ ^3P_0$. A discussion of the calculations and their limitations for this atom is given in Section 4.2.4. In particular, being restricted to taking excitations from only a few leading configurations leads to an error of up to 80 GHz amu in k_{SMS}.

In Table 6.12 we present the SMS constants for C I. We are within 1% of the values obtained using the MCHF-CI method (Refs. [77] and [78]). For most transitions the e ect of core-correlations on k_{SMS} is around 1 or 2%, however in some cases they are larger (for example, in $2s2p^3\ ^3P^{o}$ the core correlations are 8% of the total).

Table 6.12: Specific-mass-shift constants, k_{SMS}, of transitions from the ground state ($2s^2 2p^2\ ^3P_0$) in C I. Note that the MCHF-CI results are non-relativistic and hence do not distinguish ne-structure.

Level	Energy[a] (cm^{-1})	k_{SMS} (GHz amu) CI	CI + (1)	CI + (1;2)	MCHF-CI
$2s^2 2p^2\ ^1S_0$	21648	186	180	191	152[b]
$2s2p^3\ ^3S_2^o$	33735	-2540	-2579	-2588	-2583[b]
$2s^2 2p3s\ ^3P_0^o$	60333	1405	1405	1419	
$2s^2 2p3s\ ^3P_1^o$	60353	1406	1406	1420	
$2s^2 2p3s\ ^3P_2^o$	60393	1408	1408	1422	
$2s^2 2p3s\ ^1P_1^o$	61982	1549	1551	1559	1553[b]
$2s2p^3\ ^3D_3^o$	64087	-2165	-2224	-2227	
$2s2p^3\ ^3D_1^o$	64090	-2165	-2224	-2227	-2222[c]
$2s2p^3\ ^3D_2^o$	64091	-2165	-2224	-2227	
$2s2p^3\ ^3P_1^o$	75254	-1272	-1390	-1392	
$2s2p^3\ ^3P_2^o$	75255	-1272	-1389	-1391	
$2s2p^3\ ^3P_0^o$	75256	-1271	-1390	-1392	
$2s^2 2p3d\ ^1D_2^o$	77680	1334	1320	1331	
$2s^2 2p4s\ ^3P_0^o$	78105	1398	1392	1407	
$2s^2 2p4s\ ^3P_1^o$	78117	1404	1397	1412	
$2s^2 2p4s\ ^3P_2^o$	78148	1415	1408	1422	
$2s^2 2p3d\ ^3F_2^o$	78199	1378	1368	1381	
$2s^2 2p3d\ ^3F_3^o$	78216	1381	1372	1384	
$2s^2 2p3d\ ^3D_1^o$	78293	1430	1422	1434	
$2s^2 2p3d\ ^3D_2^o$	78308	1429	1421	1432	
$2s^2 2p3d\ ^3D_3^o$	78318	1430	1420	1432	
$2s^2 2p4s\ ^1P_1^o$	78340	1443	1435	1446	
$2s^2 2p3d\ ^1F_3^o$	78530	1451	1440	1452	
$2s^2 2p3d\ ^1P_1^o$	78731	1436	1426	1438	
$2s^2 2p3d\ ^3P_2^o$	79311	948	998	1010	
$2s^2 2p3d\ ^3P_1^o$	79319	956	1006	1018	
$2s^2 2p3d\ ^3P_0^o$	79323	960	1009	1021	
$2s^2 2p4d\ ^1D_2^o$	83498	1277	1258	1268	

[a] Experimental results tabulated by Moore [98]
[b] Carlsson **et al.** [77]
[c] J•onsson **et al.** [78]

Table 6.13: Comparison of calculated ^{13}C { ^{12}C isotope shifts, $^{13;12}$, with experiment.

Transition			$^{13;12}$ (cm ^{1})	
Lower Level	Upper Level	(A)	Expt.	This work
C I				
$2s^2 2p^2\ ^3P_2$	$2s2p^3\ ^5S_2^o$	2967	0:670 (5)[a]	0:674[b]
$2s^2 2p^2\ ^1S_0$	$2s^2 2p3s\ ^1P_1^o$	2479	0:156 (3)[c]	0:151
			0:156 (2)[d]	
C II				
$2s2p^2\ ^2S_{1=2}$	$2s^2 3p\ ^2P_{3=2}^o$	2837	0:612 (2)[c]	0:617
$2s2p^2\ ^2S_{1=2}$	$2s^2 3p\ ^2P_{1=2}^o$	2838	0:623 (3)[c]	0:617

[a] Bernheim and Kittrell [122]
[b] Actually, the $2s^2 2p^2\ ^3P_0$ { $2s2p^3\ ^5S_2^o$ transition was calculated. [c] Burnett [123]
[d] Holmes [124]

6.3.5 Comparison with experiment

In Table 6.13 we compare our calculations with the few experiments that exist for carbon ions; in all cases agreement is within around 0.005 cm ^{1}, which corresponds to an error in k_{SMS} of around 20 GHz amu.

In Table 6.14 we present total isotope shifts for some important transitions. These transitions can be observed in quasar absorption spectra, and can therefore be used to probe variation of and isotope abundance evolution. The results are presented both in MHz and km/s: the latter is the preferred form for use in astronomy.

Table 6.14: Total calculated ^{13}C { ^{12}C ($^{13;12}$) and ^{14}C { ^{12}C ($^{14;12}$) isotope shifts for important transitions. We believe the errors are of the order of 0.1 GHz.

Transition			13;12		14;12	
Ground State	Upper Level	(A)	(GHz)	(km/s) [a]	(GHz)	(km/s) [a]
C I						
$2s^2 2p^2\ ^3P_0$	$2s^2 2p3s\ ^3P_1^o$	1657	-2.75	0.46	-5.09	0.84
	$2s2p^3\ ^3D_1^o$	1560	21.10	-3.29	39.12	-6.10
	$2s2p^3\ ^3P_1^o$	1329	16.91	-2.25	31.34	-4.17
	$2s^2 2p4s\ ^3P_1^o$	1280	-0.82	0.10	-1.51	0.19
	$2s^2 2p3d\ ^3D_1^o$	1277	-0.94	0.12	-1.75	0.22
	$2s^2 2p4s\ ^1P_1^o$	1276	-1.01	0.13	-1.88	0.24
	$2s^2 2p3d\ ^3P_1^o$	1261	1.84	-0.23	3.42	-0.43
C II						
$2s^2 2p\ ^2P_{1=2}^o$	$2s2p^2\ ^2D_{3=2}$	1336	25.10	-3.35	46.53	-6.21
	$2s2p^2\ ^2D_{5=2}$	1336	25.10	-3.35	46.54	-6.21
	$2s2p^2\ ^2S_{1=2}$	1037	18.70	-1.94	34.66	-3.59
C III						
$2s^2\ ^1S_0$	$2s2p\ ^1P_1^o$	977	28.76	-2.81	53.33	-5.21
C IV						
$2s\ ^2S_{1=2}$	$2p\ ^2P_{1=2}^o$	1551	35.89	-5.57	66.54	-10.32
	$2p\ ^2P_{3=2}^o$	1548	35.79	-5.54	66.35	-10.27

[a] = = c (km/s). A negative velocity means that ^{14}C (and ^{13}C) are at lower wavelength than ^{12}C.

Chapter 8

Cosmological variation of deuteron binding energy, strong interaction and quark masses from big bang nucleosynthesis

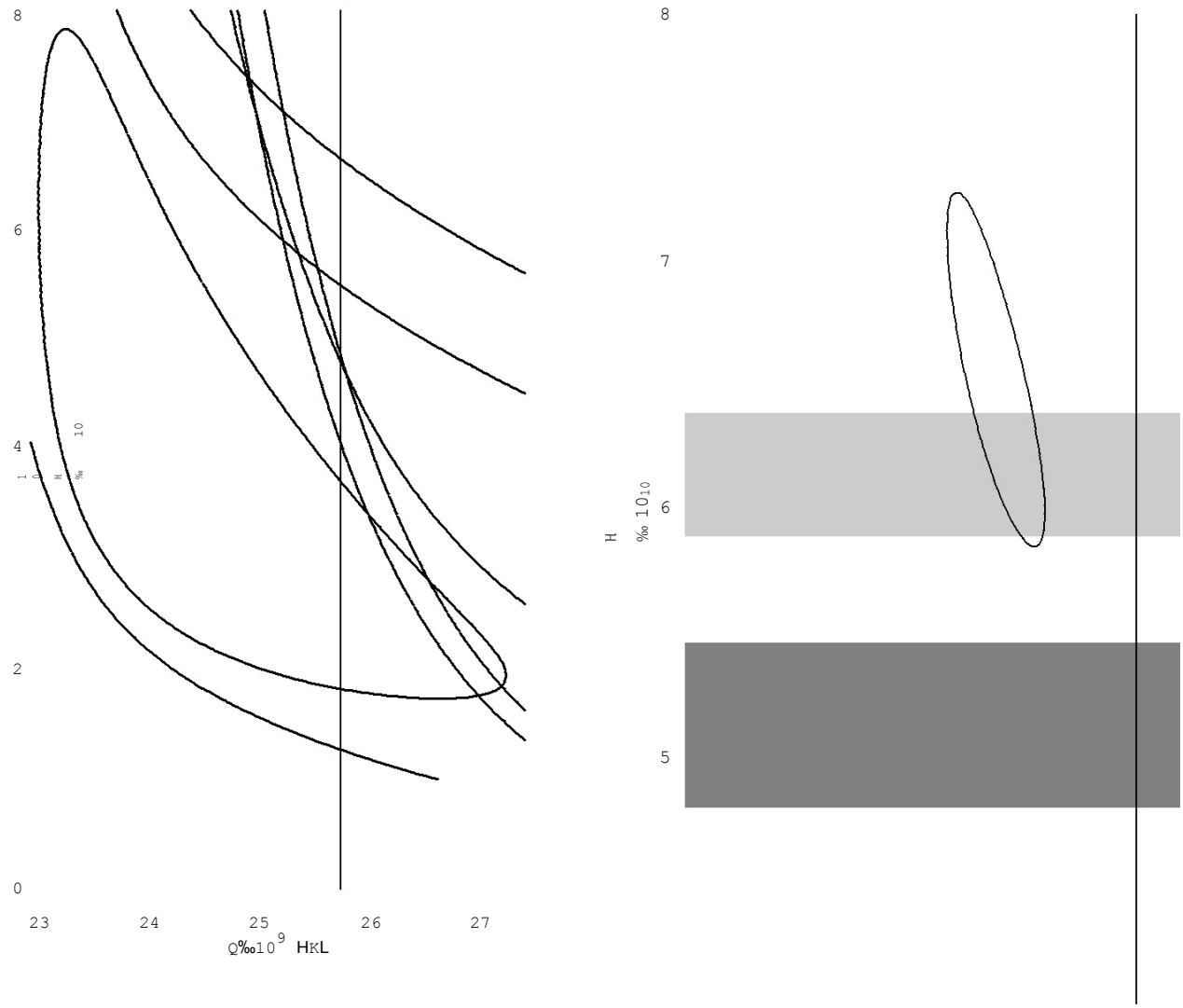

FIG. 2: 1σ-ranges around the maxima of individual likelihood functions. The solid lines show 1σ-ranges for D, the dashed lines are for ^{4}He (using Y_p from Eq.5), and the dot-dashed lines are for ^{7}Li. For lithium, there are 2 solutions for η and Q, hence the shape of the error contours is more complicated.

II. Constraint from CMB anisotropy measurements

The value of η found from CMB anisotropy measurements

$$\eta_0 = (6.14 \pm 0.25) \times 10^{-10}$$

has rather high accuracy. It is natural to use the constraint from this measurement in our study of the deuteron binding energy effects. To do this we construct another likelihood function which is a function of Q only.

If we neglect nondiagonal elements in w_{ij} we can con-struct the individual likelihood functions for D, ^{4}He, and

24 24.5 25 25.5 26 Q‰10^9 HKL

FIG. 3: 1σ-range about the maximum of Lf (η, Q) (again us-ing $Y_{\mathbf{p}}$ from Eq.5). The lighter shaded region shows CMB-WMAP data for η. The darker shaded region is the 1σ-range for η from BBN calculations using the present-day value of the deuteron binding energy, Q = 25.82. A lower value of $Y_{\mathbf{p}}$ will produce a larger deviation between the $\eta_{\mathbf{W\,M\,AP}}$ and η**BBN** .

^{7}Li. They are constructed in the same way as (7.23) using instead of general function Lf (η, Q) the individual ones

Lf_D (η, Q), Lf_{He}(η, Q) , Lf_{Li}(η, Q). These functions are plotted in Fig. 4 together with the general likelihood function (7.23)

From the deuterium likelihood function we found the position of the maximum and 1σ deviations:

$$Q_D = (25.74 + 0.92 - 0.68) \times 10^9. \quad (7.24)$$

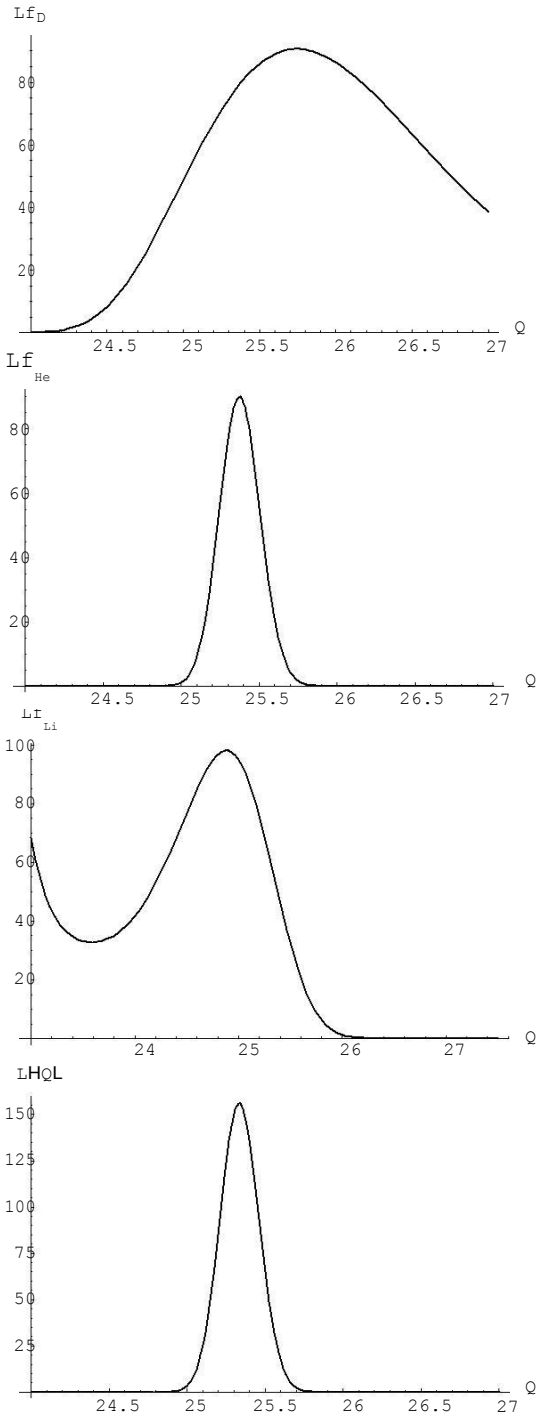

FIG. 4: Individual likelihood functions (7.23) for the light el-ements. From top to bottom: D, ^{4}He (Eq.5), Li, and the combined datset.

The shape near the maximum is apparently non-symmetric. The position of the maximum is fully com-patible with the present value of $Q = 25.82 \times 10^9$ K. The helium likelihood function is much narrower (see the sec-ond panel from the top). It gives for the maximum and

for the 1σ the values

$$Q_{He} = (25.37 \pm 0.13) \times 10^9. \qquad (7.25)$$

This value lies below the present value of the binding energy. Finally, the lithium likelihood function has the maximum at

$$Q_{Li} = (24.88 + 0.43 - 0.59) \times 10^9. \qquad (7.26)$$

The position of this maximum is compatible with the helium result.

The general likelihood function (7.23) is plotted in the lower panel in Fig. 4 The position of its maximum dif-fers only slightly from the position given by the helium likelihood function.

$$Q_{BBN} = (25.34 \pm 0.12) \times 10^9 \qquad (7.27)$$

It is interesting to compare the light element abun-dances for two values of the deuterium binding energies. In Fig. 5 we plotted the traditional curves for the light element abundances as a functions of η for two values of Q. The dotted lines in the figures correspond to a present value of $Q_{present} = 25.82 \times 10^9$ K, while the solid curves correspond to a new value $Q_{BBN} = 25.34 \times 10^9$ K. Clearly, the new value Q_{BBN} moves the curves closer to the data.

The result which we obtained may be presented as

$$\delta Q/Q = -0.019 \pm 0.005, \qquad (7.28)$$

where $\delta Q = Q_{BBN} - Q_{present}$. If we do not fix η and try to fit it simulaneously with Q we obtain

$$\delta Q/Q = -0.022 \pm 0.008, \eta = (6.51 + 0.77 - 0.66) \times 10^{-10}. \qquad (29)$$

The obtained η is fully compatible with the one measured by WMAP.

These values of $\delta Q/Q$ and η were obtained for high value of the helium mass fraction Y_p . If we use as an input the low value of Y_p from (6) we obtain

$$\delta Q/Q = -0.048 \pm 0.004, \qquad (7.30)$$

If we fit both $\delta Q/Q$ and η we obtain

$$\delta Q/Q = -0.059 \pm 0.007, \eta = (7.55 + 0.91 - 0.75) \times 10^{-10}. \qquad (31)$$

Finally if we use the value of Y_p for ^{4}He obtained using the whole sample of 14 points, with increased error bars, from Eq.(1), we obtain

$$\delta Q/Q = -0.033 \pm 0.006, \qquad (7.32)$$

and for $\delta Q/Q$ and η

$$\delta Q/Q = -0.042 \pm 0.009, \eta = (7.00 + 0.85 - 0.72) \times 10^{-10}. \qquad (33)$$

The results given in eqs.(28) and (30) therefore represent an estimate of the plausible range in $\delta Q/Q$. Despite the

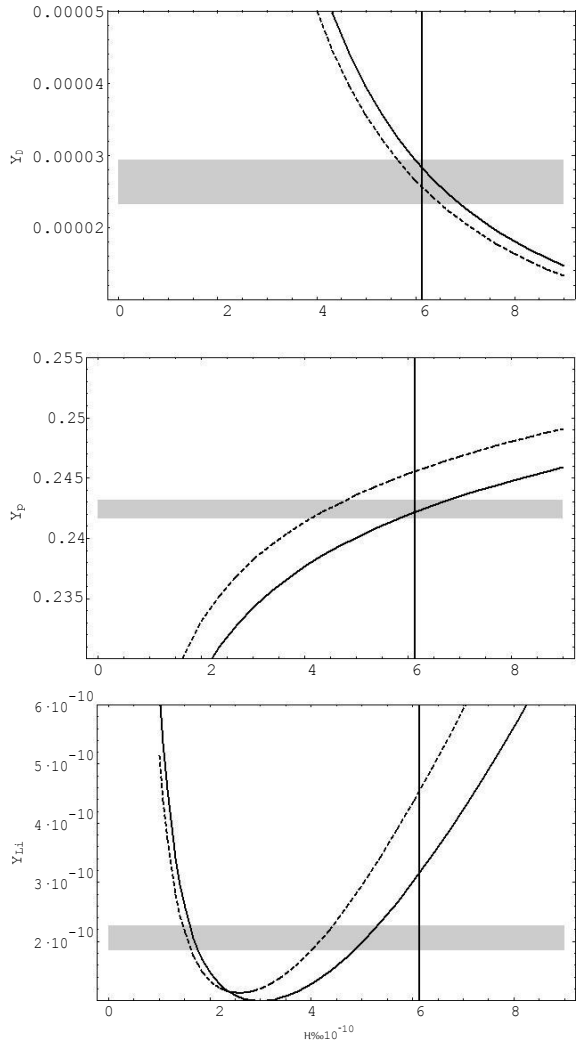

FIG. 5: The predicted light element abundance yields as a function of η, for two values of the deuteron binding energy, Q. The dotted curve corresponds to the present value of $Q_{\mathbf{present}} = 25.82 \times 10^9$ K. The solid curve corresponds to the new value of $Q = Q_{\mathbf{BBN}} = 25.34 \times 10^9$ K. The vertical line corresponds to $\eta = 6.14$ (WMAP value). The shaded regions is the 1σ-ranges for the observed light element abundances, where $Y_{\mathbf{p}}$ is from eq.5.

7

Combining eqs. (32) and (34) we obtain

$$\frac{\delta(m_s/\Lambda_{QCD})}{(m_s/\Lambda_{QCD})} = (1.1 \pm 0.3) \times 10^{-3} \quad (7.35)$$

This equation may contain an additional factor (close to one) reflecting unknown theoretical uncertainty in eq. (7.34). Note that we obtain here variation at the level 10^{-3} while the limits on variation of α [7.2, 48] and Λ_{QCD}/M_{plank} [7.2, 3] are an order of magnitude weaker. This may serve as a justification of our approach.

$$Y_p = 0.2393 \pm 0.0011 \quad \text{(BBN4DFW.1)}$$

$$Y_D = (2.63 \pm 0.31) \times 10^{-5}, \quad \text{(BBN4DFW.2)}$$

$$A = 2.315 \pm 0.051. \quad \text{(BBN4DFW.3)}$$

$$Y_{Li} = (2.02 \pm 0.22) \times 10^{-10}. \quad \text{(BBN4DFW.4)}$$

$$Y_p = 0.2424 \pm 0.0008. \quad \text{(BBN4DFW.5)}$$

$$Y_p = 0.2363 \pm 0.0008, \quad \text{(BBN4DFW.6)}$$

--

$$\frac{\dot{R}}{R} = H = \sqrt{\frac{8\pi}{3M_p^2}\rho_T}, \quad \text{(BBN4DFW.7)}$$

$$\frac{\dot{n}_b}{n_b} = -3H, \quad \text{(BBN4DFW.8)}$$

$$\dot{\rho}_T = -3H(\rho_T + p_T), \quad \text{(BBN4DFW.9)}$$

$$\dot{Y}_i = \sum_{j,k,l} N_i(\Gamma_{kl\to ij}\frac{Y_l^{N_l}Y_k^{N_k}}{N_l!N_k!} - \Gamma_{ij\to kl}\frac{Y_i^{N_i}Y_j^{N_j}}{N_i!N_j!}), \quad \text{(BBN4DFW.10)}$$

$$n_- - n_+ = \frac{n_B}{T^3}\sum_j Z_j Y_j, \quad \text{(BBN4DFW.11)}$$

$$N_i({}^{A_i}Z_i) + N_j({}^{A_j}Z_j) \leftrightarrow N_k({}^{A_k}Z_k) + N_l({}^{A_l}Z_l) \quad \text{(BBN4DFW.12)}$$

$$\rho_T = \rho_\gamma + \rho_e + \rho_\nu + \rho_B, \quad \text{(BBN4DFW.13)}$$

$$p_T = p_\gamma + p_e + p_\nu + p_B. \quad \text{(BBN4DFW.14)}$$

$$\frac{\delta\epsilon_\nu}{\sqrt{\epsilon_\nu}} = -\frac{\delta Q}{\sqrt{Q}}. \quad \text{(BBN4DFW.15)}$$

$$\sigma v \sim Q^{5/2}/\epsilon_\nu. \quad \text{(BBN4DFW.15.2)}$$

$$\Gamma_{np\to d\gamma} \to \Gamma_{np\to d\gamma}(1 + (5/2 + \sqrt{\frac{Q}{\epsilon_\nu}})\frac{\delta Q}{Q}). \quad \text{(BBN4DFW.16)}$$

$$Lf(\eta, Q) = \exp(-\frac{1}{2}\sum_{ij}(Y_i^{th}(\eta, Q) - Y_i^{ex})\omega_{ij} \times (Y_i^{th}(\eta, Q) - Y_j^{ex})). \quad \text{(BBN4DFW.17)}$$

--

$$\delta Y_i^{th} = Y_i^{th}\sum_k \lambda_{ik}\frac{\Delta R_k}{R_k}, \quad \text{(BBN4DFW.18)}$$

$$\lambda_{ik} = \frac{\partial \ln Y_i^{th}}{\partial \ln R_k} \quad \text{(BBN4DFW.18.2)}$$

-

$$\sigma_{ij}^2 = Y_i^{th}Y_j^{th}\sum_k \lambda_{ik}\lambda_{jk}\left(\frac{\Delta R_k}{R_k}\right)^2. \quad \text{(BBN4DFW.19)}$$

$$\sigma_i^{tot2} = \sigma_{ii}^2 + \sigma_i^{ex2}. \quad \text{(BBN4DFW.20)}$$

$$\omega_{ii} = 1/\sigma_i^{tot2}. \quad \text{(BBN4DFW.20.2)}$$

$$Y_i(\eta, Q) = Y_i^{ex} \quad \text{(BBN4DFW.21)}$$

$$(Y_i(\eta, Q) - Y_i^{ex})^2 = \sigma_i^{tot2} \quad \text{(BBN4DFW.22)}$$

--

$$\eta_0 = (6.14 \pm 0.25)\times 10^{10} \quad \text{(BBN4DFW.22.2)}$$

$$L(Q) = \int_{-\infty}^{+\infty} \exp\left(-\frac{(\eta-\eta_0)^2}{2\sigma_\eta^2}\right) Lf(\eta, Q)d\eta. \qquad \text{(BBN4DFW.23)}$$

$$Q_D = (25.74 + 0.92 - 0.68)\times 10^9. \qquad \text{(BBN4DFW.24)}$$

--

$$Q_{He} = (25.37 \pm 0.13)\times 10^9. \qquad \text{(BBN4DFW.25)}$$

$$Q_{Li} = (24.88 + 0.43 - 0.59)\times 10^9. \qquad \text{(BBN4DFW.26)}$$

$$Q_{BBN} = (25.34 \pm 0.12)\times 10^9 \qquad \text{(BBN4DFW.27)}$$

$$\delta Q/Q = -0.019 \pm 0.005, \qquad \text{(BBN4DFW.28)}$$

$$\delta Q/Q = -0.022 \pm 0.008, \eta = (6.51 + 0.77 - 0.66)\times 10^{-10}. \qquad \text{(BBN4DFW.29)}$$

$$\delta Q/Q = -0.048 \pm 0.004, \qquad \text{(BBN4DFW.30)}$$

$$\delta Q/Q = -0.022 \pm 0.007, \eta = (7.55 + 0.91 - 0.75)\times 10^{10}. \qquad \text{(BBN4DFW.31)}$$

$$\delta Q/Q = -0.033 \pm 0.006, \qquad \text{(BBN4DFW.32)}$$

$$\delta Q/Q = -0.042 \pm 0.009, \eta = (7.00 + 0.85 - 0.72)\times 10^{10}. \qquad \text{(BBN4DFW.33)}$$

--

$$\frac{\delta(Q/\Lambda_{QCD})}{Q/\Lambda_{QCD}} = -17\frac{\delta(m_s/\Lambda_{QCD})}{m_s/\Lambda_{QCD}} \qquad \text{(BBN4DFW.34)}$$

-

$$\frac{\delta(m_s/\Lambda_{QCD})}{m_s/\Lambda_{QCD}} = (1.1 \pm 0.3)\times 10^{-3} \qquad \text{(BBN4DFW.35)}$$

--

$$\delta U_\lambda(r) = \lambda(U_0(r) - U_t(r)), \qquad \text{(BBN4DFW.35.2)}$$

$$\frac{dE}{d\lambda} = \int_0^\infty (U_0(r) - U_t(r))\chi^2(r)dr, \qquad \text{(BBN4DFW.36)}$$

$$\int_0^R \chi^2(r)dr + b^2\int_R^\infty e^{-2\gamma r}dr = 1, \qquad \text{(BBN4DFW.37)}$$

$$\frac{dE}{\sqrt{|E|}} = d\lambda 2\sqrt{\frac{m_p}{h^2}}\int_0^\infty (U_0(r) - U_t(r))\,\tilde{\chi}^2(r)dr, \qquad \text{(BBN4DFW.38)}$$

-

$$Q = \frac{m_p}{h^2}\left(\int_0^\infty (U_0(r) - U_t(r)\,\chi^2(\tilde{r})dr\right)^2. \qquad \text{(BBN4DFW.39)}$$

$$\epsilon_v = \frac{m_p}{h^2}\left(\int_0^\infty (U_0(r) - U_s(r)\,\chi^2(\tilde{r})dr\right)^2, \qquad \text{(BBN4DFW.40)}$$

$$\frac{\delta\epsilon_v}{\sqrt{\epsilon_v}} = -\frac{\delta Q}{\sqrt{Q}}. \qquad \text{(BBN4DFW.41)}$$

Chapter 9

Searching for dark matter and variation of fundamental constants with laser and maser interferometry

Any slight variations in the fundamental constants of Nature, which may be induced by dark matter or some yet-to-be-discovered cosmic field, would characteristically alter the phase of a light beam inside an interferometer, which can be measured extremely precisely. Laser and maser interferometry may be applied to searches for the linear-in-time drift of the fundamental constants, detection of topological defect dark matter through transient-in-time effects and for a relic, coherently oscillating condensate, which consists of scalar dark matter fields, through oscillating effects. Our proposed experiments require either minor or no modifications of existing apparatus, and offer extensive reach into important and unconstrained spaces of physical parameters.

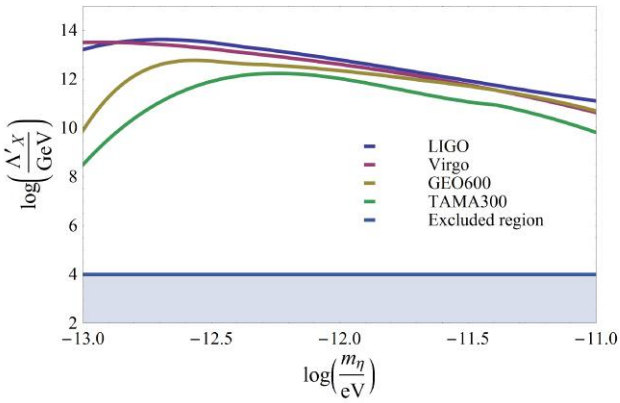

The idea that the fundamental constants of Nature might vary with time can be traced as far back as the large numbers hypothesis of Dirac, who hypothesized that the gravitational constant G might be proportional to the reciprocal of the age of the Universe [8.1]. More contemporary theories predict that the fundamental constants vary on cosmological timescales (see e.g. [8.2{4]). Astronomical observations of quasar absorption spectra hint at the existence of a spatial gradient in the value of the _ne-structure constant, _ = e2=~c [8.5, 6]. Data samples from the Keck Telescope and Very Large Telescope [8.7, 8] independently agree on the direction and magnitude of this gradient, which is significant at the 4:2_ level. A consequence of this astronomical result is that, since the solar system is moving along this spatial

gradient, there should exist a corresponding temporal shift in _ in Earth's frame of reference at the level __=_ _ 10^-19/yr [8.9]. Finding this variation with laboratory experiments could independently corroborate the astronomical result. To date, atomic clocks have provided the most sensitive laboratory limit on annual variations in _: __=_ . 10^-17/yr [8.10]. The question of dark matter (DM), namely its identity, properties and non-gravitational interactions, remains one of the most important unsolved problems in physics. Various DM candidates and searches therefor have been proposed over the years [8.11]. One such candidate is the axion, a pseudoscalar particle which was originally introduced in order to resolve the strong CP problem of Quantum Chromodynamics (QCD) [12, 13] (see also [8.14{17]). The axion is believed to have formed a condensate in the early Universe [8.18]. This relic axion condensate can be sought for through a variety of distinctive signatures (see e.g. [8.19{26]). Likewise, a condensate consisting of a scalar DM particle may also have formed. The scalar field _ comprising this condensate oscillates with frequency ! _ m_c2=~ and may couple to the fermion fields:

$$\mathcal{L}^{f}_{\text{int}} = -\sum_{f=e,p,n} \eta_0 \cos(m_\eta c^2 t/\hbar) \frac{m_f c^2}{\Lambda_f} \bar{f} f, \tag{1}$$

$$\mathcal{L}^{\gamma}_{\text{int}} = \frac{\eta_0 \cos(m_\eta c^2 t/\hbar)}{4\Lambda_\gamma} F_{\mu\nu} F^{\mu\nu}, \tag{2}$$

F is the electromagnetic _eld tensor. _X is a large energy scale, which from gravitational tests is constrained to be _X _ 1021 GeV [8.27]. Eqs. (8.1) and (8.2) alter the fundamental constants in an oscillating manner as follows, respectively:

$$m_f \to m_f \left[1 + \frac{\eta_0 \cos(m_\eta c^2 t/\hbar)}{\Lambda_f} \right], \tag{3}$$

$$\alpha \to \frac{\alpha}{1 - \eta_0 \cos(m_\eta c^2 t/\hbar)/\Lambda_\gamma} \simeq \alpha \left[1 + \frac{\eta_0 \cos(m_\eta c^2 t/\hbar)}{\Lambda_\gamma}\right]. \tag{4}$$

Quadratic couplings in _, with the replacement X is a less strongly constrained energy scale, with constraints from laboratory and astrophysical observations given by _0 X _ 10^4 GeV [8.28]. We note that the quadratic portal gives rise to not only oscillating effects, but may also lead to non-oscillating space-time variation of the fundamental constants: _X=X = _2 0=2(_0X)2, which arises due to space-time variations in. These effects may be sought for using terrestrial experiments (atomic clocks, Oklo natural nuclear reactor, and laser/maser interferometry as suggested in this paper) and astrophysical observations (quasars, white dwarves, Big Bang Nucleosynthesis, Cosmic Microwave Background measurements). Another possible DM candidate is topological defect DM, which is a stable non-trivial form of DM that consists of light DM fields and is stabilised by a self-interaction potential [8.29] (self-gravitating DM fields can also form solitons, see e.g. Ref. [8.30]). These objects may have various dimensionalities: 0D (monopoles), 1D (strings) or 2D (domain walls). The transverse size of a topological defect depends on the mass of the particle comprising the defect, d _ ~=m_c, which may be large (macroscopic or galactic) for a sufficiently light DM particle. The light DM particle comprising a topological defect can be either a scalar, pseudoscalar or vector particle. Recent proposals for pseudoscalar-type defect searches include using a global network of magnetometers to search for correlated transient spin preces-sion effects [8.31] and electric dipole moments [8.32] that arise from the coupling of the scalar field derivative to the fermion axial vector currents. Recent proposals for scalar-type defect searches include using a global net-work of atomic clocks [8.27], and Earth rotation and pul-sar timing [8.32], to search for transient-in-time alterations of the system frequencies due to transient-in-time variation of the fundamental constants that arise from the couplings of the scalar field to the fermion and photon fields. The best current sensitivities for transient-in-time variations of the fundamental constants on the time scale of t _ 1 □ 100 s with terrestrial experiments are offered by atomic clocks, with an optical/optical clock combination [33, 34] sensitive to variations in _:

__=_ _ 10□15□10□16 and a hyperfine/optical clock combination [35] to variations in the electron-to-proton mass ratio me=mp: _(me=mp)=(me=mp) _ 10□13 □ 10□14. There are many possibilities for the interactions of topological defect DM particles with the Standard Model particles. Here we consider couplings with a quadratic dependence on the scalar field, which were considered previously in Refs. [8.27, 32]. A scalar dark matter _field _ may interact with fermions via the coupling:

$$\mathcal{L}_{\rm int}^{f} = -\sum_{f=e,p,n} m_f \left(\frac{\phi c}{\Lambda'_f}\right)^2 \bar{f} f, \tag{5}$$

and with photons via the coupling:

$$\mathcal{L}_{\rm int}^{\gamma} = \left(\frac{\phi}{\Lambda'_\gamma}\right)^2 \frac{F_{\mu\nu}F^{\mu\nu}}{4}, \tag{6}$$

Eqs. (8.5) and (8.6) alter the fundamental constants in a transient manner as follows, respectively:

$$m_f \to m_f \left[1 + \left(\frac{\phi}{\Lambda'_f}\right)^2\right], \tag{7}$$

$$\alpha \to \frac{\alpha}{1-(\phi/\Lambda'_\gamma)^2} \simeq \alpha \left[1 + \left(\frac{\phi}{\Lambda'_\gamma}\right)^2\right]. \tag{8}$$

In the present work, we point out that laser and maser interferometry may be used as particularly sensitive probes to search for linear-in-time, oscillating and transient

variations of the fundamental constants of Nature, including _ and me=mp. Laser and maser interferometry are very well established techniques and have already proven to be extremely sensitive probes for exotic new physics, including searches for the aether, tests of Lorentz symmetry [8.36] and gravitational wave detection [8.37]. Laser interferometry has also recently been proposed for the detection of dilaton dark matter [8.38]. We consider the use of an interferometer with two arms of lengths L1 and L2, for which the observable is the phase difference __ = !_L=c between the two split beams, where ! is the reference frequency and _L = L1 □L2. In the absence of any variation of fundamental constants, the two split beams interfere destructively (__ = (2N + 1)_, where N is an integer). In the presence of variation of the fundamental constants, the reference frequency changes, as do the arm lengths, due to changes in the sizes of the atoms, which make up the arms. Depending on the type of laser or maser, as well as the arm lengths and materials used, the net result may be a change in the phase difference, _(__). Consider the simpler case when a laser/maser with-out a resonator is used, for example, the nitrogen laser operating on the 3_u ! 3_g electronic transition and superradiant Raman lasers [8.39{41]. In this case, ! is determined entirely by the specific atomic/molecular transition, the simplest archetypes of which are the electronic Rydberg me=mpMr) and rotational (! _(e2=aB~)(me=mpMr)) transitions, where _ is the relevant nuclear magnetic dipole moment, Krel is the derivative of the hyperfine relativistic (Casimir) correction factor with respect to _, and mpMr is the relevant reduced mass. The sensitivity coefficients KX are defined by:

$$\frac{\delta(\Delta\Phi)}{\Delta\Phi} = \sum_{X=\alpha, m_e/m_p, m_q/\Lambda_{\mathrm{QCD}}} K_X \frac{\delta X}{X}, \qquad (9)$$

where mq is the quark mass and Λ_QCD is the QCD scale, and are given in Table I for several archetypal transitions,

where we have made use of the relation _(_L)=_L _ _aB=aB for _L 6= 0 (aB is the Bohr radius). Since _(__) is proportional to __, a higher laser frequency gives a larger effect. Note that, unlike atomic clock experiments [8.10, 45, 46] and astrophysical observations [8.5, 7, 47] that search for a variation in the fundamental constants, in which two di_erent transition lines are required to form the

dimensionless ratio !A=!B, laser/maser interferometry can in principle be performed with only a single line, since the observable __ is a dimensionless parameter by itself.

TABLE I. Sensitivity coe_cients for _, me=mp and mq=_QCD for a laser or maser without a resonator and operating on typical atomic and molecular transitions. The values of Krel and Kmq=_QCD for 87Rb and 133Cs have been taken from [8.42] (see also Refs. [8.43, 44]).

Treating variations in frequencies (which depend only on the fundamental constants) and lengths independently (for variations in the latter may also arise due to undesired effects), we find

$$\delta X = \frac{c\left[\omega_A \delta(\Delta\Phi_B) - \omega_B \delta(\Delta\Phi_A)\right]}{\Delta L\left(\omega_A \frac{\partial \omega_B}{\partial X} - \omega_B \frac{\partial \omega_A}{\partial X}\right)}, \quad (10)$$

X is a particular fundamental constant. In particular, we note that shifts in the arm lengths do not ap-pear in Eq. (8.10), meaning that undesirable e_ects, such as seismic noise or tidal e_ects, are not observed with this
setup and high precision may in principle be attained for low-frequency (large timescale) e_ects. This is quite dis-tinct from conventional interferometer searches for gravi-tational waves, which have comparatively low sensitivity to low-frequency e_ects, since in this case deviations in arm lengths are sought explicitly and low-frequency sys-tematic e_ects greatly reduce the sensitivity of the appa-ratus in this region. Consider now the case when a laser/maser containing a resonator is used, for instance, the Nd:YAG solid-state laser. In this case, ! is determined by the length of the resonator, which changes if the fundamental constants change. In the non-relativistic limit, the wavelength and _L (as well as the size of Earth) have the same depen-dence on the Bohr radius and so there are no observ-able e_ects if changes of the fundamental constants are slow (adiabatic). Indeed, this may be viewed as a sim-ple change in the measurement units. Transient e_ects due to topological defect DM passage may still produce e_ects, since changes in ! and _L may occur at dif-ferent times. We note that a global terrestrial network (LIGO, Virgo, GEO600 and TAMA300) or a space-based network of interferometers (LISA) are particularly well

suited to search for topological defects through the cor-related e_ects induced by defects. Likewise, temporal correlations of homogeneous e_ects (including linear-in-time and oscillating e_ects) produced in several di_erent interferomers can also be sought for. The sensitivity of interferometry to non-transient ef-fects is determined by relativistic corrections, which we estimate as follows. The size of an atom R is determined by the classical turning point of an external atomic elec-tron. Assuming that the centrifugal term _ 1=R2 is small at large distances, we obtain (Zi + 1)e2=R = jEj.

E is the energy of the external electron and Zi is the net charge of the atomic species (for a neutral atom Zi = 0). This gives the relation: _R=R = □_jEj=jEj. The single-particle relativistic correction to the energy in a many-electron atomic species is given by [8.48]:

$$\Delta_n \simeq E_n \frac{(Z\alpha)^2}{\nu(j+1/2)}, \quad (11)$$

where En = □mee4(Zi + 1)2=2~2_2 is the energy of the external atomic electron, j is its angular momentum, Z is the nuclear charge, and _ _ 1 is the e_ective principal quantum number. The corresponding sensitivity coefficient in this case is

$$K_\alpha = 2\alpha^2 \left[\frac{Z_{\rm res}^2}{\nu_{\rm res}(j_{\rm res}+1/2)} - \frac{Z_{\rm arm}^2}{\nu_{\rm arm}(j_{\rm arm}+1/2)} \right] \quad (12)$$

Note that the sensitivity coe_cient depends particularly
strongly on the factor Z2. jK_j _ 1 for light atoms and may be of the order of unity in heavy atoms. Further-more, the arms of di_erent length can also be replaced by two arms (of the same length) made from di_erent materials, for which the coe_cients Z2=_(j + 1=2) are di_erent. We estimate the sensitivity to variations in me=mp from the di_erences in the internuclear separations in molecular H2 and D2, which are 0:74144 _A and 0:74152 _A, respectively [49]. These data give: _R=R _ □10□4 _(me=mp)=(me=mp). Since only di_erences in the coe_cients of proportionality for

the arm and resonator are observable in principle, the corresponding sensitivity coe_cient is therefore Kme=mp.

Note that for a slow variation of fundamental constants (which includes linear-in-time e_ects, transient e_ects due to a slowly moving and/or large topological defect, and low-frequency oscillating e_ects), the laser/maser resonator may be locked to an atomic/molecular fre-quency. In these cases, the sensitivity coe_cients will be the same as those for the case in which a laser/maser without a resonator is used. We estimate the sensitivity of laser and maser interfer-ometry to e_ects stemming from a relic, coherently os-cillating condensate, which consists of scalar DM _elds. The typical spread in the oscillation frequencies of the scalar DM particles, which make up the condensate, is given by 2m_v2=m_c2) _ (v2=c2), where a virial velocity of v _ 10□3c would be typical in our local Galactic neighbourhood. From the strain sensi-tivity curves of various interferometers [50{52], and as-suming that the condensate consisting of a scalar DM particle saturates the known local cold DM content, _c2=2~2 _ 0:4 GeV/cm3, we arrive at the accessi-ble region of parameter space shown in Fig. 1, in which we assume the use of a laser without a resonator. The region of parameter space accessible by the recently con-structed Fermilab Holometer (L = 40 m) [53] is expected to be similar to those accessible by the interferometers as shown in Fig. 1, but shifted toward higher scalar DM masses by several orders of magnitude.

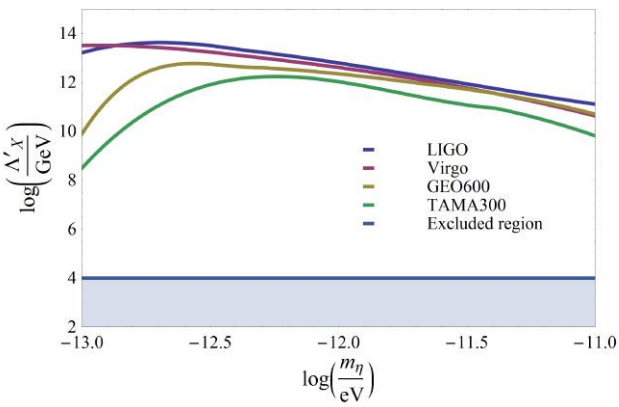

FIG. 1. (Color online) Region of dark matter parameter space accessible by various interferometers. The shaded blue region corresponds to the region of parameter space excluded by ex-isting laboratory and astrophysical observations [8.28]. Finally, we

estimate the sensitivity of laser and maser interferometry to e_ects stemming from topological de-fects, which consist of scalar DM _elds, using the simple model of a domain wall with a Gaussian cross-sectional pro_le of root-mean-square width d. The simplest do-main wall direction of incidence to consider (which pro duces non-zero e_ects) is directly along one of the inter-ferometer arms (towards the laser ource, without loss of generality). Neglecting relativistic e_ects and assuming the use of a resonator-based laser, the time-domain signal is given by

$$\frac{\delta[\Delta\Phi(t)]}{\Delta\Phi} = \frac{\rho_{\rm TDM} v \tau d \hbar c}{(\Lambda'_X)^2} \cdot \left\{ \frac{d\sqrt{\pi}}{2L} \left[\mathrm{erf}\left(\frac{L+tv}{d}\right) - \mathrm{erf}\left(\frac{tv}{d}\right) \right] - \exp\left(\frac{-t^2 v^2}{d^2}\right) \right\}, \tag{13}$$

_TDM is the energy density associated with a topological defect network, v is the typical speed of a defect, _ is the average time between encounters of a system with defect objects, and erf is the standard er-ror function. Cosmological models of topological defect DM have su_cient exibility for topological defects to be the dominant contributor to the total DM content of the universe [8.27]. For the purposes of estimating the sensi-tivity of laser interferometers to topological defects, we may hence assume _TDM _ 0:4 GeV/cm3. Also, from hints o_ered by pulsar timing data in relation to the pul-sar glitch phenomenon [8.32], we assume _ _ 1 year. The power spectrum corresponding to the time-domain signal in Eq. (8.13) is given by

$$\left|\frac{\delta[\Delta\Phi(f)]}{\Delta\Phi}\right|^2 \approx \frac{\rho_{\rm TDM}^2 v^2 \tau^2 d^4 \hbar^2 c^2}{16\pi(\Lambda'_X)^4} \cdot \left| \frac{i e^{-\frac{\pi f\left(\pi d^2 f + 4idv - 2iLv\right)}{v^2}}}{fL} \left[\mathrm{erf}\left(\frac{L}{d}+2\right) e^{\frac{\pi f\left(\pi d^2 f - 2iLv\right)}{v^2}} - e^{\frac{4i\pi df}{v}} \mathrm{erf}\left(\frac{i\pi df}{v} + \frac{L}{d} + 2\right) \right.\right.$$
$$+\mathrm{erf}(2) e^{\frac{\pi df(\pi df + 8iv)}{v^2}} + e^{\frac{4i\pi df}{v}} \mathrm{erf}\left(\frac{i\pi df}{v} - 2\right)\Big] - \frac{2\pi e^{-\frac{\pi^2 d^2 f^2}{v^2}}}{v} \left[\mathrm{erf}\left(-\frac{i\pi df}{v} + \frac{L}{d} + 2\right) + \mathrm{erf}\left(2 + \frac{i\pi df}{v}\right) \right]$$
$$\left. - \frac{i e^{-\frac{\pi df(\pi df + 4iv)}{v^2}}}{fL} \left[\mathrm{erf}(2) e^{\frac{\pi^2 d^2 f^2}{v^2}} + \mathrm{erf}\left(\frac{L}{d}+2\right) e^{\frac{\pi f\left(\pi d^2 f + 8idv + 2iLv\right)}{v^2}} - e^{\frac{4i\pi df}{v}} \mathrm{erf}\left(-\frac{i\pi df}{v} + \frac{L}{d} + 2\right) - e^{\frac{4i\pi df}{v}} \mathrm{erf}\left(2 + \frac{i\pi df}{v}\right) \right] \right|^2, \tag{14}$$

with the following asymptotic limit when d _ L:

$$\left|\frac{\delta[\Delta\Phi(f)]}{\Delta\Phi}\right|^2 \sim \frac{\pi^3 \rho_{\rm TDM}^2 \tau^2 d^4 L^2 f^2 \hbar^2 c^2 \exp\left(\frac{-2\pi^2 f^2 d^2}{v^2}\right)}{(\Lambda'_X)^4 v^2}. \tag{15}$$

From the power spectrum in (14), the plots for which are presented for interferometers of various sizes in the Supplemental Material, and the strain sensitivity curves of these interferometers [50{52], we arrive at the accessible region of parameter space shown in Fig. 2. We note that the sensitivity of interferometers drops rapidly with increasing values of d when d & L. For instance, for a LIGO interferometer (L = 4 km), the sensitivity to de-fects with d = 40 km is _0 X . 10□4 GeV. The region of parameter space accessible by the Fermilab Holometer [53] is expected to be similar to those accessible by the interferometers as shown in Fig. 2, but with a rapid drop in sensitivity occurring for d & 100 m. We hence suggest the use of laser and maser in-terferometry as particularly sensitive probes to search for linear-in-time, oscillating and transient variations of the fundamental constants of Nature, including _ and me=mp. Our proposed experiments require either minor or no modifications of existing apparatus, and offer extensive reach into important and unconstrained spaces of physical parameters. We note that oscillating variation of fundamental constants due to a scalar condensate may also be sought for using tomic clocks.

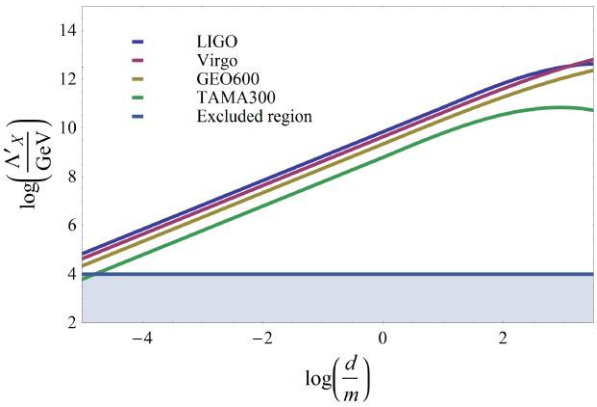

FIG. 2. (Color online) Region of dark matter parameter space accessible by various interferometers. The shaded blue region corresponds to the region of parameter space excluded by ex-isting laboratory and astrophysical observations [8.28].

SUPPLEMENTAL MATERIAL

We present the power spectra produced by a domain wall with a Gaussian cross-sectional pro_le of root-mean-square width d, passing directly along one of the arms of a Michelson Morley interferometer. The asymptotic case d _ L can be summarised by a single plot in the
combined variable fd (Fig. 3). The plots in the general case d . L are shown for the LIGO, Virgo, GEO600,TAMA300 and Fermilab Holometer interferometers in Figs. 4, 5, 6, 7 and 8, respectively. FIG. 3. (Color online) Power spectrum [in units_2 TDML2_ 2d2~2c2_3=(_0X)4v2_(m/s)2] versus fd, produced by a domain wall with a Gaussian cross-sectional pro_le passing directly along one of the arms of a Michelson-Morley interferometer with arms of equal length L.

7

FIG. 4. (Color online) Power spectra [in units _2TDM_ 2v2d2~2c2=(_0X)4_s2] versus frequency, produced by a domain wall with a Gaussian cross-sectional pro_le passing directly along one of the arms of a LIGO interferometer (L = 4 km). From left to right: d = 1 m, d = 10 m, d = 100 m, d = 1000 m, d = 4000 m. FIG. 5. (Color online) Power spectra [in units _2TDM_ 2v2d2~2c2=(_0X)4_s2] versus frequency, produced by a domain wall with a Gaussian cross-sectional pro_le passing directly along one of the arms of a Virgo interferometer (L = 3 km). From left to right: d = 1 m, d = 10 m, d = 100 m, d = 1000 m, d = 3000 m.

8

FIG. 6. (Color online) Power spectra [in units _2TDM_ 2v2d2~2c2=(_0X)4_s2] versus frequency, produced by a domain wall with a Gaussian cross-sectional pro_le passing directly along one of the arms of a GEO600 interferometer (L = 600 m). From left to right: d = 1 m, d = 10 m, d = 100 m, d = 600 m.
FIG. 7. (Color online) Power spectra [in units _2TDM_ 2v2d2~2c2=(_0X)4_s2] versus frequency, produced by a domain wall with a Gaussian cross-sectional pro_le passing directly along one of the arms of a TAMA300 interferometer (L = 300 m). From left to right: d = 1 m, d = 10 m, d = 100 m, d = 300 m.

9

FIG. 8. (Color online) Power spectra [in units _2TDM_ 2v2d2~2c2=(_0X)4_s2] versus frequency, produced by a domain wall with a Gaussian cross-sectional pro_le

passing directly along one of the arms of a Fermilab Holometer interferometer (L = 40 m). From left to right: d = 0:1 m, d = 1 m, d = 10 m, d = 40 m.

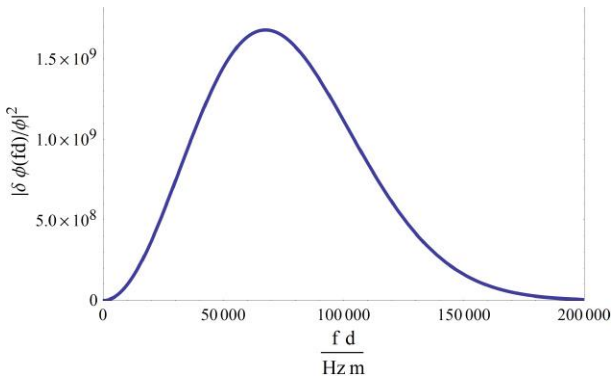

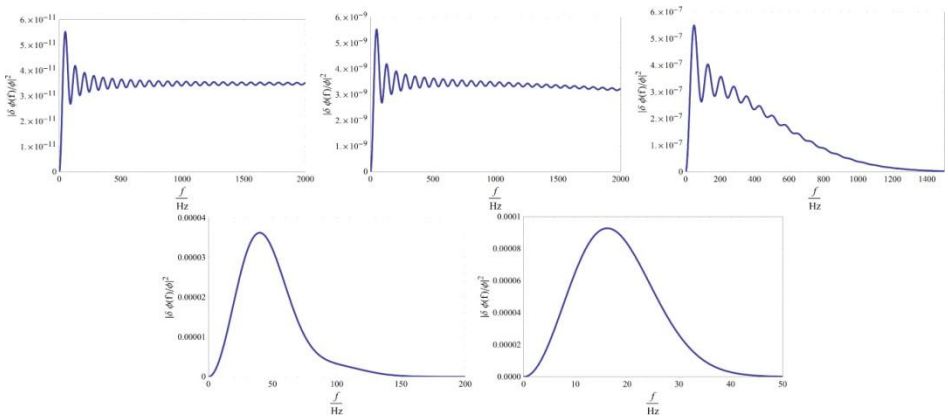

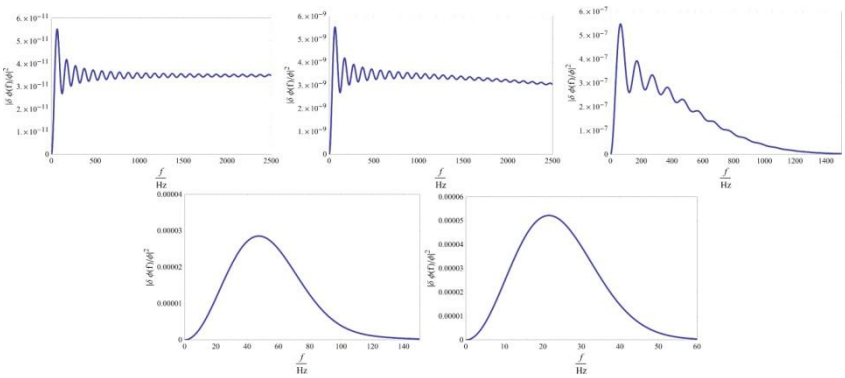

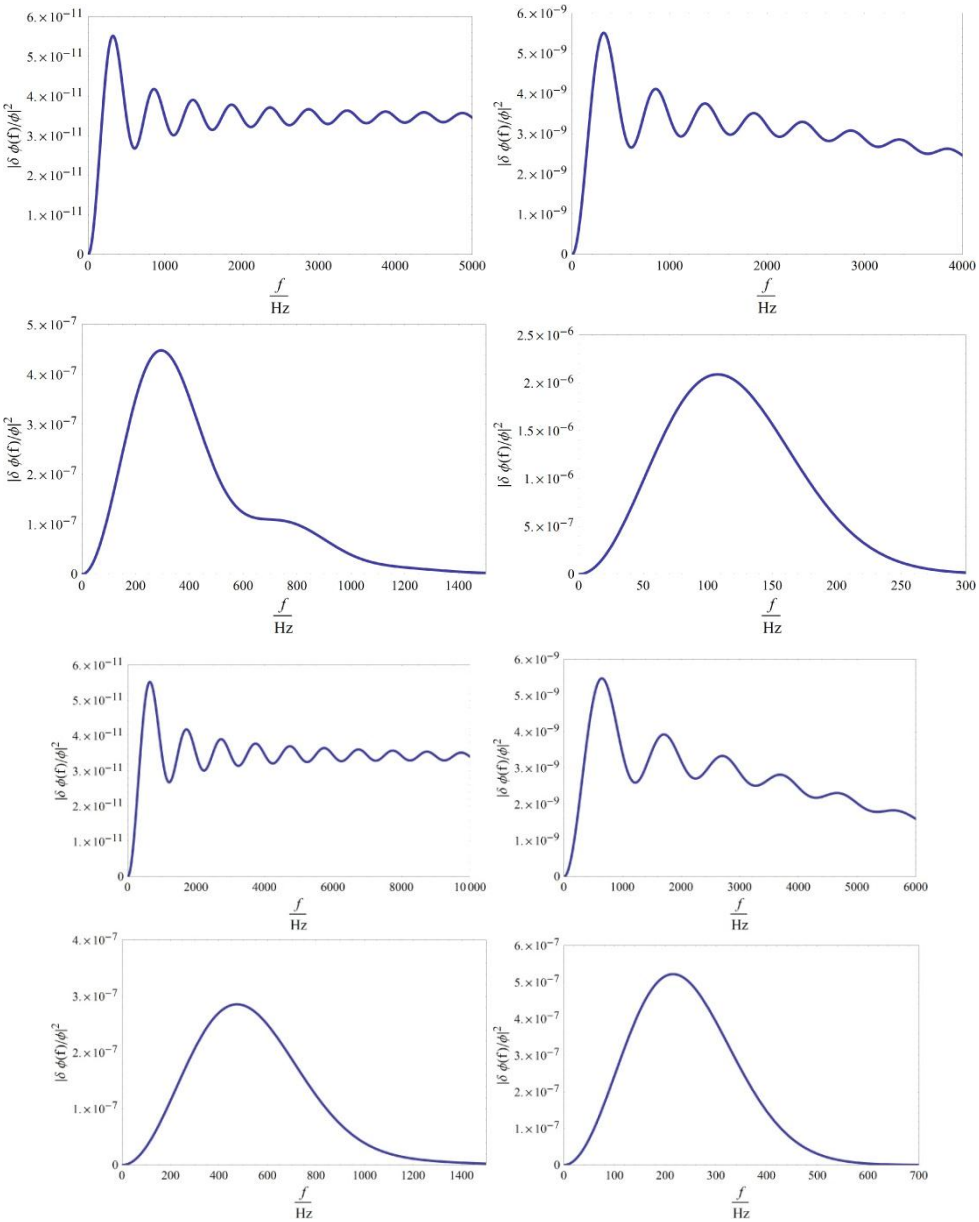
|δ ϕ(f)/ϕ|²
f/Hz

9

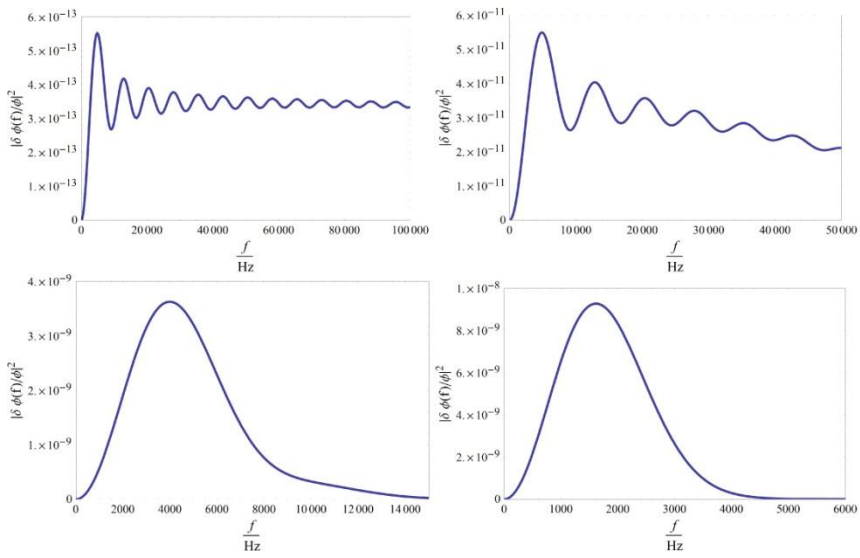

Chapter 10

Observations

Thee Sigma Rule

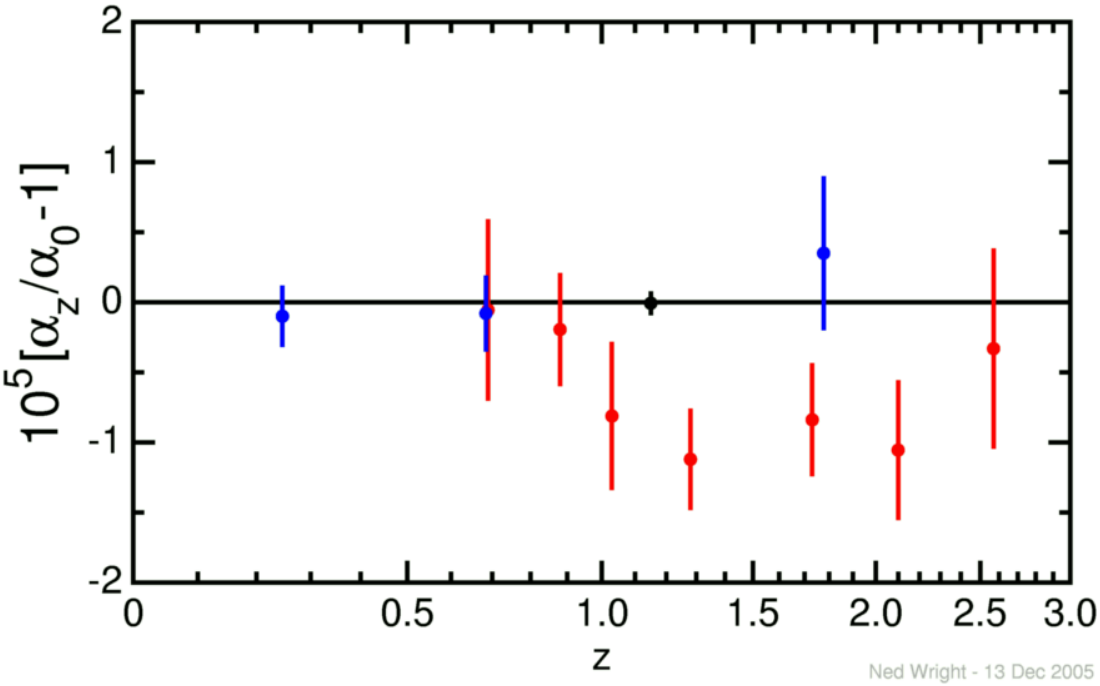

Keck/HIRES spectra

The data used here were kindly provided in reduced form by Jason X. Prochaska and Arthur M. Wolfe and are detailed in Prochaska & Wolfe (1996, 1997, 1999). Outram et al. (1999) have also kindly contributed their spectrum of Q 1759+75 taken in July 1997. Here we provide only a brief description of the observations and data reduction, deferring a more detailed discussion to Section 3-3.1.2.

All the QSO spectra were obtained at the Keck I 10-m telescope on Mauna Kea with the HIRES facility (Vogt et al. 1994) over several observing runs from 1994 to 1997. The QSOs were generally quite faint (mV $\lesssim$ 19:0) so several $\sim$1-2 hour exposures were co-added for each object. Most of the data were reduced using the HIRES data reduction package written by T. Barlow, MAKEE. This package converts the two-dimensional echelle images to fully reduced, one-dimensional, wavelength-calibrated spectra.

Thorium-argon (ThAr) spectra were taken before and after the QSO exposures and co-added to provide a calibration spectrum. ThAr lines were selected and centroided to form the wavelength solution. Some of the QSO spectra were reduced when MAKEE had no wavelength calibration facility. In these cases, wavelength calibration was carried out using IRAF routines. Spectra not reduced in MAKEE were fully reduced within IRAF. 1σ error arrays were generated assuming Poisson counting statistics. We fitted continua to regions of each spectrum containing either

or both of the Si IV doublet transitions by fitting Legendre polynomials to $\sim$500 kms^{-1} sections

The sample comprises 21 Si IV absorption systems (towards 8 QSOs) over a redshift range z = 2.0-3.1 (mean redshift (Z_{abs}) = 2.6). The S/N per pixel ranges from 15-40 with most spectra having S=N $\sim$ 30 and FWHM $\lesssim$ 7:5 kms^{-1} (R = 34000). We provide an example absorption system in Fig. 2.1. We plot all 21 absorption systems in the Appendix.

Analysis

Although equation 2.1 is a simple approach to the specific case of an alkali doublet, a more general approach is to write down the energy equation for any individual transition, within any multiplet and for any species. Dzuba et al. (1999a,b) and Webb et al. (1999) suggested the convenient formulation

$$\omega_z = \omega_0 + q_1 x_z + q_2 y_z, \qquad (2.3)$$

where ω_z is the wavenumber in the rest-frame of the cloud, at redshift z, in which α_z/α_0 may not equal unity. ω_0 is the wavenumber as measured in the laboratory and x_z and y_z contain the information about $\triangle_{\alpha/\alpha}$:

$$x_z \equiv (\alpha_z/\alpha_0)^2 - 1 \text{ and } y_z \equiv (\alpha_z/\alpha_0)^4 - 1 \qquad (2.4)$$

The q_1 and q_2 coefficients represent the relativistic corrections to the energy for a particular transition. The q_1 coefficients are typically an order of magnitude larger than the q_2 coefficients and so it is the relative magnitudes of q_1 for different transitions.

Conclusions

In this paper we present new refined calculations of the parameters q, which determine α-dependence of the transition frequencies for a number of ions used in the astrophysical search for α-variation. These ions appear to be very different from the theoretical point of view. Because of that we had to use different methods and dif-ferent levels of approximation for them. The final accu-racy of our results differs not only for different ions, but also for different transitions.

The simplest system is Zn II, which has one valence electron. On the other hand, this is the heaviest ion and it has the largest core, which includes $3d^{10}$-shell. That gave us the opportunity to study corrections to q from the core-valence correlations and from Breit interaction. We found the former to be about 17% and the latter to be less than 1%. For lighter ions Breit interaction should be even smaller and can be safely neglected. Other ions also have much smaller and more rigid cores, so one might expect that core-valence correlations are few times weaker there in comparison to Zn. That allows us to neglect core-valence correlations for all other ions discussed in this paper.

Si II has the smallest core $1s^2 \ldots 2p^6$ and three valence electrons. For neutral Mg, which has the same core, the core-valence corrections to the 3s → 3p transition frequencies were found to be about 4% [33, 36]. CI calculation for Si II is relatively simple and the errors associated with incompleteness of CI space are small. Thus, our estimate of the accuracy for Si on 6% level seems to be rather conservative.

Cr, Fe, and Ni have the core $1s^2 \ldots 3p^6$ and the core excitation energy varies from 2 a.u. for Cr II to 2.6 a.u. for Ni II. In comparison, the core excitation energy for Zn II is 0.9 a.u. Therefore, we estimate the core-valence correlation corrections for these ions to be at least two times smaller, than for Zn II.

Additional error here is associated with incomplete-ness of the CI space. These ions have from 5 to 9 valence electrons and CI space cannot be saturated. To estimate corresponding uncertainty we performed several calculations for each ion

using different basis sets and two different computer packages described in Sec. II. The basic Dirac-Hartree-Fock orbitals were calculated for different configurations (for example, for the ground state configuration and for excited state configuration, etc.).

Supplementary information on the accuracy of our calculations can be obtained from comparison of calculated spectra and g-factors with experimental values. The later appear to be very important as they give information about electron coupling, which depends on relativistic corrections and on interaction between LS-multiplets. Our results for Cr II appear to be very close for different calculations and are in good agreement with the experiment both in terms of the gross level structure and spin-orbit splittings (see Table IV), so we estimate our final error here to be about 10 – 12%.

In this paper we present new refined calculations of the parameters q, which determine α-dependence of the transition frequencies for a number of ions used in the astrophysical search for α-variation. These ions appear to be very different from the theoretical point of view. Because of that we had to use different methods and dif-ferent levels of approximation for them. The final accu-racy of our results differs not only for different ions, but also for different transitions.

The simplest system is Zn II, which has one valence electron. On the other hand, this is the heaviest ion and it has the largest core, which includes $3d^{10}$-shell. That gave us the opportunity to study corrections to q from the core-valence correlations and from Breit interaction. We found the former to be about 17% and the latter to be less than 1%. For lighter ions Breit interaction should be even smaller and can be safely neglected. Other ions also have much smaller and more rigid cores, so one might expect that core-valence correlations are few times weaker there in comparison to Zn. That allows us to neglect core-valence correlations for all other ions discussed in this paper.

Si II has the smallest core $1s^2 \ldots 2p^6$ and three valence electrons. For neutral Mg, which has the same core, the core-valence corrections to the 3s → 3p transition

frequencies were found to be about 4% [33, 36]. CI calculation for Si II is relatively simple and the errors associated with incompleteness of CI space are small. Thus, our estimate of the accuracy for Si on 6% level seems to be rather conservative.

Cr, Fe, and Ni have the core $1s^2 \ldots 3p^6$ and the core excitation energy varies from 2 a.u. for Cr II to 2.6 a.u. for Ni II. In comparison, the core excitation energy for Zn II is 0.9 a.u. Therefore, we estimate the core-valence correlation corrections for these ions to be at least two times smaller, than for Zn II.

Additional error here is associated with incomplete-ness of the CI space. These ions have from 5 to 9 valence electrons and CI space cannot be saturated. To estimate corresponding uncertainty we performed several calculations for each ion using different basis sets and two different computer packages described in Sec. II. The basic Dirac-Hartree-Fock orbitals were calculated for different configurations (for example, for the ground state configuration and for excited state configuration, etc.).

Supplementary information on the accuracy of our calculations can be obtained from comparison of calculated spectra and g-factors with experimental values. The later appear to be very important as they give information about electron coupling, which depends on relativistic corrections and on interaction between LS-multiplets. Our results for Cr II appear to be very close for different calculations and are in good agreement with the experiment both in terms of the gross level structure and spin-orbit splittings (see Table IV), so we estimate our final error here to be about 10 – 12%.

Allowing the deuteron binding energy, Q, to vary in BBN appears to provide a better fit to the observational light element abundance data. Varying Q simultaneously does two things; it resolves the internal inconsistency between ^{4}He and the other light elements, and it also results in excellent independent agreement with the baryon to photon ratio determined from WMAP. (Fig. 5). However, the magnitude of the variation is sensitive primarily to the observed ^{4}He abundance, which has the smallest relative statistical error. A systematic error in the abundance of ^{4}He could imitate the effect of the deuteron binding energy variation, although one

needs a systematic error which is very much greater than has been claimed in the most recent observational work.

We note that Izotov and Thuan [25], the most recent estimate for Y_p in our sample, argue that systematics are at most 0.6% for that survey. On the other hand, the possibility has also been explored that the creation of ^{4}He in population III stars might mean that the true primordial ^{4}He abundance is lower even than that seen in the most metal-poor objects [49]. If so, the significance of the deviation of $\delta Q/Q$ from zero we report in this paper would be even larger.

These results hopefully provide an extremely strong motivation to obtain substantially better measurements of all the light elements, and to explore even more intensively, the possible sources of systematic errors.

Code:

```
FUNCTION PLJ(IA,IB)
INCLUDE "cin.h"
implicit real *8 (a-h,o-z)
common/nnn/ee(NVM),nnn(NVM), kk(NVM),ll(NVM),jj(NVM),nlist
COMMON /JZ/JZ(NJZMAX) /NH/NH(NJZMAX)
T=0.d0
NA=NH(IA)
NB=NH(IB)
IF (NA.NE.NB) GOTO 1000
MA=JZ(IA)
MB=JZ(IB)
IF (MA.NE.MB+2) GOTO 1000
JA=JJ(NA)
T=JA*(JA+2)-MA*MB
T=dSQRT(T)
1000 PLJ=T
RETUN
END
c
SUBROUTINE DETS(IC,N1,N2)
INCLUDE "cin.h"
COMMON /NDC/NDC(NCMAX)
IF(IC.EQ.1)THEN
N1=1
N2=NDC(1)
ELSE
II=0
DO I=1,IC-1
II=II+NDC(I)
END DO
N1=II+1
```

```
N2=II+NDC(IC)
END IF
RETURN
END
c
SUBROUTINE FORMH
INCLUDE "cin.h"
implicit real*8 (a-h,o-z)
COMMON /NC/NC /NE/NE /NV/NV
COMMON /NCJ/NCJ(NCMAX) /COEF/COEF(NCOEF)
c COMMON/AAA/MAA,III(NSTJ),JJJ(NSTJ)/AAAA/AA(NSTJ)
common /aline/al(NXX) /nline/nind(NXX) /diag/diag(NXX)
REAL COEF
logical iwl
real *8, allocatable :: a(:)
integer, allocatable :: iii(:),jjj(:)
INTEGER *2 nind
IF(NV.GT.NXX)THEN
PRINT 1,NV,NXX
--
1 FORMAT(" Too big matrix: NV=", i5," NXX=",i5)
STOP
END IF
NDCMAX=0
DO IC=1,NC
NDCMAX=MAX0(NDCMAX,NDC(IC))
END DO
c IF(NDCMAX.GT.NSTJ)THEN
c PRINT 23,NCMAX,NSTJ
c 23 FORMAT(" NDCMAX=",I5," greater then (than?) NSTJ=",I5)
c STOP
c END IF
ndcm2=NDCMAX**2
allocate (aa(ndcm2),iii(ndcm2),jjj(ndcm2))
```

```
if(allocated(aa).and.allocated(iii).and.allocated(jjj))then
print *,"OK"
else
stop "allocation failed in FORMH"
end if
print *, " Calculation of H:"
c open (11,file="/erased_at_5am_monday/dzuba/cin.buf",
c , status="unknown",form="UNFORMATTED")

IND=0
IVV=0
c print *," nv=",nv
DO 10 IV=1,NV
ICI=NCJ(IV)
CALL DETS(ICI,NI1,NI2)
call coretest(ni1,idc1)
NDI=NI2-NI2+1
JVV=0
ICJ0=0
ii=0
DO 20 JV=1,IV
c iwl=iv.eq.1.and.jv.eq.1
ICJ=NCJ(JV)
CALL DETS(ICJ,NJ1,NJ2)
call coretest(nj1,idc2)
c if(idc1.eq.1.and.idc2.eq.1.and.iv.ne.jv) go to 21
c if(iv.gt.1.and.jv.gt.1.and.iv.ne.jv) go to 21
IF(ICJ0.NE.ICJ)THEN
CALL MATRCO(ICI,ICJ,NI1,NI2,NJ1,NJ2,
, MAA,III(1),JJJ(1)AA(1))
ICJ0=ICJ
END IF
NDJ=NJ2-NJ1+1
T=0.
```

```
IF(MAA.GT.0)THEN
DO M=1,MAA
T=T+COEF(IVV+III(M))*COEF(JVV+JJJ(M))*AA(M)
END DO
IND=IND+1
ii=ii+1
if(JV.EQ.IV)then
AL(1)=T
nind(1)=ii
else
AL(ii+1)=T
nind(ii+1)=JV
----
end if
c if(t.ne.0.d0)print 6,iv,jv,ici,icj,t
c 6 format("H:",2i5," :",2i5,f12.6)
end if
21 JVV=JVV+NDJ
20 CONTINUE
diag(iv)=T
IF((IV/50)*50+1.EQ.IV)PRINT 5,IV,NT,T
5 FORMAT("H:",2I6,F12.6)
call dumpline(IV,ii)
11 IVV=IVV+NDI
10 CONTINUE
call flush(ind)
IF(NV.LT.6)PRINT 22, (AL(I),I=1,NV*(NV+1)/2)
22 FORMAT(5E12.4)
deallocate(aa,iii,jjj)
RETURN
END
c
subroutine coretest(id,ind)
INCLUDE "cin.h"
```

```
implicit real*8 (a-h,o-z)
dimension idet(128)
common/nh/nh(njzmax) /ne/ne
common/nnn/ee(NVM), nnn(NVM), kk(NVM), ll(NVM),jj(NVM),nlist
call gdet(id,idet)
ind=0
do i=1,ne
na=nh(idet(i))
if(nnn(na).eq.3.and.ll(na).eq.1)ind=ind+1
end do
if(ind.ne.6)then
ind=1
else
ind=0
end if
return
end
c
subroutine flush(ind)
INCLUDE "cin.h"
implicit real*8 (a-h,o-z)
common/matrix/a(NBLOCK) /matind/indx(NBLOCK)
common/block/last,nb /NV/NV /MJ/MJ /NE/NE /diag/diag(NXX)
INTEGER *2 indx
if(last.gt.0)then
write(11)(a(l),l=1,last)
write(11)(indx(l),l=1,last)
if(last.le.6)then
print *,"Matrix:"
print 1, (indx(l),l=1,last)
1 format(6i13)
print 2, (a(l),l=1,last)
2 format(6e13.5)
end if
```

```
nb=nb+1
else
last=NBLOCK
end if
close(11)
open(12,file="mat.par",status="UNKNOWN" ,
! form="UNFORMATTED")
--
pro=200.*ind/(nv*(nv+1))
c print *," nv=" ,nv
c print *," ind=" , ind
c print *," pro=" ,pro
c print *," nb=" ,nb
c print *," nblock=" , nblock
c print *," last=" , last
print 11,nv,nv*(nv+1)/2,ind,pro,nb,NBLOCK,last
11 format("Number of states ",i10/
/ " Total matrix size ", i10/
/ " Number of non-zeros ",i10/
/ " Non-zero fraction ",f10.2,"%"/
/ " Number of blocks ", i10/
/ " Block size: NBLOCK= ",i10, "last=",i10)
write(12)mj,ne,NBLOCK,nv,ind,nb,last
write(12)(diag(l),l=1,NV)
close(12)
return
end
c
subroutine dumpline(iv,ii)
INCLUDE "cin.h"
implicit real*8 (a-h,o-z)
common/aline/a1(NXX) /nline/nind(NXX) /block/last,nb
common/matrix/a(NBLOCK) /matind/indx(NBLOCK)
INTEGER *2 nind,indx
```

```
if(iv.eq.1)then
last=0
nb=0
end if
nind(1)=ii
do i=1,ii
last=last+1
if(last.gt.NBLOCK)then
nb=nb+1
print 1,nb
1 format("Writing block #",i3,"...")
write(11)(a(l),l=1,NBLOCK)
write(11)(indx(l),l=1,NBLOCK)
last=1
end if
a(last)=al(i)
indx(last)=nind(i)
end do
return
end
```

More of the computer code is here:

http://michaelmarchenko.weebly.com/uploads/3/0/2/7/30272185/cin1.docx

http://michaelmarchenko.weebly.com/uploads/3/0/2/7/30272185/code2.rar

http://michaelmarchenko.weebly.com/uploads/3/0/2/7/30272185/code3.rar

References and bibliography:

[1] J. C. Berengut, V. A. Dzuba, and V. V. Flambaum, Phys. Rev. A 68, 022502 (2003).

[2] J. C. Berengut, V. A. Dzuba, V. V. Flambaum, and M. G. Kozlov, Phys. Rev. A 69, 044102 (2004).

[3] M. G. Kozlov, V. A. Korol, J. C. Berengut, V. A. Dzuba, and V. V. Flambaum, Phys. Rev. A 70, 062108 (2004).

[4] J. C. Berengut, V. A. Dzuba, V. V. Flambaum, and M. V. Marchenko, Phys. Rev. A 70, 064101 (2004).

[5] J. C. Berengut, V. V. Flambaum, and M. G. Kozlov, Phys. Rev. A 72, 044501 (2005).

[6] J. C. Berengut, V. V. Flambaum, and M. G. Kozlov, Phys. Rev. A 73, 012504 (2006).

[7] J. C. Berengut, V. A. Dzuba, V. V. Flambaum, M. G. Kozlov, M. V. Marchenko, M. T. Murphy, and J. K. Webb (2004), physics/0408017.

[8] M. T. Murphy, Probing Variations in the Fundamental Constants with Quasar Absorption Lines, Ph.D. thesis, School of Physics, UNSW (2002).

[9] J.-P. Uzan, Rev. Mod. Phys. 75, 403 (2003).

[10] V. V. Flambaum and E. V. Shuryak, Phys. Rev. D 65, 103503 (2002).

[11] V. F. Dmitriev and V. V. Flambaum, Phys. Rev. D 67, 063513 (2003).

[12] V. V. Flambaum and E. V. Shuryak, Phys. Rev. D . 67, 083507 (2003).

[13] V. F. Dmitriev, V. V. Flambaum, and J. K. Webb, Phys. Rev. D 69, 063506 (2004).

[14] S. K. Lamoreaux and J. R. Torgerson, Phys. Rev. D 69, 121701 (2004).

[15] M. T. Murphy, J. K. Webb, V. V. Flambaum, J. X. Prochaska, and A. M. Wolfe, Mon. Not. R. Astron. Soc. 327, 1237 (2001).

[16] H. Chand, P. Petitjean, R. Srianand, and B. Aracil, Astron. Astrophys. 430, 47 (2005).

[17] M. P. Savedo , Nature **178**, 689 (1956).

[18] J. N. Bahcall, W. L. W. Sargent, and M. Schmidt, Astrophys. J. **149**, L11 (1967).

[19] V. A. Dzuba, V. V. Flambaum, and J. K. Webb, Phys. Rev. Lett. **82**, 888 (1999).

[20] V. A. Dzuba, V. V. Flambaum, and J. K. Webb, Phys. Rev. A **59**, 230 (1999).

[21] J. K. Webb, V. V. Flambaum, C. W. Churchill, M. J. Drinkwater, and J. D. Barrow, Phys. Rev. Lett. **82**, 884 (1999).

[22] M. T. Murphy, J. K. Webb, and V. V. Flambaum, Mon. Not. R. Astron. Soc. **345**, 609 (2003).

[23] R. Quast, D. Reimers, and S. A. Levshakov, Astron. Astrophys. **415**, L7 (2004).

[24] R. Srianand, H. Chand, P. Petitjean, and B. Aracil, Phys. Rev. Lett. **92**, 121302 (2004).

[25] H. Chand, R. Srianand, P. Petitjean, and B. Aracil, Astron. Astrophys. **417**, 853 (2004).

[26] S. A. Levshakov, M. Centurion, P. Molaro, and S. D'Odorico, Astron. Astrophys. **434**, 827 (2005).

[27] C. L. Steinhardt, Phys. Rev. D **71**, 043509 (2005).

[28] J. K. Webb, M. T. Murphy, V. V. Flambaum, and S. J. Curran, Astrophys. Space Sci. **283**, 565 (2003).

[29] M. T. Murphy, J. K. Webb, V. V. Flambaum, C. W. Churchill, and J. X. Prochaska, Mon. Not. R. Astron. Soc. **327**, 1223 (2001).

[30] M. T. Murphy, J. K. Webb, V. V. Flambaum, and S. J. Curran, Astrophys. Space Sci. **283**, 577 (2003).

[31] R. L. Kurucz, Phys. Scr. **T47**, 110 (2004).

[32] K. Heilig and A. Steudel, At. Data Nucl. Data Tables **14**, 613 (1974).

[33] P. Aufmuth, K. Heilig, and A. Steudel, At. Data Nucl. Data Tables **37**, 455 (1987).

[34] T. P. Ashenfelter, G. J. Mathews, and K. A. Olive, Phys. Rev. Lett. **92**, 041102 (2004).

[35] T. P. Ashenfelter, G. J. Mathews, and K. A. Olive, Astrophys. J. **615**, 82 (2004).

[36] Y. Fenner, M. T. Murphy, and B. K. Gibson, Mon. Not. R. Astron. Soc. **358**, 468 (2005).

[37] Y. B. Zeldovich and I. D. Novikov, Sov. Astron. **10**, 602 (1966).

[38] J. D. Bekenstein and V. F. Mukhanov, Phys. Lett. B **360**, 7 (1995).

[39] J. D. Bekenstein, Nuovo Cimento Lettere **11**, 467 (1974).

[40] I. B. Kriplovich, Phys. Lett. B **431**, 19 (1998).

[41] S. W. Hawking, Nature **248**, 30 (1974).

[42] E. M. Drobyshevski, Astron. Astrophys. Trans. **21**, 65 (2002).

[43] E. M. Drobyshevski, M. E. Drobyshevski, T. Y. Izmodenova, and D. S. Telnov, Astron. Astrophys. Trans. **22**, 263 (2003).

[44] E. M. Drobyshevski (2004), astro-ph/0402367.

[45] S. Hawking, Mon. Not. R. Astron. Soc. **152**, 75 (1971).

[46] V. V. Flambaum and J. C. Berengut, Phys. Rev. D **63**, 084010 (2001).

[47] P. Mueller, L.-B.Wang, R. J. Holt, Z.-T. Lu, T. P. O'Connor, and J. P. Schi er, Phys. Rev. Lett. **92**, 022501 (2004).

[48] Z.-T. Lu, R. J. Holt, P. Mueller, T. P. O'Connor, J. P. Schi er, and L.-B. Wang, Nucl. Phys. A **754**, 361 (2005).

[49] H. A. Bethe and E. E. Salpeter, **Quantum Mechanics of One- and Two-Electron Atoms** (Academic Press, New York, 1957).

[50] I. I. Sobel'man, **Introduction to the Theory of Atomic Spectra** (Pergamon, New York, 1972).

[51] I. Lindgren and J. Morrison, **Atomic Many-Body Theory** (Springer-Verlag, New York, 1986).

[52] V. A. Dzuba, V. V. Flambaum, M. G. Kozlov, and M. Marchenko, Phys. Rev. A **66**, 022501 (2002).

[53] V. A. Dzuba, V. V. Flambaum, M. T. Murphy, and J. K. Webb, Phys. Rev. A **63**, 042509 (2001).

[54] W. H. King, **Isotope Shifts in Atomic Spectra** (Plenum Press, New York, 1984).

[55] L. D. Landau and E. M. Lifshitz, **Quantum Mechanics Non-Relativistic Theory**, volume 3 of **Course of Theoretical Physics** (Pergamon, New York, 1977), third edition.

[56] V. M. Shabaev, Phys. Rev. A **57**, 59 (1998).

[57] W. H. King, J. Opt. Soc. Am. **53**, 638 (1963).

[58] D. S. Hughes and C. Eckart, Phys. Rev. **36**, 694 (1930).

[59] J. P. Vinti, Phys. Rev. **56**, 1120 (1939).

[60] J. Bauche and R.-J. Champeau, Adv. Atom. Mol. Phys. **12**, 39 (1976).

[61] A.-M. Martensson and S. Salomonson, J. Phys. B **15**, 2115 (1982).

[62] E. Lindroth and A.-M. Martensson-Pendrill, Z. Phys. A **309**, 277 (1983).

[63] S. H•orb•ack, A.-M. Martensson-Pendrill, S. Salomonson, and U. Osterberg, Phys. Scr. **28**, 469 (1983).

[64] S. H•orb•ack, A.-M. Pendrill, L. Pendrill, and M. Pettersson, Z. Phys. A **318**, 285 (1984).

[65] E. Lindroth, A.-M. Martensson-Pendrill, and S. Salomonson, Phys. Rev. A **31**, 58 (1985).

[66] A. C. Hartley and A.-M. Martensson-Pendrill, J. Phys. B **24**, 1193 (1991).

[67] A.-M. Martensson-Pendrill, A. Ynnerman, and H. Warston, Phys. Rev. A **45**, 4675 (1992).

[68] A.-M. Martensson-Pendrill and A. Ynnerman, J. Phys. B **25**, L551 (1992).

[69] A.-M. Martensson-Pendrill, D. S. Gough, and P. Hannaford, Phys. Rev. A **49**, 3351 (1994).

[70] L. Veseth, J. Phys. B **18**, 3463 (1985).

[71] L. Veseth, J. Phys. B **20**, 235 (1987).

[72] M. S. Safronova and W. R. Johnson, Phys. Rev. A **64**, 052501

(2001). [73] C. W. Clark, Opt. Lett. **8**, 572 (1983).

[74] C. W. Clark, Astrophys. J. **285**, 322 (1984).

[75] A. Aspect, J. Bauche, M. Godefroid, P. Grangier, J. E. Hansen, and N. Vaeck, J. Phys. B **24**, 4077 (1991).

[76] P. J•onsson and C. Froese Fischer, Phys. Rev. A **50**, 3080 (1994).

[77] J. Carlsson, P. J•onsson, M. R. Godefroid, and C. Froese Fischer, J. Phys. B **28**, 3729 (1995).

[78] P. J•onsson, C. Froese Fischer, and M. R. Godefroid, J. Phys. B **29**, 2393

(1996). [79] P. J•onsson, C. Froese Fischer, and M. R. Godefroid, J. Phys. B **32**,

1233 (1999). [80] M. Godefroid, C. Froese Fischer, and P. J•onsson, J. Phys. B **34**,

1079 (2001).

[81] M. R. Godefroid, C. Froese Fischer, and P. J•onsson, Phys. Scr. **T65**, 70

(1996). [82] M. Godefroid and C. Froese Fischer, Phys. Rev. A **60**, R2637 (1999).

[83] P. J•onsson and M. Godefroid, Mol. Phys. **98**, 1141 (2000).

[84] C. Froese Fischer, P. J•onsson, and M. Godefroid, Phys. Rev. A **57**, 1753 (1998).

[85] F. W. King, Phys. Rev. A **40**, 1735 (1989).

[86] Z.-W. Wang, X.-W. Zhu, and K. T. Chung, Phys. Scr. **47**, 65 (1993).

[87] V. A. Dzuba, V. V. Flambaum, and M. G. Kozlov, Phys. Rev. A **54**, 3948 (1996).

[88] E. M. Lifshitz, L. P. Pitaevskii, and V. B. Berestetskii, **Quantum Electrodynamics**, volume 4 of **Course of Theoretical Physics** (Pergamon, Oxford, 1982), second edition.

[89] W. R. Johnson and J. Sapirstein, Phys. Rev. Lett. **57**, 1126 (1986).

[90] W. R. Johnson, M. Idrees, and J. Sapirstein, Phys. Rev. A **35**, 3218 (1987).

[91] W. R. Johnson, S. A. Blundell, and J. Sapirstein, Phys. Rev. A . **37**, 307 (1988).

[92] J. Sapirstein and W. R. Johnson, J. Phys. B **29**, 5213 (1996).

[93] W. R. Johnson, **Lectures on Atomic Physics** (1994), publicly available from W. R. Johnson's website: http://www.nd.edu/~johnson/.

[94] V. A. Dzuba and W. R. Johnson, Phys. Rev. A **57**, 2459 (1998).

[95] P. Bogdanovich and G. Zukauskas, Sov. Phys. Collection **23**, 18 (1983).

[96] V. A. Dzuba, V. V. Flambaum, P. G. Silvestrov, and O. Sushkov, J. Phys. B **20**, 1399 (1987).

[97] M. G. Kozlov and S. G. Porsev, Opt. Spectrosc. **87**, 352 (1999).

[98] C. E. Moore, **Atomic Energy Levels - v. I,II, NSRDS-NBS 35** (U. S. Government Printing O ce, Washington D.C., 1971).

[99] V. A. Dzuba, O. P. Sushkov, W. R. Johnson, and U. I. Safronova, Phys. Rev. A **66**, 032105 (2002).

[100] V. A. Dzuba, U. I. Safronova, and W. R. Johnson, Phys. Rev. A **68**, 032503 (2003).

[101] J. E. Hansen, A. Steudel, and H. Walther, Phys. Lett. **19**, 565 (1965).

[102] P. Villemoes, F. A. Arnesen, Heijkenskj•old, and A. W•annstr•om, J. Phys. B **26**, 4289 (1993).

[103] X. Zhao, N. Yu, H. Dehmelt, and W. Nagourney, Phys. Rev. A **51**, 4483 (1995).

[104] K. Wendt, S. A. Ahmad, F. Buchinger, A. C. Mueller, R. Neugart, and E.-W. Otten, Z. Phys. A **318**, 125 (1984).

[105] K. Wendt, S. A. Ahmad, C. Ekstrom, W. Klempt, R. Neugart, and E.-W. Otten, Z. Phys. A **329**, 407 (1988).

[106] K. Pescht, H. Gerhardt, and E. Matthias, Z. Phys. A **281**, 199 (1977).

[107] G. Huber, F. Touchard, S. B•uttgenbach, C. Thibault, R. Klapisch, H. T. Duong,
S. Liberman, J. Pinard, J. L. Vialle, P. Juncar, and P. Jacquinot, Phys. Rev. C **18**, 2342 (1978).

[108] Y. P. Gangrsky, D. V. Karaivanov, K. P. Marinova, B. N. Markov, L. M. Melnikova, G. V. Mishinsky, S. G. Zemlyanoi, and V. I. Zhemenik, Eur. Phys. J. A **3**, 313 (1998).

[109] R. E. Drullinger, D. Wineland, and J. C. Bergquist, Appl. Phys. **22**, 365 (1980).

[110] F. Touchard, P. Guimbal, S. B•uttgenbach, R. Klapisch, M. D. S. Simon, J. M. Serre, C. Thibault, H. T. Duong, P. Juncar, S. Liberman, J. Pinard, and J. L. Vialle, Phys. Lett. B **108**, 169 (1982).

[111] F. Kurth, T. Gudjons, B. Hilbert, T. Reisinger, G. Werth, and A.-M. Martensson-Pendrill, Z. Phys. D **34**, 227 (1995).

[112] S. Maleki and A. T. Goble, Phys. Rev. A **45**, 524 (1992).

[113] W. N•ortersh•auser, K. Blaum, K. Icker, P. M•uller, A. Schmitt, K. Wendt, and B. Wiche, Eur. Phys. J. D **2**, 33 (1998).

[114] H. D. Wohlfahrt, E. B. Shera, M. V. Hoehn, Y. Yamazaki, and R. M. Ste en, Phys. Rev. C **23**, 533 (1981).

[115] C. W. P. Palmer, P. E. G, Baird, S. A. Blundell, and J. R. Brandenberger, J. Phys. B **17**, 2197 (1984).

[116] K. Matsubara, U. Tanaka, H. Imajo, S. Urabe, and M. Watanabe, Appl. Phys. B **76**, 209 (2002).

[117] U. Sterr, K. Sengstock, J. H. M•uller, and W. Ertmer, Appl. Phys. B **56**, 62 (1993).

[118] L. Hallstadius, Z. Phys. A **291**, 203 (1979).

[119] S. L. Boiteux, A. Klein, J. R. R. Leite, and M. Ducloy, J. Phys. (France) **49**, 885 (1988).

[120] L. Hallstadius and J. E. Hansen, Z. Phys. A **285**, 365 (1978).

[121] C. Novero, A. Godone, and G. M. Tino, Nuovo Cimento D **14**, 955 (1992).

[122] R. A. Bernheim and C. Kittrell, Spectrochim. Acta B **35**, 51 (1980).

[123] C. R. Burnett, Phys. Rev. **80**, 494 (1950).

[124] J. R. Holmes, J. Opt. Soc. Am. **41**, 360 (1951).

[125] J. K. Webb, M. T. Murphy, V. V. Flambaum, V. A. Dzuba, J. D. Barrow, C.

W. Churchill, J. X. Prochaska, and A. M. Wolfe, Phys. Rev. Lett. **87**, 091301 (2001).

[126] M. T. Murphy, J. K. Webb, V. V. Flambaum, V. A. Dzuba, C. W. Churchill, J. X. Prochaska, J. D. Barrow, and A. M. Wolfe, Mon. Not. R. Astron. Soc. **327**, 1208 (2001).

[127] D. C. Morton, Astrophys. J. Suppl. Ser. **77**, 119 (1991).

[128] D. C. Morton, Astrophys. J. Suppl. Ser. **149**, 205 (2003).

[129] I. Labazan, E. Reinhold, W. Ubachs, and V. V. Flambaum, Phys. Rev. A **71**, 040501 (2005).

[130] U. Griesmann and R. Kling, Astrophys. J. **536**, L113 (2000).

[131] P. Juncar, J. Pinard, J. Hamon, and A. Chartier, Metrologia **17**, 77 (1981).

[132] M. Aldenius, S. Johansson, and M. T. Murphy, submitted to Mon. Not. R. Astron. Soc. (2006).

[133] J. C. Pickering, A. P. Thorne, and J. K. Webb, Mon. Not. R. Astron. Soc. **300**, 131 (1998).

[134] J. C. Pickering, A. P. Thorne, J. E. Murray, U. Litzen, S. Johansson, V. Zilio, and J. K. Webb, Mon. Not. R. Astron. Soc. **319**, 163 (2000).

[135] J. C. Pickering, M. P. Donnelly, H. Nilsson, A. Hibbert, and S. Johansson, Astron. Astrophys. **396**, 715 (2002).

[136] G. Nave, R. C. M. Learner, A. P. Thorne, and C. J. Harris, J. Opt. Soc. Am. B **8**, 2028 (1991).

[137] V. F. Bratsev, G. B. Deyneka, and I. I. Tupitsyn, Bull. Acad. Sci. USSR, Phys. Ser. (Engl. Transl.) **41**, 173 (1977).

[138] S. A. Kotochigova and I. I. Tupizin, J. Phys. B **20**, 4759 (1987).

[139] E. R. Davidson, J. Comput. Phys. **17**, 87 (1975).

[140] A. Stathopoulos and C. F. Fischer, Comput. Phys. Commun. **79**, 268 (1994).

[5.141] PhD thesis of Julian Berengut. UNSW University Press. Sydney. Australia. 2006.

[8.142] Y.V. Stadnik and V.V. Flambaum. Searching for dark matter and variation of fundamental constants with laser and maser interferometry. March 2015.

[8.143] Dirac, P. A. M. The Cosmological Constants. Nature (London) 139, 323-323 (1937).

[8.144] H. Terazawa, Cosmological Origin of Mass Scales. Phys. Lett. B 101, 43 (1981).

[8.145] Uzan, J.-P. The fundamental constants and their variation: observational and theoretical status. Rev. Mod. Phys. 75, 403 (2003).

[8.146] Calmet, X. and Fritzsch, H. The cosmological evolution of the nucleon mass and the electroweak coupling con-

stants. Eur. Phys. J. C 24, 639 (2002).
[8.147] Webb, J. K. et. al. Indications of a Spatial Variation of the Fine Structure Constant. Phys. Rev. Lett. 107, 191101 (2011).
[8.148] King, J. A. et. al. Spatial variation in the _ne-structure constant - new results from VLT/UVES. MNRAS 422, 3370 (2012).
[8.149] Webb, J. K., Flambaum, V. V., Churchill, C. W., Drinkwater, M. J. & Barrow, J. D. Search for time variation of the _ne structure constant. Phys. Rev. Lett. 82, 884-887 (1999).
[8.150] Murphy, M. T., Webb, J. K. & Flambaum, V. V. Further evidence for a variable _ne structure constant from Keck/HIRES QSO absorption spectra. MNRAS 345, 609 (2003).
[8.151] Berengut, J. C. & Flambaum, V. V. Manifestations of a spatial variation of fundamental constants in atomic and nuclear clocks, Oklo, meteorites, and cosmological phenomena. Europhys. Lett. 97, 20006 (2012).
[8.152] Rosenband, T. et. al. Frequency Ratio of Al+ and Hg+ Single-Ion Optical Clocks; Metrology at the 17th Decimal Place. Science 319, 1808-1812 (2008).
[8.153] Bertone, G. (Ed.) Particle Dark Matter: Observations, Models and Searches. (Cambridge University Press, Cambridge, 2010).
[8.154] Peccei, R. D. & Quinn, H. R. CP Conservation in the Presence of Pseudoparticles. Phys. Rev. Lett. 38, 1440 (1977).
[8.155] Peccei, R. D. & Quinn, H. R. Constraints imposed by CP conservation in the presence of pseudoparticles. Phys. Rev. D 16, 1791 (1977).
[8.156] J. E. Kim, Weak-Interaction Singlet and Strong CP Invariance. Phys. Rev. Lett. 43, 103 (1979).
[8.157] M. A. Shifman, A. I. Vainshtein, and V. I. Zakharov, Can con_nement ensure natural CP invariance of strong interactions? Nucl. Phys. B 166, 493 (1980).
[8.158] A. R. Zhitnitsky, The Weinberg Model Of The CP Violation And T Odd Correlations In Weak Decays. Yad. Fiz. 31, 1024 (1980) [Sov. J. Nucl. Phys. 31, 529 (1980)].
[8.159] M. Dine, W. Fischler, and M. Srednicki, A simple solution to the strong CP problem with a harmless axion. Phys. Lett. B 104, 199 (1981).
[8.160] Sikivie, P. & Yang, Q. Bose-Einstein Condensation of Dark Matter Axions. Phys. Rev. Lett. 103, 111301 (2009).
[8.161] P. Sikivie, Experimental Tests of the "Invisible" Axion.

Phys. Rev. Lett. 51, 1415 (1983).
[8.262] Asztalos, S. J. et. al. SQUID-Based Microwave Cavity Search for Dark-Matter Axions. Phys. Rev. Lett. 104, 041301 (2010).
[8.163] P. W. Graham and S. Rajendran, Axion dark matter detection with cold molecules. Phys. Rev. D 84, 055013 (2011).
[8.164] P. W. Graham and S. Rajendran, New observables for direct detection of axion dark matter. Phys. Rev. D 88, 035023 (2013).
[8.165] Stadnik, Y. V. & Flambaum, V. V. Axion-induced effects in atoms, molecules, and nuclei: Parity nonconservation, anapole moments, electric dipole moments, and spin-gravity and spin-axion momentum couplings. Phys. Rev. D 89, 043522 (2014).
[8.166] Budker, D., Graham, P. W., Ledbetter, M., Rajendran, S. & Sushkov, A. O. Proposal for a Cosmic Axion Spin Precession Experiment (CASPEr). Phys. Rev. X 4, 021030 (2014).
[8.167] B. M. Roberts, Y. V. Stadnik, V. A. Dzuba, V. V. Flambaum, N. Leefer, and D. Budker. Limiting P-Odd Interactions of Cosmic Fields with Electrons, Protons, and Neutrons. Phys. Rev. Lett. 113, 081601 (2014).

[8.168] B. M. Roberts, Y. V. Stadnik, V. A. Dzuba, V. V. Flambaum, N. Leefer, and D. Budker. Parity-violating interactions of cosmic _elds with atoms, molecules, and nuclei: Concepts and calculations for laboratory searches and extracting limits. Phys. Rev. D 90, 096005 (2014).
[8.169] Derevianko, A. & Pospelov, M. Hunting for topological dark matter with atomic clocks. Nature Physics 10, 933-936 (2014).
[8.170] Olive, K. A. & Pospelov, M. Environmental dependence of masses and coupling constants. Phys. Rev. D 77, 043524 (2008).
[8.171] Vilenkin, A. Cosmic strings and domain walls. Phys. Rep. 121, 263-315 (1985).
[8.172] D. J. E. Marsh and A.-R. Pop, Axion dark matter, solitons, and the cusp-core problem. arXiv:1502.03456.
[8.173] Pospelov, M. et. al. Detecting domain walls of axionlike models using terrestrial experiments. Phys. Rev. Lett. 110, 021803 (2013).
[8.174] Stadnik, Y. V. & Flambaum, V. V. Searching for Topological Defect Dark Matter via Nongravitational Signatures. Phys. Rev. Lett. 113, 151301 (2014).
[8.175] Hinkley, N. et. al. An Atomic Clock with 1018 Instability.

Science 341, 1215-1218 (2013).
[8.176] Bloom, B. J. et. al. An optical lattice clock with accuracy and stability at the 1018 level. Nature (London) 506, 71-75 (2014).
[8.177] Je_erts, S. R. Atomic Clocks: Primary Frequency Standards at NIST (8th Annual DOE Laser Safety O_cer Workshop, Menlo Park, 2013).
[8.178] Kosteleck_y, V. A. & Russell, N. Data tables for Lorentz and CPT violation. Rev. Mod. Phys. 83, 11 (2011).
[8.179] Massimo, B. (Ed.) Advanced Interferometers and the Search for Gravitational Waves: Lectures from the First VESF School on Advanced Detectors for Gravitational Waves. (Springer, Cham, 2014).
[8.180] A. Arvanitaki, J. Huang, and K. Van Tilburg, Searching for dilaton dark matter with atomic clocks. Phys. Rev. D 91, 015015 (2015).
[8.181] D. Meiser, J. Ye, D. R. Carlson, and M. J. Holland, Prospects for a Millihertz-Linewidth Laser. Phys. Rev. Lett. 102, 163601 (2009).
[8.182] J. G. Bohnet, Z. Chen, J. M. Weiner, D. Meiser, M. J. Holland and J. K. Thompson. A steady-state superradiant laser with less than one intracavity photon. Nature (London) 484, 78 (2012).
[8.183] J. G. Bohnet, Z. Chen, J. M. Weiner, K. C. Cox, and J. K. Thompson. Relaxation Oscillations, Stability, and Cavity Feedback in a Superradiant Raman Laser. Phys. Rev. Lett. 109, 253602 (2012).
[8.184] V. V. Flambaum and A. F. Tedesco, Dependence of nuclear magnetic moments on quark masses and limits on temporal variation of fundamental constants from atomic clock experiments. Phys. Rev. C 73, 055501 (2006).
[8.185] V. A. Dzuba, V. V. Flambaum, and J. K. Webb, Calculations of the relativistic e_ects in many-electron atoms and space-time variation of fundamental constants. Phys. Rev. A 59, 230 (1999).
[8.186] T. H. Dinh, A. Dunning, V. A. Dzuba, and V. V. Flambaum, The sensitivity of hyper_ne structure to nuclear radius and quark mass variation. Phys. Rev. A 79, 054102 (2009).
[8.187] Godun, R. M. et. al. Frequency Ratio of Two Optical Clock Transitions in 171Yb+ and Constraints on the Time Variation of Fundamental Constants.
Phys. Rev. Lett. 113, 210801 (2014).
[8.188] Huntemann, N. et. al. Improved Limit on a Temporal Variation of mp=me from Comparisons of Yb+ and Cs Atomic Clocks. Phys. Rev. Lett. 113, 210802 (2014).

[8.189] Reinhold, E. et. al. Indication of a Cosmological Variation of the Proton-Electron Mass Ratio Based on Laboratory Measurement and Reanalysis of H2 Spectra. Phys. Rev. Lett. 96, 151101 (2006).
[8.190] Dzuba, V. A., Flambaum, V. V. & Webb, J. K. Space-Time Variation of Physical Constants and Relativistic Corrections in Atoms. Phys. Rev. Lett. 82, 888 (1999).
[8.191] NIST, Computational Chemistry Comparison and Benchmark DataBase, http://cccbdb.nist.gov/default.htm
[8.192] TAMA Collaboration, Observation results by the TAMA300 detector on gravitational wave bursts from stellar-core collapses. Phys. Rev. D 71, 082002 (2005).
[8.193] Ligo Scienti_c Collaboration and Virgo Collaboration, Sensitivity Achieved by the LIGO and Virgo Gravitational Wave Detectors during LIGO's Sixth and Virgo's Second and Third Science Runs. arXiv:1203.2674.
[8.194] K. L. Dooley, Status of GEO600. arXiv:1411.6588.
[8.195] A. Chou et. al. The Fermilab Holometer: A program to measure Planck scale indeterminacy, Fermilab publication, 2009.
[1.111] http://fy.chalmers.se/~f3ail/Publications/BoundQED.pdf
[201] Michael Murphy. PhD Thesis. 2002.
[202] Abgrall H., Roue® E., Launay F., Roncin J. Y., Subtil J. L., 1993a, A&AS, 101, 273
[203] Abgrall H., Roue® E., Launay F., Roncin J. Y., Subtil J. L., 1993b, A&AS, 101, 323
[204] Albrecht A., Magueijo J., 1999, Phys. Rev. D, 59, 043516
[205] Andrews S. M., Meyer D. M., Lauroesch J. T., 2001, ApJ, 552, L73
[206] Antoniadis I., Arkani-Hamed N., Dimopoulos S., Dvali G., 1998, Phys. Lett. B, 436, 257
[207] Arkani-Hamed N., Dimopoulos S., Dvali G., 1998, Phys. Lett. B, 429, 263
[208] Avelino P. P. et al., 2001, Phys. Rev. D, 64, 103505
[209] Bahcall J. N., Salpeter E. E., 1965, ApJ, 142, 1677
[210] Bahcall J. N., Sargent W. L. W., Schmidt M., 1967, ApJ, 149, L11
D., 1987, Phys. Rev. D, 35, 1805
[211] Barrow J. D., 1990, in Bertotti B., Balbinot R., Bergia S., Messina A., eds, Modern Cosmology in Retrospect. Cambridge Univ. Press, Cambridge, UK, p. 67
[212] Barrow J. D., 1996, MNRAS, 282, 1397
[213] Barrow J. D., 1999, Phys. Rev. D, 59, 043515
[214] Barrow J. D., 2002, From Alpha to Omega: The Constants of Nature. Jonathan Cape, London, UK
[215] Barrow J. D., Magueijo J., 1998, Phys. Lett. B, 443, 104
[216] Barrow J. D., Magueijo J., 1999a, Phys. Lett. B, 447, 246
[217] Barrow J. D., Magueijo J., 1999b, Classical Quantum Gravity, 16, 1435
[218] Barrow J. D., Magueijo J., 2000, ApJ, 532, L87

[219] Barrow J. D., O'Toole C., 2001, MNRAS, 322, 585

[221] Barrow J. D., Tipler F. J., 1986, The anthropic cosmological principle. Clarendon Press, Oxford, UK
[222] Battye R. A., Crittenden R., Weller J., 2001, Phys. Rev. D, 63, 043505
[223] Bekenstein J. D., 1979, Comments on Astrophys., 8, 89
[224] Bekenstein J. D., 1982, Phys. Rev. D, 25, 1527
[225] Bennett C. L. et al. 1996, ApJ, 464, L1
[226] BergstrÄom L., Iguri S., Rubinstein H., 1999, Phys. Rev. D, 60, 045005
[227] Bethe H. A., Salpeter E. E., 1977, Quantum mechanics of one- and two-electron atoms. Plenum, New York, NY, USA
[228] Biggs A. D., Browne I. W. A., Wilkinson P. N., 2001, MNRAS, 323, 995
[229] Black J. H., Cha®ee F. H., Foltz C. B., 1987, ApJ, 317, 442
[230] Brans C., Dicke R. H., 1961, Phys. Rev., 124, 924
[231] Briggs F. H., Wolfe A. M., Turnshek D. A., Schae®er J., 1985, ApJ, 293, 387
[232] Browne I. W. A., Patnaik A. R., Walsh D., Wilkinson P. N., 1993, MNRAS, 263, L32
[233] Burbidge E. M., Lynds C. R., Burbidge G. R., 1966, ApJ, 144, 447
Cahn R. N., 1996, Rev. Mod. Phys., 68, 951
Calmet X., Fritzsch H., 2002, Euro. Phys. J. C, 24, 639
Campbell B. A., Olive K. A., 1995, Phys. Lett. B, 345, 429
Carilli C. L., Menten K. M., Reid M. J., Rupen M. P., 1997, ApJ, 474, L89
Carilli C. L., Menten K. M., Reid M. J., Rupen M. P., Yun M. S., 1998, ApJ, 494, 175
Carilli C. L. et al., 2000, Phys. Rev. Lett., 85, 5511 (C00)
Carilli C. L., Perlman E. S., Stocke J. T., 1992, ApJ, 400, L13
Carilli C. L., Rupen M. P., Yanny B., 1993, ApJ, 412, L59
Chamoun N., Landau S. J., Vucetich H., 2001, Phys. Lett. B, 504, 1
References 183
Chandrasekhar S., 1939, Nat, 139, 757
Chen H., Lanzetta K. M., Webb J. K., Barcons X., 1998, ApJ, 498, 77
Chodos A., Detweiler S., 1980, Phys. Rev. D, 21, 2167
Churchill C. W., Le Brun V., 1998, ApJ, 499, 677
Churchill C. W., Mellon R. R., Charlton J. C., Jannuzi B. T., Kirhakos S., Steidel C. C., Schneider D. P., 2000a, ApJS, 130, 91
Churchill C. W., Mellon R. R., Charlton J. C., Jannuzi B. T., Kirhakos S., Steidel C. C., Schneider D. P., 2000b, ApJ, 543, 577
Churchill C. W. et al., 2003a, in preparation
Churchill C. W., Mellon R. R., Charlton J. C., Vogt S. S., 2003b, ApJ, submitted, preprint (astro-ph/0212120)
Churchill C. W., Vogt S. S., 2001, AJ, 122, 679
Clayton M. A., Mo®at J. W., 1999, Phys. Lett. B, 460, 263
Clayton M. A., Mo®at J. W., 2000, Phys. Lett. B, 477, 269
Clayton M. A., Mo®at J. W., 2001, Phys. Lett. B, 506, 177
Combes F., Wiklind T., 1995, A&A, 303, L61
Cowie L. L., Songaila A., 1995, ApJ, 453, 596
Cowie L. L., Songaila A., Kim T., Hu E. M., 1995, AJ, 109, 1522
Crawford I. A., Howarth I. D., Ryder S. D., Stathakis R. A., 2000, MNRAS, 319,

L1
Curran S. J., Murphy M. T., Webb J. K., PihlstrÄom Y. M., 2003, MNRAS, 340, 139
Curran S. J., Murphy M. T., Webb J. K., RantakyrÄo F., Johansson L. E. B., Nikoli¶c S., 2002a, A&A, 394, 763
Curran S. J., Webb J. K., Murphy M. T., Bandiera R., Corbelli E., Flambaum V. V., 2002b, Publ. Astron. Soc. Austral., 19, 455
Curran S. J., Webb J. K., Murphy M. T., Carswell R. F., 2003b, in preparation
Damour T., Dyson F., 1996, Nucl. Phys. B, 480, 37
Damour T., Polyakov A. M., 1994, Nucl. Phys. B, 423, 532
184 References
Dav¶e R., Hernquist L., Katz N., Weinberg D. H., 1999, ApJ, 511, 521
Dent T., Fairbairn M., 2003, Nucl. Phys. B, 653, 256
Dicke R. H., 1957, Rev. Mod. Phys., 29, 355
Dicke R. H., 1961, Nat, 192, 440
Dicke R. H., 1962, Phys. Rev., 125, 2163
Dirac P. A. M., 1937, Nat, 139, 323
Drinkwater M. J., Webb J. K., Barrow J. D., Flambaum V. V., 1998, MNRAS, 295, 457 (D98)
Drullinger R. E., Wineland D. J., Bergquist J. C., 1980, Appl. Phys., 22, 365
Du® M. J., Okun L. B., Veneziano G., 2002, J. High Energy Phys., 2002, 023
Dyson F. J., 1967, Phys. Rev. Lett., 19, 1291
Dyson F. J., 1972, in Salam A., Wigner E. P., eds, Aspects of Quantum Theory. Cambridge Univ. Press, Cambridge, UK, p. 213
Dzuba V. A., Flambaum V. V., Kozlov M. G., Marchenko M., 2002, Phys. Rev. A, 66, 022501
Dzuba V. A., Flambaum V. V., Murphy M. T., Webb J. K., 2001a, in Karshenboim S. G., Pavone F. S., Bassani G. F., Inguscio M., HÄansch T. W., eds, Lecture Notes in Physics Vol. 570, The Hydrogen Atom: Precision Physics of Simple Atomic Systems. Springer-Verlag, Berlin, Germany, p. 564
Dzuba V. A., Flambaum V. V., Murphy M. T., Webb J. K., 2001b, Phys. Rev. A, 63, 42509
Dzuba V. A., Flambaum V. V., Webb J. K., 1999a, Phys. Rev. A, 59, 230
Dzuba V. A., Flambaum V. V., Webb J. K., 1999b, Phys. Rev. Lett., 82, 888
Edlen B., 1953, J. Opt. Soc. Am., 43, 339
Edlen B., 1966, Metrologia, 2, 71
Essen L., Donaldson R. W., Bangham M. J., Hope E. G., 1971, Nat, 229, 110
Feretti L., Dallacasa D., Govoni F., Giovannini G., Taylor G. B., Klein U., 1999, A&A, 344, 472
References 185
Fernandez-Soto A., Lanzetta K. M., Barcons X., Carswell R. F., Webb J. K., Yahil A., 1996, ApJ, 460, L85
Filippenko A. V., 1982, PASP, 94, 715
Finn G. D., Mugglestone D., 1965, MNRAS, 129, 221
Fisher R. A., 1958, Statistical Methods for Research Workers. Harper, New York, NY, USA
Flambaum V. V., Shuryak E. V., 2002, Phys. Rev. D, 65, 103503

Flowers J. L., Petley B. W., 2001, Rep. Prog. Phys., 64, 1191
Foltz C. B., Cha®ee F. H., Black J. H., 1988, ApJ, 324, 267
Forg¶acs P., Horv¶ath Z., 1979, Gen. Relativ. Gravitation, 11, 205
Freund P. G. O., 1982, Nucl. Phys. B, 209, 146
Fujii Y., Iwamoto A., Fukahori T., Ohnuki T., Nakagawa M., Hidaka H., Oura Y., MÄoller P., 2000, Nucl. Phys. B, 573, 377
Gaillard M. K., Grannis P. D., Sciulli F. J., 1999, Rev. Mod. Phys., 71, 96
Gamow G., 1967, Phys. Rev. Lett., 19, 913
Gay P. L., Lambert D. L., 2000, ApJ, 533, 260
Ge J., Bechtold J., 1997, ApJ, 477, L73
Ge J., Bechtold J., 1999, in Carilli C. L., Radford S. J. E., Menten K. M., Langstom G. I., eds, ASP Conf. Ser. Vol. 156, Highly Redshifted Radio Lines. Astron. Soc. Pac., San Francisco, CA, U.S.A, p. 121
Ge J., Bechtold J., Kulkarni V. P., 2001, ApJ, 547, L1
Gill P. E., Murray W., Wright M. H., 1981, Practical optimization. Academic Press, London, UK
Griesmann U., Kling R., 2000, ApJ, 536, L113
Gunn J. E., Peterson B. A., 1965, ApJ, 142, 1633
Haehnelt M. G., Steinmetz M., Rauch M., 1998, ApJ, 495, 647
Haldane J. B. S., 1937a, Nat, 139, 1002
Haldane J. B. S., 1937b, Nat, 158, 555
186 References
Hallstadius L., 1979, Z. Phys. A, 291, 203
Hannestad S., 1999, Phys. Rev. D, 60, 023515
Harris D. L., 1948, ApJ, 108, 112
Hazard C., 1963, MNRAS, 126, 489
Herbig G. H., 1975, ApJ, 196, 129
Hogan C. J., 2000, Rev. Mod. Phys., 72, 1149
Ho·rava P., 1996, Phys. Rev. D, 54, 7561
Ho·rava P., Witten E., 1996, Nucl. Phys. B, 475, 94
Huml¶³·cek J., 1979, J. Quant. Spectrosc. Radiat. Transfer, 21, 309
Huml¶³·cek J., 1982, J. Quant. Spectrosc. Radiat. Transfer, 27, 437
Hummer D. G., 1965, MNRAS, 70, 1
Ivanchik A. V., Potekhin A. Y., Varshalovich D. A., 1999, A&A, 343, 439
Ivanchik A. V., Rodriguez E., Petitjean P., Varshalovich D. A., 2002, Astron. Lett., 28, 423
Ivanchik A. V., Rodriguez E., Petitjean P., Varshalovich D. A., 2003, in Martins C. J. A. P., ed., The cosmology of extra dimensions and varying fundamental constants. Kluwer, Netherlands
Jenkins E. B., Peimbert A., 1997, ApJ, 477, 265
Jenkins E. B., Wo¶zniak P. R., So¯a U. J., Sonneborn G., Tripp T. M., 2000, ApJ, 538, 275
Jenniskens P., Desert F.-X., 1994, A&AS, 106, 39
Jordan P., 1937, Naturwiss., 25, 513
Jordan P., 1939, Z. Phys., 113, 660
Kaluza T., 1921, Preuss. Akad. Wiss. K, 1, 966

Kaplinghat M., Scherrer R. J., Turner M. S., 1999, Phys. Rev. D, 60, 023516
Kelly R. L., 1987, J. Phys. Chem. Ref. Data Suppl., 16, 1
Klein O., 1926, Z. Phys., 37, 895
References 187
Kolb E. W., Perry M. J., Walker T. P., 1986, Phys. Rev. D, 33, 869
Kothari D. S., 1938, Nat, 142, 354
Kujat J., Scherrer R. J., 2000, Phys. Rev. D, 62, 023510
Kupka F., Piskunov N., Ryabchikova T. A., Stempels H. C., Weiss W. W., 1999, A&AS, 138, 119
Landau L. D., 1955, in Pauli W., ed., Neils Bohr and the Development of Physics. McGraw-Hill, New York, NY, USA, p. 52
Landau S. J., Harari D. D., Zaldarriaga M., 2001, Phys. Rev. D, 63, 083505
Landau S. J., Vucetich H., 2002, ApJ, 570, 463
Langacker P., Segrµe G., Strassler M. J., 2002, Phys. Lett. B, 528, 121
Lanzetta K. M., Bowen D. V., 1992, ApJ, 391, 48
Lanzetta K. M., Bowen D. V., Tytler D., Webb J. K., 1995, ApJ, 442, 538
Lauroesch J. T., Meyer D. M., Blades J. C., 2000, ApJ, 543, L43
Le Brun V., Bergeron J., 1998, A&A, 332, 814
Le Brun V., Bergeron J., Boisse P., 1996, A&A, 306, 691
Ledoux C., Srianand R., Petitjean P., 2002, A&A, 392, 781
Levshakov S. A., Dessauges-Zavadsky M., D'Odorico S., Molaro P., 2002a, MNRAS, 333, 373
Levshakov S. A., Dessauges-Zavadsky M., D'Odorico S., Molaro P., 2002b, ApJ, 565, 696
Levshakov S. A., Molaro P., Centuri¶on M., D'Odorico S., Bonifacio P., Vladilo G., 2000, A&A, 361, 803
Levy-Leblond J. M., 1979, in Toraldo di Francini G., ed., Proc. Enrco Fermi Int. School Phys. Vol. 52, Problems in the foundations of physics. Elsevier, Netherlands, p. 237
Li L., Gott J. R. III, 1998, Phys. Rev. D, 58, 103513
Lineweaver C. H., Tenorio L., Smoot G. F., Keegstra P., Banday A. J., Lubin P., 1996, ApJ, 470, 38
188 References
Liske J., 2003, A&A, 398, 429
Litzen U., Brault J. W., Thorne A. P., 1993, Phys. Scr., 47, 628
Livio M., Stiavelli M., 1998, ApJ, 507, L13
Lopez S., Reimers D., Rauch M., Sargent W. L. W., Smette A., 1999, ApJ, 513, 598
Lu L., Sargent W. L. W., Barlow T. A., Churchill C. W., Vogt S. S., 1996, ApJS, 107, 475
Lu L., Sargent W. L. W., Womble D. S., Takada-Hidai M., 1996, ApJ, 472, 509
Lynds R., 1971, ApJ, 164, L73
Maeda K. I., 1988, Mod. Phys. Lett. A, 3, 242
Magueijo J., 2000, Phys. Rev. D, 62, 103521
Magueijo J., Barrow J. D., Sandvik H. B., 2002, Phys. Lett. B, 549, 284
Maller A., Somerville R. S., Prochaska J. X., Primack J. R., 1999, in Bunker A. J., van Breugel W. J. M., eds, ASP Conf. Ser. Vol. 193, The Hy-Redshift Universe:

Galaxy Formation and Evolution at High Redshift. Astron. Soc. Pac., San Francisco, CA, U.S.A, p. 608
Marciano W. J., 1984, Phys. Rev. Lett., 52, 489
Marcy G. W., Butler R. P., 1992, PASP, 104, 270
Martin W. C., Zalubas R., 1983, J. Phys. Chem. Ref. Data, 12, 323
Martins C. J. A. P., ed., 2003, Proceedings of JENAM2002, The cosmology of extra dimensions and varying fundamental constants. Kluwer, Netherlands
Martins C. J. A. P., Melchiorri A., Trotta R., Bean R., Rocha G., Avelino P. P., Viana P. T. P., 2002, Phys. Rev. D, 66, 023505
Maurette M., 1976, Annu. Rev. Nuc. Sci., 26, 319
McDonald P., Miralda-Escud¶e J., 1999, ApJ, 519, 486
Menten K. M., Reid M. J., 1996, ApJ, 465, L99
Mills I., Cvitas T., Homann K., Kallay N., Kuchitsu K., 1988, in Quantities, Units and Symbols in Physical Chemistry. Blackwell Scienti¯c Publications, Oxford, UK
Milne E. A., 1935, Relativity, Gravitation and World Structure. Clarendon Press, References 189
Oxford, UK
Milne E. A., 1937, Proc. R. Soc. A, 158, 324
Miralda-Escude J., Cen R., Ostriker J. P., Rauch M., 1996, ApJ, 471, 582
Mo®at J., 1993, Int. J. Mod. Phys. D, 2, 351
Mohr P. J., Taylor B. N., 2000, Rev. Mod. Phys., 72, 351
Molaro P., Bonifacio P., Centuri¶on M., D'Odorico S., Vladilo G., Santin P., Di Marcantonio P., 2000, ApJ, 541, 54
Molaro P., Levshakov S. A., D'Odorico S., Bonifacio P., Centuri¶on M., 2001, ApJ, 549, 90
Monaghan J. J., 1971, MNRAS, 152, 509
Moore C. E., 1971, Atomic Energy Levels as Derived from Analyses of Optical Spectra. Natl. Stand. Rel. Data Ser. Vol. 1{3, Natl. Bur. Stand. (USA), US Govt. Printing O±ce, Washington DC, USA
Morton D. C., 1991, ApJS, 77, 119
Morton D. C., 1992, ApJS, 81, 883
Morton D. C., Dinerstein H. L., 1976, ApJ, 204, 1
Murphy M. T., Curran S. J., Webb J. K., 2003b, MNRAS, 342, 830
Murphy M. T., Webb J. K., Flambaum V. V., 2003c, MNRAS, accepted, preprint (astro-ph/0306483)
Murphy M. T., Webb J. K., Flambaum V. V., Churchill C. W., Prochaska J. X., 2001b, MNRAS, 327, 1223
Murphy M. T., Webb J. K., Flambaum V. V., Curran S. J., 2002, in Dong S., Burchat P., eds, Proceedings of the XXII Physics in Collision Conference. Stanford, CA, U.S.A, p. 116
Murphy M. T., Webb J. K., Flambaum V. V., Curran S. J., 2003a, Ap&SS, 283, 577
Murphy M. T.,Webb J. K., Flambaum V. V., Drinkwater M. J., Combes F., Wiklind T., 2001d, MNRAS, 327, 1244
190 References
Murphy M. T., Webb J. K., Flambaum V. V., Dzuba V. A., Churchill C. W.,

Prochaska J. X., Barrow J. D., Wolfe A. M., 2001a, MNRAS, 327, 1208
Murphy M. T., Webb J. K., Flambaum V. V., Prochaska J. X., Wolfe A. M., 2001c, MNRAS, 327, 1237
Nagourney W., Dehmelt H. G., 1981, Bull. Am. Phys. Soc., 26, 805
Naudet R., 1974, Bull. Inf. Sci. Tech., 193, 1
Nave G., Learner R. C. M., Thorne A. P., Harris C. J., 1991, J. Opt. Soc. Am. B, 8, 2028
Nollett K. M., Lopez R. E., 2002, Phys. Rev. D, 66, 063507
Norl¶en G., 1973, Phys. Scr., 8, 249
Nulsen P. E. J., Barcons X., Fabian A. C., 1998, MNRAS, 301, 168
O'Dea C. P., Baum S. A., Stanghellini C., Dey A., van Breugel W., Deustua S., Smith E. P., 1992, AJ, 104, 1320
Olive K. A., Pospelov M., Qian Y.-Z., Coc A., Cass¶e M., Vangiona-Flam E., 2002, Phys. Rev. D, 66, 045022
Outram P. J., Carswell R. F., Theuns T., 2000, ApJ, 529, L73
Outram P. J., Cha®ee F. H., Carswell R. F., 1999, MNRAS, 310, 289
Pagel B. E. J., 1977, MNRAS, 179, 81P
Palmer B. A., Engleman R., 1983, Technical report, Atlas of the Thorium spectrum. Los Alamos National Laboratory, NM, USA
Patnaik A. R., Browne I. W. A., King L. J., Muxlow T. W. B., Walsh D., Wilkinson P. N., 1993, MNRAS, 261, 435
Peacock J. A., 1999, Cosmological physics. Cambridge Univ. Press, Cambridge, UK
Peck E. R., Reeder K., 1972, J. Opt. Soc. Am., 62, 958
Peebles P. J., Dicke R. H., 1962, Phys. Rev., 128, 2006
Peebles P. J. E., 1993, Principles of physical cosmology. Princeton Univ. Press, Princeton, NJ, USA
Perlman E. S., Carilli C. L., Stocke J. T., Conway J., 1996, AJ, 111, 1839
References 191
Petitjean P., Rauch M., Carswell R. F., 1994, A&A, 291, 29
Petitjean P., Srianand R., Ledoux C., 2000, A&A, 364, L26
Petitjean P., Srianand R., Ledoux C., 2002, MNRAS, 332, 383
Petrov Y. V., 1977, Sov. Phys. Uspekhi, 20, 937
Pettini M., King D. L., Smith L. J., Hunstead R. W., 1997, ApJ, 478, 536
Pickering J. C., Donnelly M. P., Nilsson H., Hibbert A., Johansson S., 2002, A&A, 396, 715
Pickering J. C., Thorne A. P., Murray J. E., Litz¶en U., Johansson S., Zilio V., Webb J. K., 2000, MNRAS, 319, 163
Pickering J. C., Thorne A. P., Webb J. K., 1998, MNRAS, 300, 131
Pickett H. M., Poynter R. L., Cohen E. A., Delitsky M. L., Pearson J. C., Muller H. S. P., 1998, J. Quant. Spectrosc. Radiat. Transfer, 60, 883
Piskunov N. E., Kupka F., Ryabchikova T. A., Weiss W. W., Je®ery C. S., 1995, A&AS, 112, 525
Poppe G. P. M., Wijers C. M. J., 1990, Trans. Math. Software, 16, 38
Potekhin A. Y., Ivanchik A. V., Varshalovich D. A., Lanzetta K. M., Baldwin J. A., Williger G. M., Carswell R. F., 1998, ApJ, 505, 523
Prestage J. D., Tjoelker R. L., Maleki L., 1995, Phys. Rev. Lett., 74, 3511

Price R. J., Crawford I. A., Barlow M. J., 2000, MNRAS, 312, L43
Prochaska J. X., 2003, ApJ, 582, 49
Prochaska J. X., Wolfe A. M., 1996, ApJ, 470, 403
Prochaska J. X., Wolfe A. M., 1997, ApJ, 474, 140
Prochaska J. X., Wolfe A. M., 1999, ApJS, 121, 369
Prochaska J. X., Wolfe A. M., 2000, ApJ, 533, L5
Prochaska J. X. et al., 2001, ApJS, 137, 21
Randall L., Sundrum R., 1999a, Phys. Rev. Lett., 83, 3370
Randall L., Sundrum R., 1999b, Phys. Rev. Lett., 83, 4690
192 References
Rao S. M., Turnshek D. A., 2000, ApJS, 130, 1
Rauch M., 1998, ARA&A, 36, 267
Riazuelo A., Uzan J., 2002, Phys. Rev. D, 66, 023525
Rosman K. J. R., Taylor P. D. P., 1998, J. Phys. Chem. Ref. Data, 27, 1275
Safronova M. S., Johnson W. R., 2001, Phys. Rev. A, 64, 52501
Sandvik H. B., Barrow J. D., Magueijo J., 2002, Phys. Rev. Lett., 88, 31302
Savedo® M. P., 1956, Nat, 178, 689
Schaye J., 2001, ApJ, 559, L1
Schmidt M., 1963, Nat, 197, 1040
Shlyakhter A. I., 1976, Nat, 264, 340
Sievers J. L. et al., 2002, ApJ, submitted, preprint (astro-ph/0205387)
Smoot G. F. et al., 1992, ApJ, 396, L1
Sommerfeld A., 1911, Z. Phys., 12, 1057
Songaila A., Cowie L. L., 1996, AJ, 112, 335
Songaila A. et al., 1994, Nat, 371, 43
Sortais Y. et al., 2001, Phys. Scr., T95, 50
Srianand R., Petitjean P., 1998, A&A, 335, 33
Srianand R., Petitjean P., Ledoux C., 2000, Nat, 408, 931
Stockton A. N., Lynds C. R., 1966, ApJ, 144, 451
Struve O., Elvey C. T., 1934, ApJ, 79, 409
Teller E., 1948, Phys. Rev., 73, 801
Theuns T., Leonard A., Efstathiou G., 1998a, MNRAS, 297, L49
Theuns T., Leonard A., Efstathiou G., Pearce F. R., Thomas P. A., 1998b, MNRAS, 301, 478
Thompson R. I., 1975, Astron. Lett., 16, 3
Timmes F. X., Clayton D. D., 1996, ApJ, 472, 723
Tripp T. M., Lu L., Savage B. D., 1998, ApJ, 508, 200
References 193
Tubbs A. D., Wolfe A. M., 1980, ApJ, 236, L105
Uzan J., 2003, Rev. Mod. Phys., 75, 403
Valenti J. A., Butler R. P., Marcy G. W., 1995, PASP, 107, 966
Varshalovich D. A., Levshakov S. A., 1993, J. Exp. Theor. Phys. Lett., 58, 237
Varshalovich D. A., Panchuk V. E., Ivanchik A. V., 1996, Astron. Lett., 22, 6
Varshalovich D. A., Potekhin A. Y., 1995, Space Sci. Rev., 74, 259
Varshalovich D. A., Potekhin A. Y., 1996, Astron. Lett., 22, 1 (VP96)
Varshalovich D. A., Potekhin A. Y., Ivanchik A. V., 2000, in Dunford R. W., Gemmel

D. S., Kanter E. P., Kraessig B., Southworth S. H., Young L., eds, AIP Conf. Proc. Vol. 506, X-Ray and Inner-Shell Processes. Argonne National Laboratory, Argonne, IL, USA, p. 503 (VPI00)
Vogt S. S. et al., 1994, in Crawford D. L., Craine E. R., eds, Proc. SPIE Vol. 2198, Instrumentation in Astronomy VIII. p. 362
Walker M., Wardle M., 1998, ApJ, 498, L125
Weast R. C., 1979, Handbook of Chemistry and Physics, 60th edn. CRC Press, Boca Raton, FL, USA
Webb J. K., 1987, PhD thesis, Univ. Cambridge
Webb J. K., Flambaum V. V., Churchill C. W., Drinkwater M. J., Barrow J. D., 1999, Phys. Rev. Lett., 82, 884 (W99)
Webb J. K., Murphy M. T., Flambaum V. V., 2003, in preparation
Webb J. K., Murphy M. T., Flambaum V. V., Curran S. J., 2003, Ap&SS, 283, 565
Webb J. K., Murphy M. T., Flambaum V. V., Dzuba V. A., Barrow J. D., Churchill C. W., Prochaska J. X., Wolfe A. M., 2001, Phys. Rev. Lett., 87, 091301
Weinberg S., 1983, Phil. Trans. R. Soc. London, 310, 249
Wells R. J., 1999, J. Quant. Spectrosc. Radiat. Transfer, 62, 29
Whaling W., Anderson W. H. C., Carle M. T., Brault J. W., Zarem H. A., 1995, J. Quant. Spectrosc. Radiat. Transfer, 53, 1
Wheeler J. A., 1980, in Woolf H., ed., Some strangeness in the proportion. Addison194 References
Wesley, London, UK, p. 341
Wiklind T., Combes F., 1994, A&A, 286, L9
Wiklind T., Combes F., 1995, A&A, 299, 382
Wiklind T., Combes F., 1996, A&A, 315, 86
Wiklind T., Combes F., 1997, A&A, 328, 48
Wiklind T., Combes F., 1998, ApJ, 500, 129
Wolfe A. M., Brown R. L., Roberts M. S., 1976, Phys. Rev. Lett., 37, 179
Wolfe A. M., Davis M. M., 1979, AJ, 84, 699
Wolfe A. M., Prochaska J. X., 2000, ApJ, 545, 603
Wu Y., Wang Z., 1986, Phys. Rev. Lett., 57, 1978

Tables list:

http://michaelmarchenko.weebly.com/uploads/3/0/2/7/30272185/tables4phd4physics.rtf

Formulas list:

http://michaelmarchenko.weebly.com/uploads/3/0/2/7/30272185/formulas_17jan07.rtf
http://michaelmarchenko.weebly.com/uploads/3/0/2/7/30272185/formulas_18jan07.rtf
http://michaelmarchenko.weebly.com/uploads/3/0/2/7/30272185/formulas_19jan07.rtf
http://michaelmarchenko.weebly.com/uploads/3/0/2/7/30272185/formulas25mar07__.rtf